SKARN AND SULPHIDE MINERALISATION OF THE SYLVESTER PROSPECT, ZEEHAN, WESTERN TASMANIA

by

Michael Iain Taylor B.Sc.

A research thesis submitted in partial fulfilment of the requirements for the degree of Bachelor of Science with Honours.

Centre for Ore Deposits and Exploration Studies,
Geology Department
Univerersity of Tasmania

December 1993.

CODES

ABSTRACT

The Sylvester prospect is a Zn-Pb-Ag skarn located in the Zeehan mineral field approximately 4 kms west of Zeehan, western Tasmania. The skarn and sulphide mineralisation is hosted in dolomitic carbonate units of the Late Precambrian Upper Oonah Formation. Mineralisation occurs in the footwall of a major NNW trending Devonian fault (Balstrup Fault), where carbonates and shales of the Upper Oonah Formation are in contact with sandstones and siltstones of the Lower Oonah Formation and turbiditic greywackes of the Eo-Cambrian Crimson Creek Formation. Approximately 3 kms west of the Sylvester prospect is the Late Devonian (S-type) Heemskirk Granite.

Three stages of skarn formation can be observed in rocks of the prospect: (a) contact metamorphism produced restricted occurrences of biotite hornfels in pelites of the Oonah Formation, and resulted in the recrystallisation of Upper Oonah Formation dolomitic carbonate to marble; (b) early stage metasomatism produced isolated patches of andradite-diopside-tremolite-talc skarn in carbonate units; and (c) late stage (hydrous) metasomatism development resulting in the extensive massive serpentine-magnetite ± brucite skarn which replaces a dolomitic carbonate unit in the immediate footwall of the Balstrup Fault.

Sulphide mineralisation is characterised by a near-vertical lens of massive pyrrhotite + sphalerite + galena + chalcopyrite ± arsenopyrite ± marcasite ± pyrite (called the Comstock massive sulphide body) replacing the late (hydrous) stage skarn, whereas massive pyrite + sphalerite + galena + chalcopyrite + quartz replaces dolomite in the footwall of the Balstrup Fault. Quartz + pyrite ± sphalerite ± galena stockwork veins are developed in the Balstrup Fault and non-carbonate units of the Oonah Formation. Mineral textures indicate deposition of the sulphides closely followed late stage (hydrous) skarn formation.

A weak west to east metal zonation is expressed in the prospect by decreasing tin grades in the late stage skarn, and decreasing copper grades in the sulphide body. The ratio of zinc to lead is constant at 2:1 throughout the sulphide body.

Sulphur isotope values of sulphide phases range from +3.3 to +7.6 ‰. The more positive $\delta^{34}S$ values (compared with sulphide phases in skarns known to be of magmatic origin; $\delta^{34}S$ 0 ± 3‰) are consistant with being a mixture of ^{34}S enriched sedimentary sulphur leached from the Oonah Formation and lighter magmatic sulphur derived from the Heemskirk Granite. Carbon and oxygen isotopes values of calcite formed in the late (hydrous) metasomatic stage range from $\delta^{13}C$ values of -2.6 to -4.6 ‰ and $\delta^{18}O$ 3.8 to 8.2 ‰ (SMOW). The depleted $\delta^{18}O$ values are interpretated as indicating a mixing of magmatic and meteoric fluids.

The skarn and sulphide mineralisation in the Sylvester prospect originated by metasomatic replacement of carbonate units of the Oonah Formation by fluids intially derived directly from the Heemskirk Granite. Later mixing of these fluids with meteoric fluids that circulated through the Oonah Formation resulted in precipitation of the late stage hydrous skarn assemblages and sulphide mineralisation in the carbonate unit in the footwall of the Balstrup Fault.

ACKNOWLEDGMENTS

I would like to thank Dr Bruce Gemmell and Prof. Ross Large for helpful criticism, guidance and advice throughout the development of this thesis. Thanks must also go to Dr Garry Davidson and Paul Kitto.

I am very grateful to the assistance provided by RGC Exploration, Zeehan, in particularly Scott Halley, Bruce and Deb.

I would also like to thank the following people for their invaluable assistance: S. Stephens for thin section preparation; M. Power for isotope analysis; W. Jablonski, A. McNeil and M. Kamperman for microprobe analysis; R. Botrill for inspirational XRD analysis.

My sincere apologies must go to the rest of the Honours for having to put up with me this year. In particular, Jonesy, Rohan, Joe, Lauzza, Karen and John B, who provided desperately needed distraction.

Finally, a big thanks to my family for their support, encouragement and help throughout the year.

TABLE OF CONTENTS

LIST OF FIGURES

LIST OF TABLES

LIST OF APPENDICES

CHAPTER ONE

INTRODUCTION

1.1 Location and Physiography

The Sylvester prospect is situated four kilometres west of the township of Zeehan, western Tasmania. It lies within the western portion of the Zeehan mineral field (Figure 1.1).

Access to the area is provided by the Trial Harbour Road which bisects the field area. Numerous 4WD tracks and old, partially overgrown, tramways provide access to the furthest parts of the map area.

The topography of the area consists of a broad swampy lowlands in the centre of the map area surrounded by a number of large hills and steep ridges. Vegetation ranges from buttongrass-Ti-Tree swamp to mature dense regrowth eucalyptus rainforest.

1.2 History of the Zeehan mineral field

The Zeehan mineral field is located between the south-eastern margin of the Heemskirk Granite and the township of Zeehan, covering an area approximately sixty five km^2. The extent of the Zeehan field and the numerous deposits that make up the field are shown in Figure 1.2.

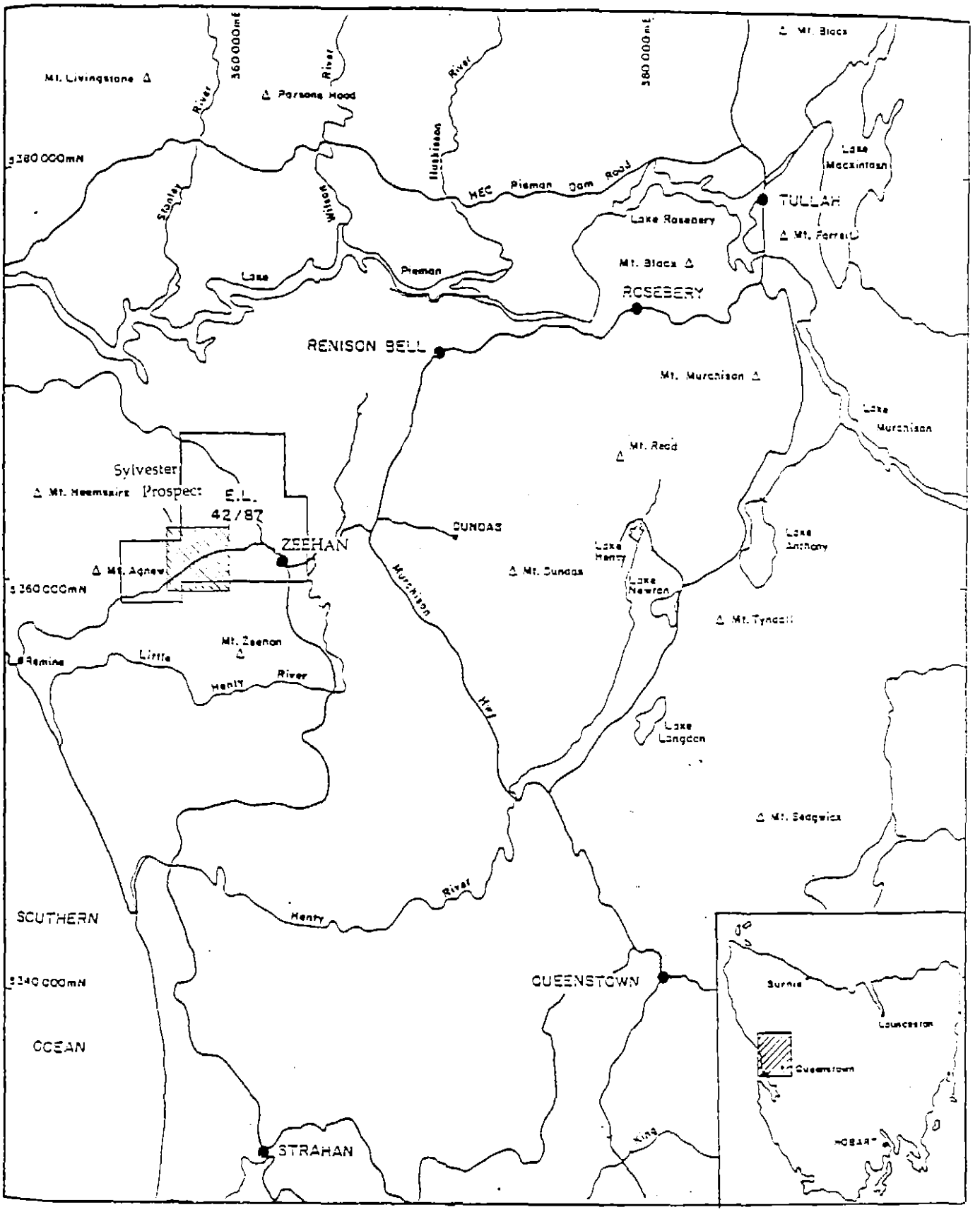

Figure 1.1 Location of the Sylvester prospect.

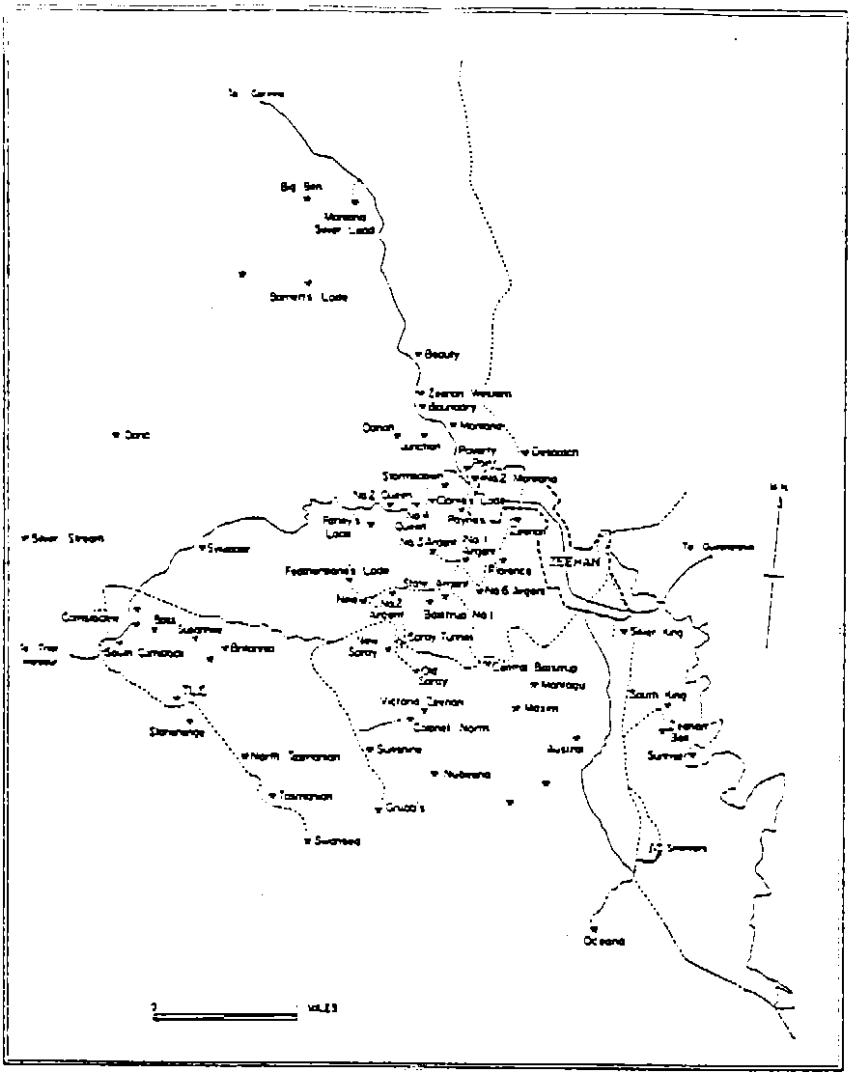

Figure 1.2 Zeehan mineral field (Both and Williams, 1969)

5 cm

Mine or Prospect	Lead (tons)	Silver (oz.)	Zinc (tons)	
Argent Mines (Nos 2, 5, 6)	4,248	561,110		
Austral, North Austral, Watt & McAuliffe's	1,050	93,000	50	
Boss	70	6,500		
Britannia	*See* Spray Mine			
Central Balstrup	12	1,250		
Colonel North (including Grubb's)	1,549	128,075		
Comstock and South Comstock	1,625	165,000	2,100	
Doric	0·44	30		
Florence	10,200	1,400,000		
Grubb's	*See* Colonel North			
Junction (including Hanrahan's Adit)	15	8,728		
Maxim	60	10,000		
Montagu No. 1	115	1,500		
Montana S.L.	2,304	279,348		
Mount Zeehan	1,540	166,350		
Nike	2,149	225,330	7·8	
Nubeena and South Nubeena	375	49,000		
Oceana	14,902	614,981	12·3	
Oonah	11,724	2,050,135		** Copper 941 tons
Silver King and South King	5,000	350,000		Copper 4 tons
Silver Stream	165	9,200		
Spray*	41,700	6,456,674		
Stonehenge	30	2,700		
Stormsdown				Tin 5 tons
Sunrise	36	4,760		
Susannite	20	3,500		
Swansea	1,319	35,630	570	Cadmium 40 tons
Sylvester	274	26,560		
Tasmanian and North Tasmanian	720	41,299	8	
Tasmanian Crown	113	15,738		
T.L.E.	203	30,031	1	
Zeehan Bell	600	27,500		
Zeehan-Montana	49,580	7,058,122		
Zeehan Queen	16,532	1,973,746		**
Zeehan-Western	26,300	4,800,000		

Table 1.1 Production records of silver-lead mined from the Zeehan mineral field. (Both and Williams, 1969)

Silver-lead veins were first discovered by Frank Long in 1882 near the present day township of Zeehan. The subsequent discovery of further silver-lead mineralisation in and around the township of Zeehan between 1882 and 1887 lead to the rapid establishment of the Zeehan mineral field. Silver-lead ore was mined continuously from the Zeehan field until its decline in 1913 and subsequent closure by 1914 (Both and Williams, 1968).

Towards the end of the 19th century mining of quartz-tourmaline-cassiterite veins and associated alluvial tin deposits in the Heemskirk mineral field, west of Zeehan, was well established. With intense prospecting moving outside of the Heemskirk field, tin (in the form of stanniferous veins) was eventually discovered in the Zeehan area (Waller, 1904). However, only a few prospects were mined for economic grades of stannite (Clarkes Lode, Oonah Mine, Bradshaws and Pastkuchens Lodes) and by 1914 tin production had ceased (Both and Williams, 1968).

In 1937 cassiterite was discovered on Queen Hill as a part of the Stormsdown Lode. Between the period 1937 to 1960 5.4 tonnes of tin was worked by the Zeehan Tin Development NL from the Stormsdown mine. The Stormsdown mine was the last tin mine in the Zeehan field (Blissett, 1962b).

The resurgence of tin mining was paralleled by the resurrection of silver-lead mining. With the discovery of the Montana Silver Lead mine and the re-development of the Oceana mine in the late 1940's, silver, lead, and zinc was again mined from the area until their closure in the early 1960's (Both and Williams, 1968).

By the end of mining activity in 1960, the Zeehan Field had produced approximately 200,000 tonnes of lead, 826,000 kg's of silver, 2,700 tons of zinc and 5.4 tons of tin (Blissett, 1962b). Production records of silver-lead mined from individual mines is given in Table 1.1.

Modern exploration in the Zeehan field began in the late 1970's and has to date resulted in the discovery of the large Queen Hill-Severn cassiterite/sulphide replacement deposit; a cluster of three presently sub economic cassiterite bodies. Presently, only minor exploration is being conducted in the Zeehan field.

1.3 Previous Workers

There are numerous references on the geology and ore-gangue mineralogy of the Zeehan district by early regional workers and mining company reports. Reports of relevance are Waller (1904), Twelvetrees and Ward (1910), Blissett (1962a, 1962b), and Both and Williams (1968). More comprehensive studies of the geology of the area, and its regional relationships include Brown (1986) and more recently Everard et al., (1992), as part of the revision of the 25- year old Zeehan Quadrangle 1:50,000 map series.

1.4 Modern Exploration in the Sylvester area

Since the early 1970's several exploration companies have explored the areas adjacent to the Sylvester prospect. Gold Fields Exploration Pty. Ltd. (later to become Renison Goldfields Consolidated (RGC) Exploration) held the E.L. 11/76 from 1974 to 1986 which was centred near the Stonehenge area (The Stonehenge area is situated within the extreme south western part of the current E.L. 42/87). The target in the Stonehenge area was replacement-style

tin hosted in altered dolomites of the Precambrian Oonah Formation. Work completed on this lease was drilling of six diamond drill holes into moderate lead and tin geochemical anomalies. Exploration in the Tenth Legion area (north west of the current lease) began in 1958 with the drilling of two holes by the Tasmanian Mines Department , and later thirteen holes by IMI Pty. Ltd, into the largest of the magnetite skarn bodies, targeting iron ore. Between 1980 and 1982 CRA Exploration in joint venture with IMI Pty. Ltd completed fourteen drill holes targeting tin mineralisation within the magnetite-serpentinite skarn bodies. Currently the Sylvester area is incorporated in E.L. 42/87 being explored by RGC Exploration. As part of the current exploration fifteen diamond drill holes (SY002-SY016) have been drilled.

1.5 Terminology

The term "Sylvester prospect" refers to the 1:5000 scale mapping area Map pocket, Figure 1.4
The term "Comstock massive sulphide body" refers to the pyrrhotite-sphalerite-galena orebody in the footwall of the Balstrup Fault.

1.6 Aims

The primary aims of this research thesis are;

1. To log the diamond drill core from the Sylvester prospect, in particular detailed logging of holes intersecting magnetite-serpentinite skarn and base metal sulphide mineralisation, in order to establish the geological characteristics of the skarn and sulphide mineralisation as a framework for petrologic and isotropic investigations.

2. Establish the sulphur isotopic signature of the Comstock massive sulphide mineralisation. Correlate this data with other mineralisation in the Zeehan field to investigate if a regional pattern exists.

1.7 Methods

Fieldwork, undertaken June to early August 1993, involved detailed logging of fifteen diamond drill holes (SY 002 - SY 016) and collection of samples for subsequent petrological and isotopic analyses. Laboratory research involved sulphur and carbon/oxygen isotope and electron probe analyses. Analyses of all samples were carried out by facilities at the University of Tasmania. All samples discussed in this thesis are referred to by their Department of Geology catalogue number.

CHAPTER TWO

REGIONAL GEOLOGY

The general geology of the Heemskirk-Zeehan area is shown in Figure 2.1.

2.1 STRATIGRAPHY

2.1.1 Proterozoic

The oldest rocks are multiply-deformed, low grade greenschist facies sediments (Turner, 1989) called the Oonah Formation (Blissett, 1962a). The Oonah Formation typically consists of abundant thin-bedded micaceous quartzite and siltstone, sandstones, black shales (Blissett 1962a). The upper portion of the formation becomes increasingly dominated by dolomites, interbedded carbonaceous shales and spilitic volcanics; which includes lava flows and pyroclastic bands (Blissett 1962). On the basis of lithological differences between the lower sandstone-siltstone-shale sequences and the upper sandstone-siltstone-carbonate-shale-spilitic sequences the Oonah Formation can be divided into two successions; the Upper Oonah Succession and the Lower Oonah Succession (Brown 1986). The age of Oonah Formation is regarded as Late Precambrian, based on the K-Ar dating of rocks from the Oonah Formation deformed during the Late Precambrian Pengiun Orogeny (Turner, 1989).

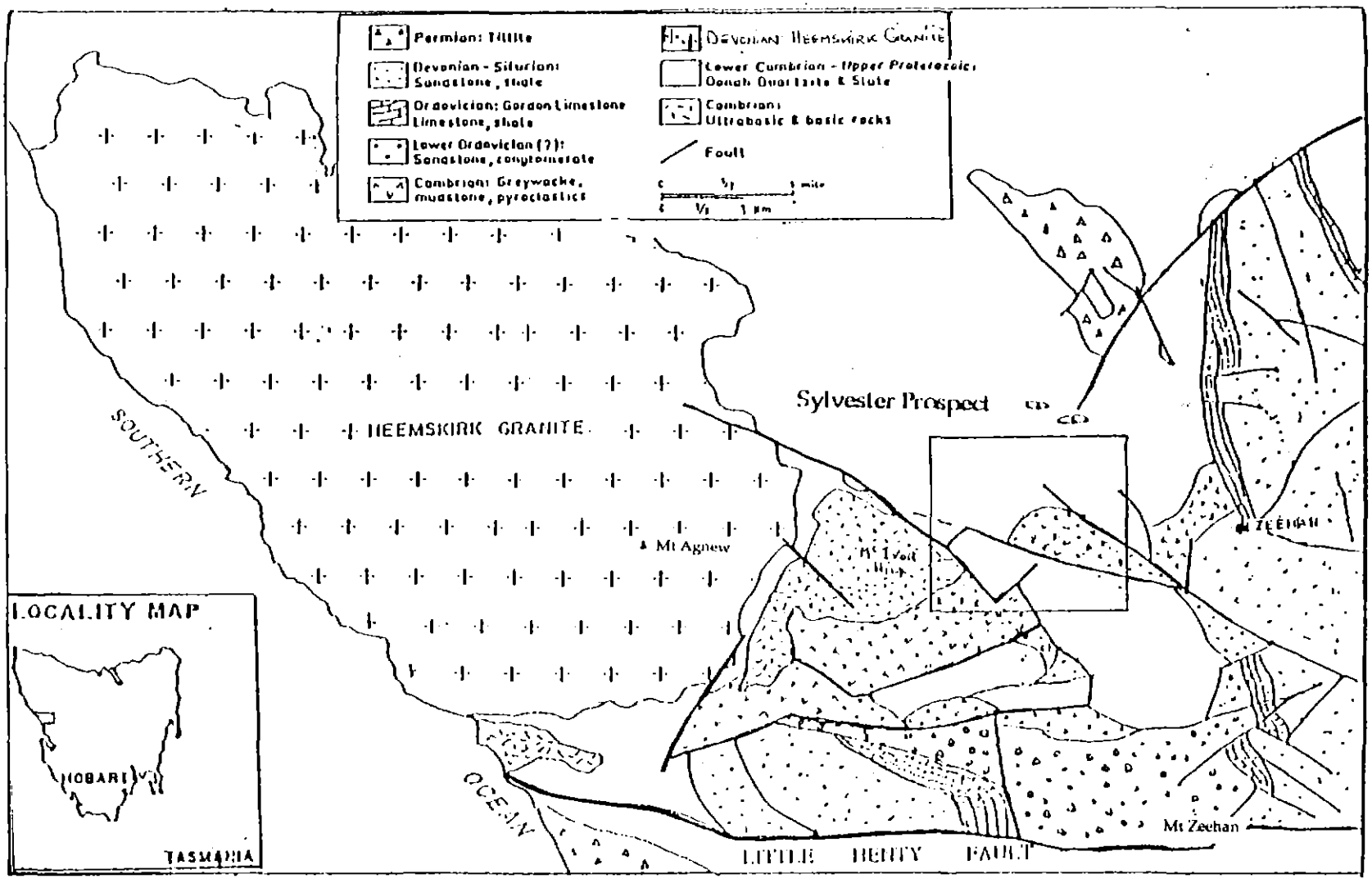

Figure 2.1 Regional geology of the Heemskirk-Zeehan region. (modified after Both et al., 1969)

5 cm

2.1.2 Late Precambrian to Cambrian

A sequence of unfossiliferous shallow water sediments, the Success Creek Group (absent in the Zeehan area), unconformably overlies the upper successions of the Oonah Formation, and is itself conformably overlain by the Crimson Creek Formation (Brown, 1986). The Crimson Creek Formation is a latest Precambrian or Early Cambrian turbidite sequence (Brown 1986). The sequence is dominated overall by green to brown greywackes, laminated siltstones and mudstones, volcaniclastic lithic wackes and interbedded tholeiitic basalts (Brown 1986).

Fault contacts separate the Crimson Creek Formation from the overlying fossiliferous Middle to Upper Cambrian sequences of the Dundas Group (Brown, 1986). The Dundas Group consists of two successions, both composed of lithic mudstones, sandstone and conglomerates. East of the Sylvester prospect, shales and greywackes containing fossils {Diplagnostus sp.} outcrop, and these have been correlated with the Hodge Slate (Crossing, 1989), one of five formations assigned to the lower successions of the Dundas Group. Fossiliferous, as well as non fossiliferous, siltstones, wackes and tuffs south of the Tenth Legion Fault have also been tentatively correlated to the Dundas Group (Crossing, 1989).

The McIvor Hill Complex is a large fault-bounded igneous body consisting of serpentinite, gabbros and mafic volcanics. The complex is one of fifteen Cambrian mafic-ultramafic bodies that define a discontinuous belt in western Tasmania (Brown, 1986; Olubus, 1989). The mafic-ultramafic complexes are considered to have been tectonically emplaced into western Tasmania during the Early to Middle Cambrian (Berry and Crawford, 1988).

2.1.3 Devonian Granitiods

The Heemskirk Granite intruded the Precambrian Oonah Formation in the Late Devonian (330-360 Ma) (Brooks, 1966) The granite is composite body consisting of two intrusions, a red granite which has been intruded by a white granite (Klominsky, 1972). Both the red and white granite consist of quartz, K-feldspar, plagioclase and varying amounts of biotite, muscovite and minor hornblende. Acessory magnetite and sphene is confined to the red granite suggesting that it is an I-type granite, whereas the minerlogy of the white granite is consistent with it being and S-type granite (McClenaghan, 1989). Exsolution of hydrothermal fluids following crystallisation of the granite was greatest for the white granite, producing quartz-tourmaline-cassiterite veins in the southern part of the body (McClenaghan, 1989). The granite outcrops as a large elongate body of 140 km^2, approximately 8 kms west of Zeehan.

2.1.4 Permian

Tillite of Permian age outcrops in a number of small patches north of Zeehan. The tillite occurs as a blue-grey clay containing unsorted sub angular pebbles and fragments of quartzite and sandstone (Blissett, 1962a). The main outcrop of tillite, north of the Montana SL Mine, is less than 20 metres thick (Blissett, 1962a).

2.2 STRUCTURE

Three major deformational events may be observed within the rocks of the Zeehan district. The earliest phase of deformation (D1) is evident only in the Proterozoic sediments of the Oonah Formation and has been assigned to the Late Precambrian Penguin Orogeny (Berry et al., 1990). The D1 event is characterised by an early S_1 cleavage associated with mesoscale isoclinal folding in well bedded units, a S_2 crosscutting crenulation cleavage associated with shallowly reclined refolding of F1 fold axes, and a later S3 crenulation foliation occurring dominantly in the closure zones of large scale upright folds which produced regional anticlinorial-synclinorial folding (Turner, 1989). Associated with these third generation folds is the occurrence of reverse faults and cataclasite formation. These two features may possibly represent the second phase of deformation, associated with the mid-Cambrian thrusting event which produced the emplacement of the ultramafic complexes (Berry et al., 1990).

The final orogenic phase is part of the multi-deformational mid-Devonian Tabberabberan Orogeny. The mid-Devonian Tabberabberan Orogeny produced the most significant period of deformation in the area. It involved two main phases of deformation; an early NE-SW compression that produced large tight NW trending folds with half wavelengths of 4.5 km (Heemskirk Anticlinorium) (termed the West Coast Range/Valentines Peak Trend). ; and a later NW-SE compression that produced northward plunging, NE trending open folds with wavelengths of less than 1km (termed the Zeehan/ Gormanston Trend) (Williams and Seymour, 1989).

2.3 GRANITE MORPHOLOGY

The extent of the contact aureole and the eastward trend of the mineralogical zonation of ores in the Zeehan mineral field has been thought to indicate that the sub surface form of the Heemskirk Granite batholith shelves shallowly toward the east of Zeehan (Johnson, 1967). Leaman and Richardson (1989) confirmed this idea through a geophysical interpretation of the sub surface form of the Heemskirk Granite (Fig. 2.2).

Gravity data indicates that the granite surface occurs within two kilometres of the ground surface over a large part of the Zeehan field. East of Zeehan the surface plunges to depths of six and eight kilometres, at these depths the granite is interpreted to continue regionally toward Pine Hill (Leaman and Richardson, 1989). The gravity interpretation of the granite form allows for recognition of topographical features on the granite surface. Irregularities on this surface have been suggested to have controlled the occurrence of mineralisation in the Zeehan district (Collins and Williams, 1986; Leaman and Richardson, 1989). These irregularities are seen as "roof spines" or cupolas which intrude into the overlying rock, and act as channels for mineralising fluids. It is proposed that the sulphide -cassiterite mineralisation centred on the Queen Hill- Severn area is genetically related to a cupola located at depth. Leaman (1990) does not rule out the possibility of a cupola below the Sylvester prospect.

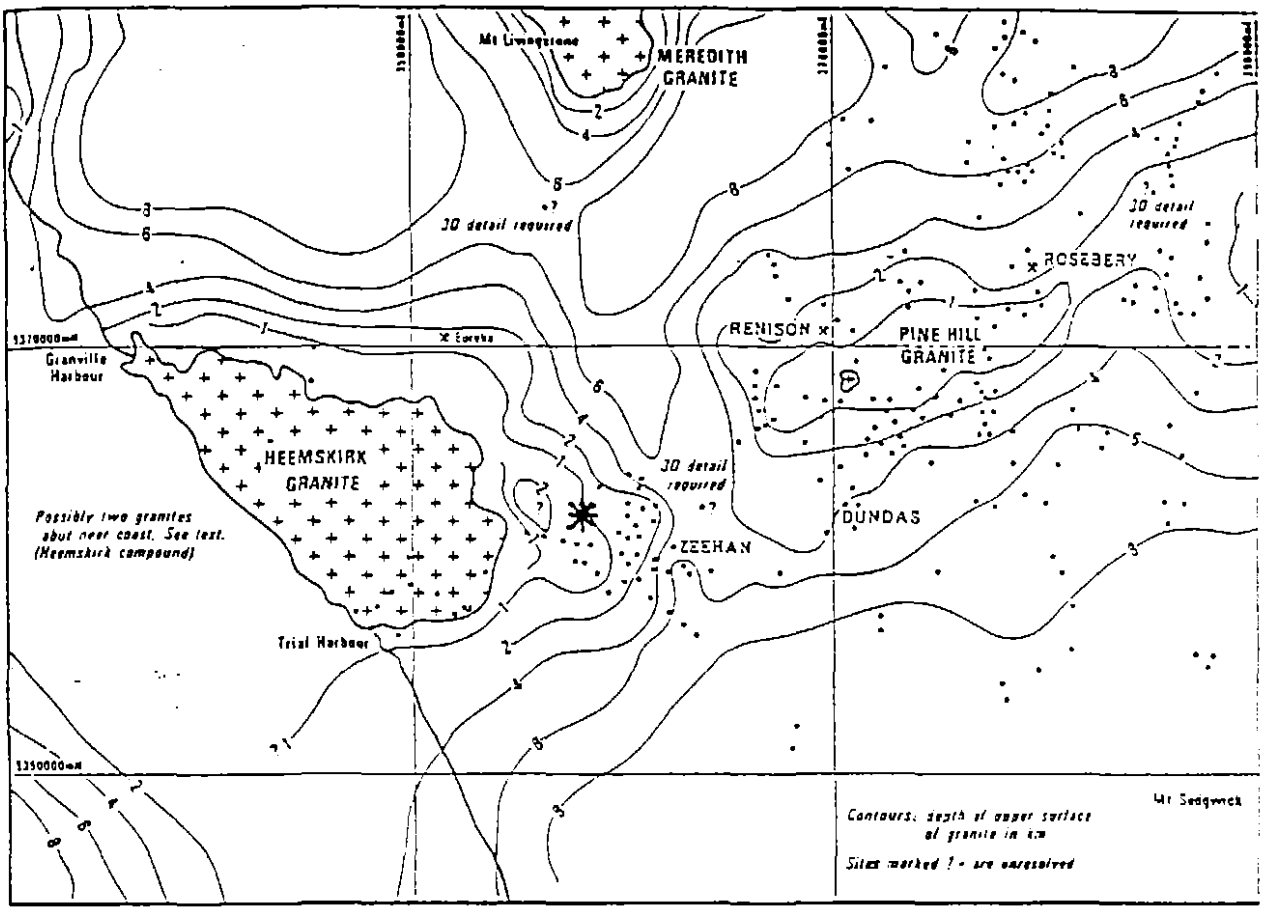

Figure 2.2 The interpretation of the sub-surface form of the Heemskirk Granite below the Zeehan mineral field. Depth contour intervals is 1km. Mineralisation sites in the Zeehan field are indicated by dots. (after Leaman and Richardson, 1989). Star indicates location of Sylvester prospect

5 cm

2.4 MINERALOGICAL ZONATION OF THE ZEEHAN FIELD

The ore bodies at Zeehan occupy a complex system of faults and fractures apparently related to the mid-Devonian deformation (Waller, 1904; Blissett, 1962a; Both and Williams, 1968; Williams and Both, 1969). Most of the lodes strike between NNW and NNE, are steeply dipping, and occur in rocks of Late Precambrian to Early Devonian age, although most deposits occur in the Precambrian Oonah Formation and Early Cambrian Crimson Creek Formation. The lodes consist of relatively small but rich shoots of argentiferous galena, sphalerite in a gangue of pyrite, siderite and quartz. The

lenticular or highly irregular shoots vary in width from less than 2 cm's up to at least 5 m, but average less than 0.25 m and pinch out below 100 m. Their strike lengths rarely exceed 200 m (Both et al., 1969).

The lead-zinc ores of the Zeehan mineral field have long been regard as a classic example of hydrothermal ore zonation, based primarily on distance from the Heemskirk Granite (eg. Waller, 1903; Twelvetrees and Ward, 1910; Both and Williams, 1968; Solomon, 1981). The regional mineralogical zonation pattern proposed by Both and Williams (1968) is generalised into the following zones: (1) a cassiterite zone, (2) a pyritic zone, (3) a sidero-pyrite zone, and (3) a siderite zone (Fig. 2.4). The *cassiterite zone* consists of the cassiterite, tourmaline veins that occur within and adjacent to the Heemskirk Granite. This zone also includes tin deposits associated with skarn replacing carbonates of the Oonah Formation (eg. Tenth Legion). The ores of the *pyritic zone* consist essentially of sphalerite-galena with pyrite as the dominant gangue mineral. This zone includes the areas from the contact aureole of the Heemskirk Granite to the Comstock area. The *sidero-pyrite zone* includes all the sphalerite and galena lodes but with siderite is comparable in abundance to pyrite. The *siderite zone* is marked by the predominance of siderite as the gangue phase and galena dominant over sphalerite.

The exception to this zonation is the Queen Hill-Oonah Hill area where pyritic tin ores occur in the sideritic zone. This anomalous zone is genetically related to the Queen Hill-Severn cassiterite deposit, which is inturn thought to be spatially related to the presence of a cupola located at depth beneath the area (Both and Williams, 1969).

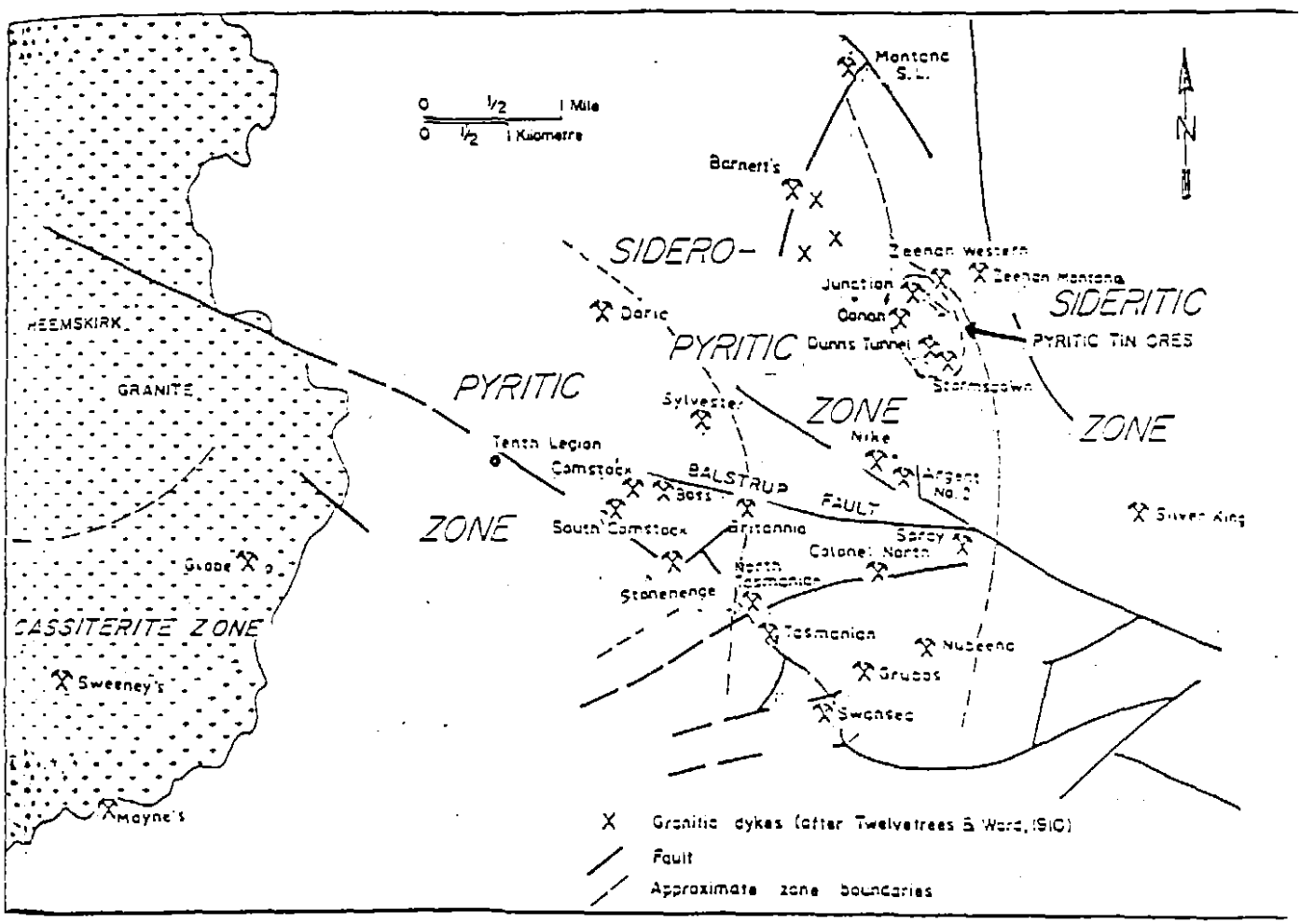

Figure 2.3 Regional Mineralogical zontion pattern of the Heemskirk-Zeehan area. (modified after Both and Willians, 1968)

5 cm

CHAPTER THREE

LOCAL GEOLOGY

3.1 INTRODUCTION

The Comstock massive sulphide body and related serpentine-magnetite skarn are located within a generally shallow dipping wedge of carbonates and interbedded carbonaceous shales of the Upper Oonah Formation. The wedge of Upper Oonah Formation is bound to the north by quartzitic sandstone and siltstone of the Lower Oonah Formation and greywackes of the Crimson Creek Formation. To the south the wedge is in Fault contact with gabbros of the McIvor Hill Complex, The structural aspect of the Sylvester prospect is dominated by three major NW trending faults. The geology of the Sylvester prospect is given in (Fig. 1.4).

J. Crossing of R.G.C Exploration Pty Ltd compiled the geology of the Sylvester prospect into a 1:5000 scale map (Fig. 1.4). Data on the stratigraphy in outcrop compiled by Crossing (1989-1992) is presented in this Chapter, along with information on the stratigraphy acquired through logging of drill core.

3.2 STRATIGRAPHY

3.2.1 Oonah Formation

The Oonah Formation consists of two distinct successions, a Lower Oonah Succession (Po) and an Upper Oonah Succession (Pou) (Brown, 1986). The lower succession is occurs predominantly in the north western part of the Sylvester prospect where it outcrops as thinly bedded sequences of fine-grained micaceous sandstone and siltstone, and medium-grained massive quartzitic sandstones interbedded with minor siltstone and mudstone. In hand specimen, the thinly bedded parts of the sequence the sand-grade units form 60 - 80mm thick sequences of 2 - 4mm thick beds separated by laminae of mudstone. The medium-grained sandstone sequence is composed of 50 - 100 mm thick beds of sandstone separated by 5 mm beds of siltstone and mudstone.

The upper succession consists of similar lithology's as seen in the basal portions, with the exception of an increase in laminated sandstones, siltstones sequences (Post), as well as the inclusion of grey dolomitic and calcareous sequences interbedded with black carbonaceous shale units (Pocs), and vesicular pillow lavas, pyroclastics and breccias (Poms). The dolomitic and carbonaceous shale units occur predominantly in the wedge of Oonah Formation situated between the Balstrup and Tenth Legion Faults.

In drill core, the laminated sandstones - siltstones sequence consists of 10 to 50 mm thick beds of alternating grey siltstone, interbedded with sand-grade units varying between 50 to 100mm and 1 to 5 mm laminae of black mudstone (Plate 3.1). Sedimentary structures are rarely observed, as the majority of the thinly bedded to laminated siltstones and sandstones show

strong overprinting by later deformational events, which has resulted in the disruption and contortion of beds (Plate 3.1). In places, however, what appears as slumping and soft sediment deformation has been preserved.

In thin section, the coarse-silt to fine-sand size layers are well sorted with a continuous framework, and consist of up to 60% clastic quartz grains, 20% opaque minerals, zircon, rutile and accessory tourmaline, and only minor muscovite and siltstone grains. The grains are typically sub-rounded and of medium sphericity, with an average size of 0.05-0.2 mm. The matrix, constituting 10-15%, is predominantly quartz, sericite and minor chlorite. Although the quartz grains show undulose extinction in part, they exhibit an orientation sub-parallel with muscovite and sericite which are aligned parallel to bedding, suggesting that the orientation is a depositional feature.

The dark mudstone laminae consist of fine-grained (0.015 mm) clastic quartz grains in a matrix supported framework, where the matrix is highly carbonaceous and clay rich. Muscovite and the opaque minerals present in the sand and silt size layers are absent. Small scale cross bedding and ripple marks are commonly observed in these bands.

The carbonaceous shale units are typically massive, strongly graphitic, occasionally pyritic (up to 5%), and vary in thickness from less than ten centimetres to over 50 metres (in drill core) (Plate 3.2). In a number of drill holes (eg SY005) the carbonaceous shale units commonly show a transition into massive carbonate units. It is these carbonate units that host the skarn and sulphide mineralisation.

The carbonate units are predominantly beds of grey dolomite (Plate 3.2), and vary in drill core thickness from 50 cm's up to 300m (eg SY005). The units are

typically interbedded with minor shale and siltstone layers. The dolomite is fine-grained and consists exclusively of crystalline dolomite with minor interstitial quartz. Irregular occurrences of magnesite, siderite and ferro-dolomite, and strong talcose overprinting are observed in places. These later features were most probably developed during recrystallisation related to granite emplacement and /or mineralisation, as will be discussed in Chapter 4.

The occurrence of slump structures in the laminated siltstone and sandstones sequences, and the occurrence of gypsum in carbonates (Anderson, 1986), indicate deposition in a shallow water, possibly sabkha-type, environment (Crossing, 1991).

3.2.2 Crimson Creek Formation

The Crimson Creek Formation forms a fault-sided Y-shaped outcrop stretching from the old Sylvester mine to Argent Flats (Fig. 1.4). It consists of grey to grey-green lithic greywacke-sandstones and siltstones, red-brown greywackes interbedded with green to brown laminated mudstones, and rare cherts and carbonates. The volcaniclastic/tuffaceous wacke units are rarely observed in the mapping area (Crossing, 1991).

In drill core, the individual lithic greywacke-sandstone, siltstone and mudstone units range in thickness from 1 to 5 cm. The greywacke beds usually have a sharp irregular contact with the underlying beds, and commonly display scour marks and ripple marks. Grading and cross bedding is common with in the sandstone, as are parallel-laminations of sandstone and mudstone. The interbedded mudstone units are frequently thinly bedded to silt-laminated, passing into, brown, more massive non laminated mudstone

beds. The overall sedimentary features of these units are indicative of Bouma sequences B, C and D of a turbidity current (Fig. 3.1).

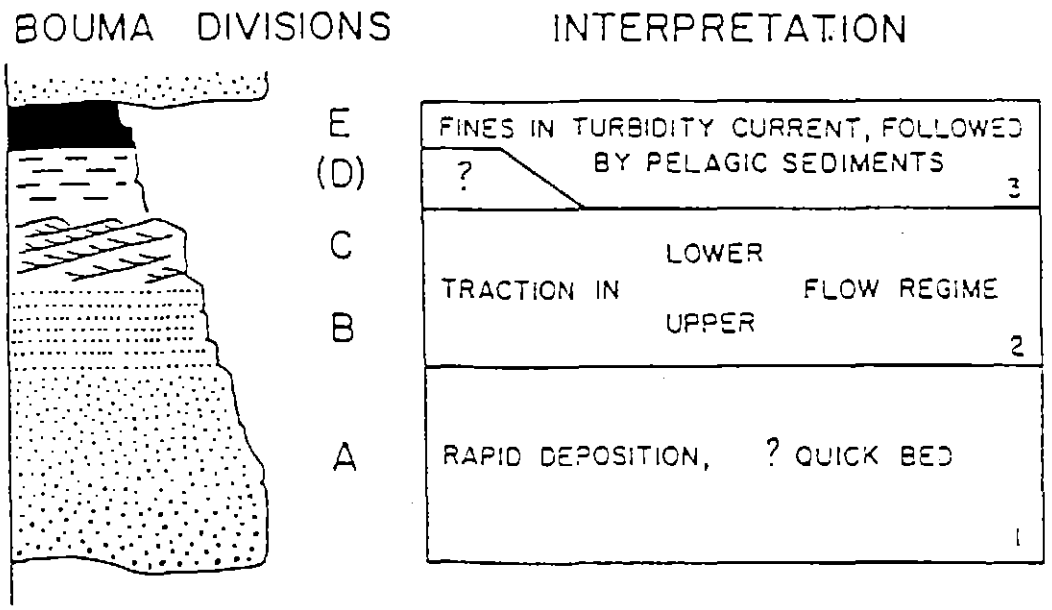

Figure 3.1 The five divisions of the Bouma model for turbidites: A-graded or massive sandstone; B-parallel laminated sandstone; C-ripple cross-laminated fine sandstone; D-faint parallel laminations of silt and mud; and E-pelitic division (after Walker, 1979b).

In thin section, the sand to fine silt size rocks are immature, poorly sorted, and consist of sub angular to angular fragments of polycrystalline quartz, K-feldspar and chlorite-sericite altered fragments of clinopyroxene and orthopyroxene in a finer grained clay matrix that forms 30% of the rock. Accessory fragments include chert, embayed quartz, carbonate, chlorite and magnetite.

The clay-rich rocks are extremely fine grained, and the composition cannot be determined microscopically. The red to brown colouration of the mudstones represent iron oxidation-reduction colours, possibly due to limonite and haematite. The mudstones also display irregular colour variations through alteration. The extensive development of chlorite, epidote, sericite, and calcite suggests that pervasive hydrothermal alteration has affected the rock.

3.2.2.1 Cataclasite

A significant feature of the Upper Oonah Formation is the occurrence of broad zones (<20m) of cataclasite. The cataclasite consists of chaotic, unsorted angular to lenticular clasts of varying size of the Upper Oonah Formation in a black to grey fine carbonaceous matrix (Plate 3.3). The cataclasite commonly exhibits gradational contacts with highly strained graphitic shales and phylittic siltstones. Cataclasite occurs throughout the Upper Oonah Formation and ubiquitous along the contact between the Upper Oonah Formation and the Crimson Creek Formation, where they include clasts derived from the Crimson Creek Formation. The zones of cataclasite are not restricted to regions of major faults, although they are ubiquitous in the Balstrup and Tenth Legion Fault zones.

3.2.3 McIvor Hill Complex

A gabbroic rock, inferred to be part of the McIvor Hill Complex, is observed in drill core SY001. The rock is massive and highly altered. In thin section, the rock is composed of approximately 60 modal % of clinopyroxene (2-5 mm), 40 % stubby grains of plagioclase, and magnetite. The pyroxenes minerals have been pseudomorphed by tremolite-actinolite, epidote, and occasionally chlorite. The plagioclase crystals are altered to turbid masses of saussuritite. The magnetite occurs as large skeletal crystals displaying triangular exsolution patterns.

1

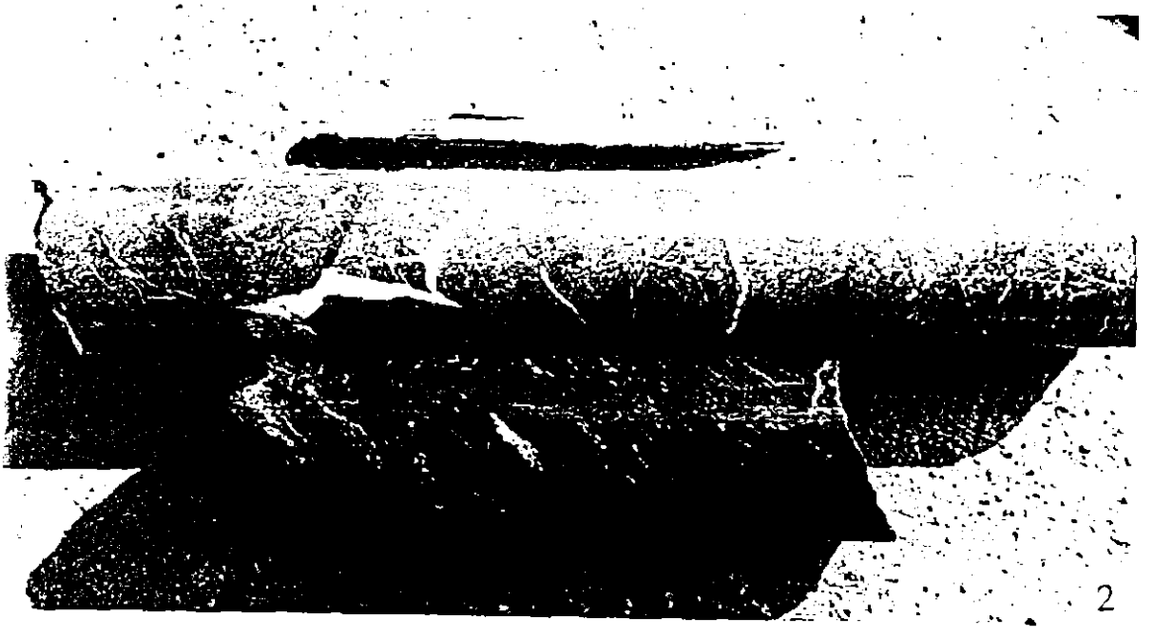

2

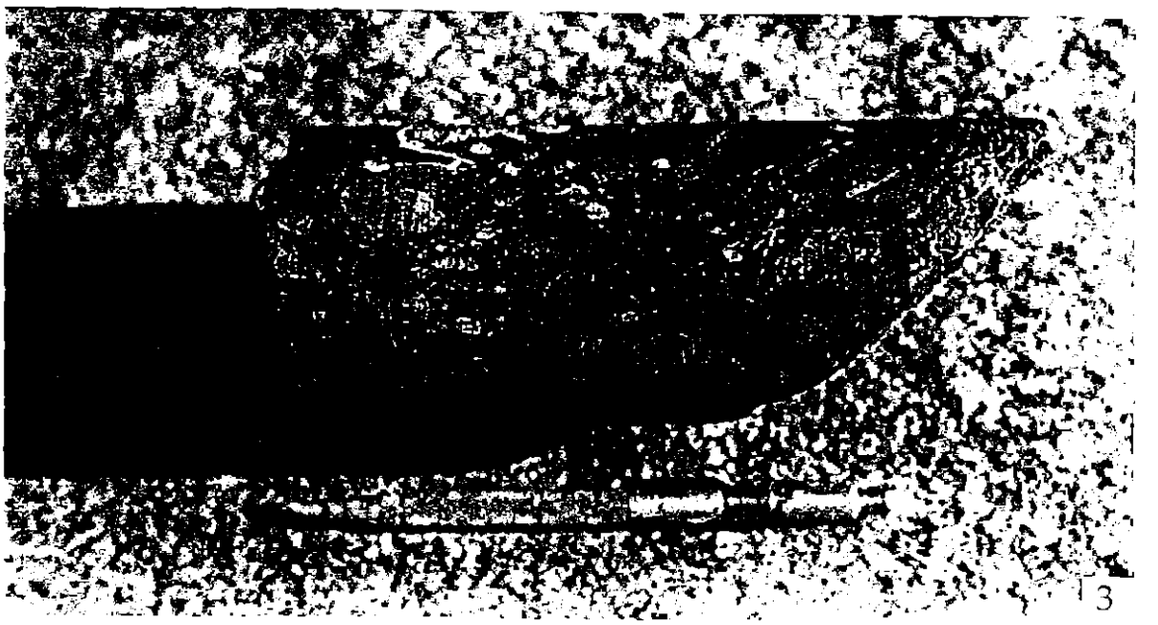

3

The pervasive tremolite-actinolite alteration is regarded as typical of "ocean-floor metamorphism", where pyroxenes are altered to amphiboles via convection of seawater during early stages of burial (A.J Crawford, pers comm). However, similar fibrous amphiboles has been observed in hornfelsic sediments adjacent to the Heemskirk Granite (Olubus, 1989), indicating possible formation of the amphiboles after the emplacement of the granite.

3.2.4 Mafic intrusives

A number of small mafic intrusive dyke bodies are observed in strongly deformed Crimson Creek Formation in the hangingwall of the Balstrup Fault (SY016 and SY012). The dykes display a distinct chilled margin and have produced hornfelsing of the adjacent brecciated sediments.

In thin section, the dykes are porphyritic, consisting of sanidine-feldspar, and minor clinopyroxene phenocrysts. The phenocrysts are dominantly altered to chlorite, actinolite-tremolite and/or serpentine. The groundmass is highly altered, permeated by secondary quartz, serpentine and carbonate. The exact origin of these dykes is unknown, although intrusive dykes have been observed in several mines of the Zeehan field (Twelvetrees and Ward, 1910).

3.3 STRUCTURE

3.3.1 Folding

Stereographic analysis by Crossing (1991) of over 400 bedding readings from the Oonah Formation taken throughout the study area indicate the presence

of two distinct spatial domains. The first domain corresponds to the upper and lower successions of the Oonah Formation that outcrop north of the Balstrup Fault (Fig. 1.4). The second domain corresponds to the upper successions of the Oonah Formation that form the wedge shape outcrop between the Balstrup and Tenth Legion Faults.

The stereographic projections of bedding readings in domain 1 indicate that the rocks are associated with folding plunging 30 degrees toward 100 degrees AMG (Fig. 3.2). In the field, these folds correspond to series of major ESE plunging fold axes with axial planes inclined northward. These folds typically have wavelengths of 1 to 1.5 km (Crossing, 1992). Measurements of fold axes of small scale folds in the limbs of these folds show two sets of folds, one conformable with the abovementioned folds, and a second set with average fold axes plunge of 54 degrees toward 041 AMG (Fig 3.3) (Crossing, 1991).

The dominant ESE-WNW fold axis trend of folds observed in domain 1 corresponds to the early phase of folding characteristic of the mid-Devonian Tabberabberan Orogeny.

Stereographic analysis by Crossing (1991) of bedding readings of the Upper Oonah Formation in domain 2 show a wide spread of attitudes, with an average dip of 16 degrees SE (Fig. 3.4). No consistent pattern of folding is indicated by this data, although the data is consistent with open fold axes plunging at 20 degrees 050 AMG, and 40 degrees 090 AMG. This data may represent folds produced during the early phase of the mid Devonian Orogeny that have been subsequently deformed in response to thrust and wrench movements on the Balstrup and Tenth Legion Faults (ref. 3.3.3).

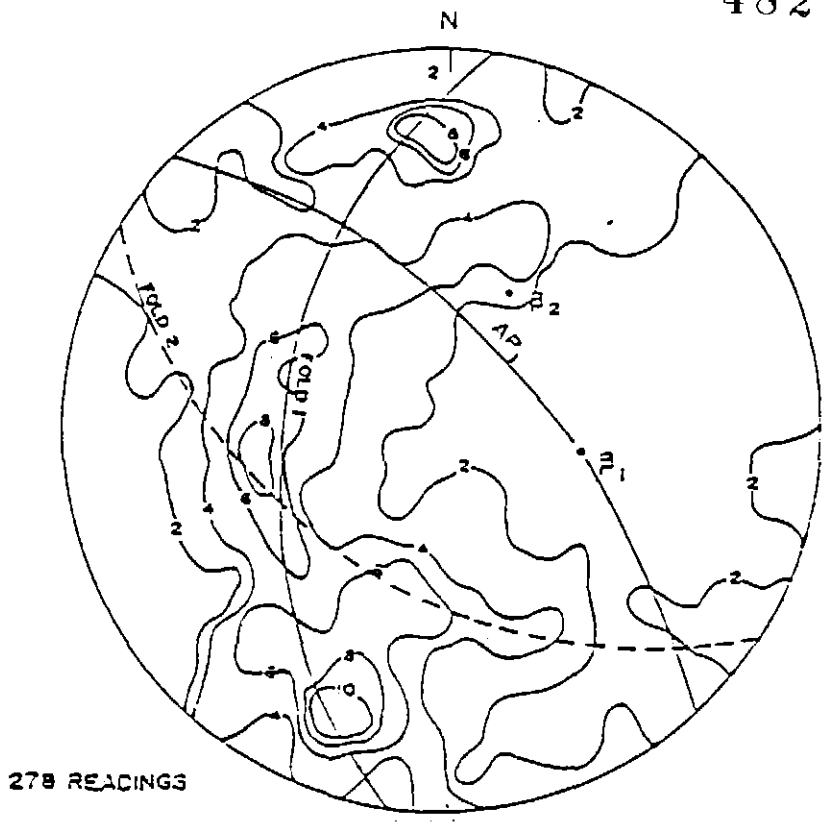

Figure 3.2 Domain 1: Poles to bedding. Fold 1; average fold axes ($ß_1$) 46 097° AMG, Axial Plane (AP) 60 134. Fold 2; average fold axes ($ß_2$) 44 023° AMG, not well developed. (after Crossing, 1991).

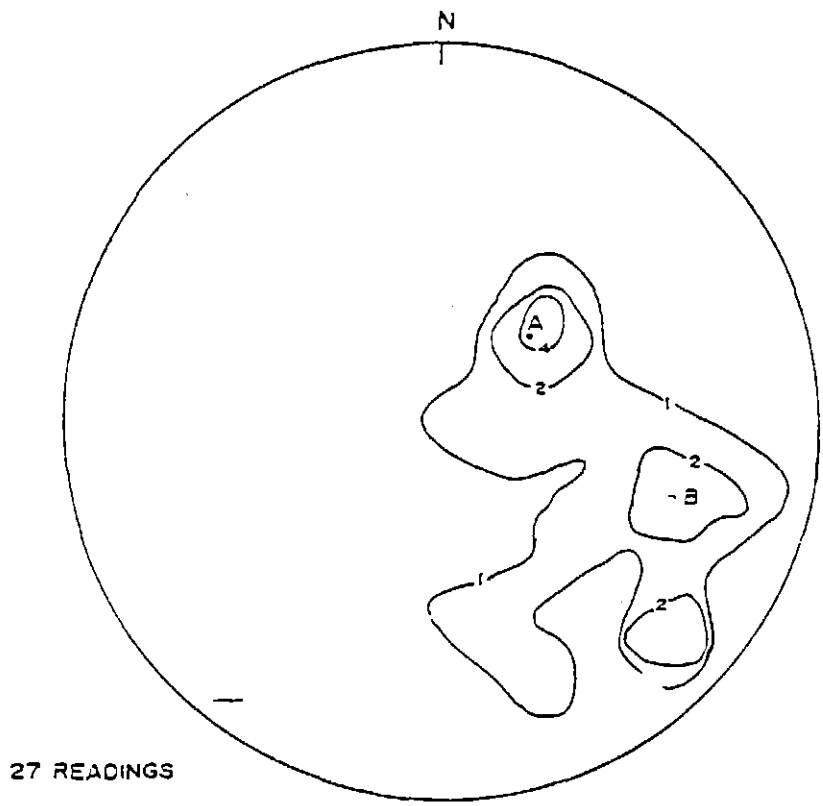

Figure 3.3 Domain 1: Measurement of fold axes plunge. Average fold axes

A 54 041° AMG

B 22 108° AMG

Structural measurements of orientated core indicate that the carbonate beds of the Upper Oonah Formation in domain 2 steepen as they approach the footwall of the Balstrup Fault zone, in a manner similar to the steeping of Carbonate beds in the footwall of the Federal-Bassett Fault at the Renison Bell Tin (Crossing, 1991).

3.3.2 Cleavage

The dominant cleavage orientation measured in Oonah Formation sediments in both domain 1 and 2 is 90 degrees trending 112 degrees AMG (Fig. 3.5) (Crossing, 1991). The trend of the cleavage is consistent with having developed as an axial plane cleavage to the NW trending fold phase.

Localised development of a strong penetrative cleavage is observed within the siltstone and sandstone successions of the Upper Oonah Formation adjacent to the Balstrup and Tenth Legion Faults. This cleavage inturn develops into a C-S fabric at, and within, the margins of the cataclasite rock (ref 3.1 3) associated with the two faults.

3.3.3 Faulting

The Sylvester prospect is transected by three extensive WNW trending faults; the Sylvester Fault, the Balstrup Fault, and the Tenth Legion Fault (Fig. 1.4). The largest of the three faults, the Tenth Legion Fault, has been mapped in considerable detail in the Sylvester area by Crossing (1991) and Findlay and Brown (1992). It is regarded as a major regional low angle thrust along which sediments of the Upper Oonah Formation have been thrust over rocks of the

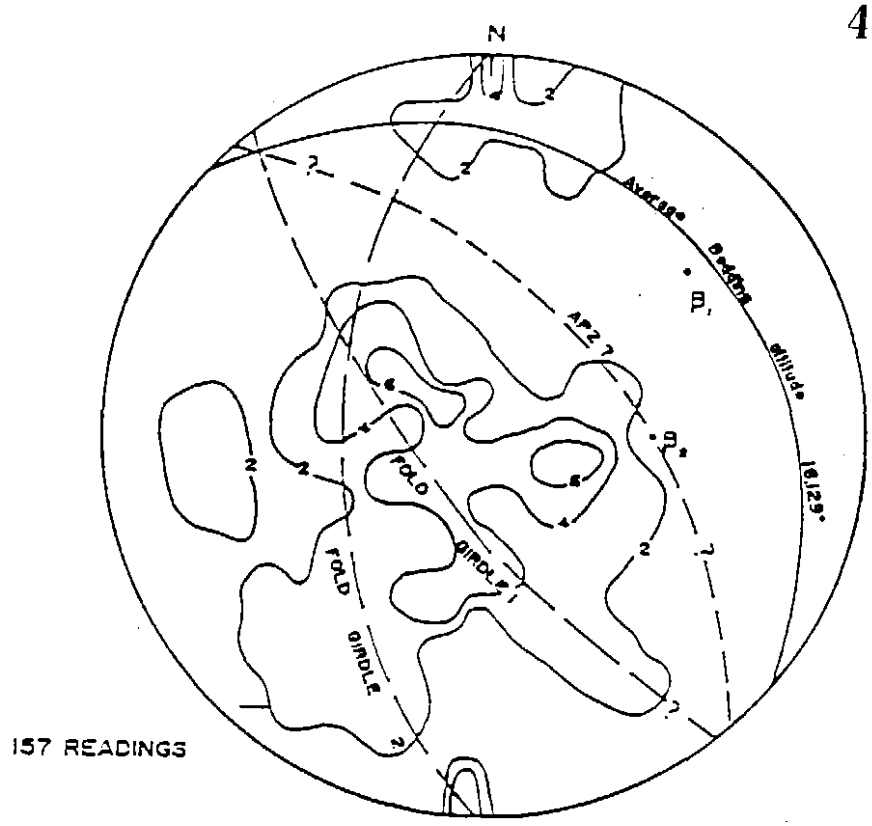

Figure 3.4 Domain 2: Poles to bedding. Average bedding altitude 16 129° ($ß_1$) 20 050° AMG, ($ß_2$) 40 090° AMG. (after Crossing, 1991).

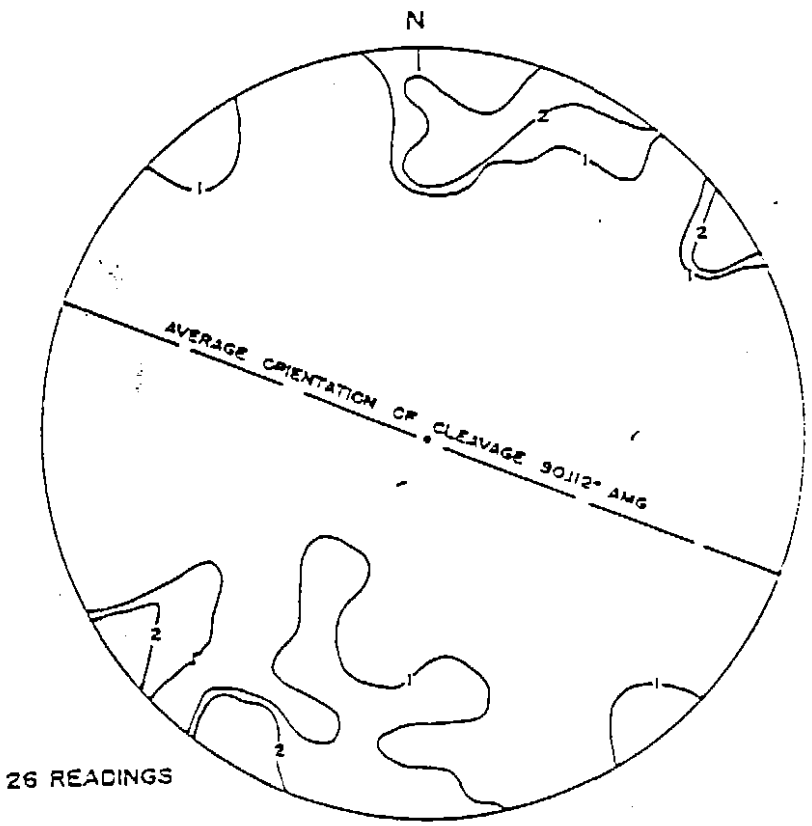

Figur e 3.5 Poles to cleavage. (after Crossing, 1991).

McIvor Hill complex, west of the South Comstock mine, and sediments of the Dundas Group.

The structure is characterised by a dip of about 45 degrees NNE trending 110 degrees AMG in the South Comstock mine area. To the east of the South Comstock area the strike of the structure follows the topographic contours of the land, suggesting a very low angle dip. In the Swansea area (bottom right hand corner of Fig. 1.4) dips of 25 degrees N and 40 degrees SE were observed (Crossing, 1991). The fault trace in this area is strongly convoluted.

The most important structural feature in the Sylvester prospect, with respect to controls on mineralisation is the Balstrup Faults. The fault is a complex, composite structure characterised by multiple discrete fault zones (total fault zone 40 m), marked by the presence of cataclasite (ref. 3.1.2.1), and highly strained, often graphitic, brecciated/ boundinaged sandstones (Crossing, 1992).

The Balstrup Fault is a well defined structure between holes SY003 and SY005, characterised by calcareous, angular breccias, and only minor cataclasite. The average dip of the fault in this area is 70 degrees NNE, striking 118 degrees AMG (Crossing, 1991). West of SY005 the fault splays, producing the West Balstrup Fault which merges with the Tenth Legion Fault in the Kynance area. (Fig. 1.4). The average dip of the West Balstrup Fault is 60 degrees NNE trending 090 degrees AMG (Crossing, 1992).

The movement on the Balstrup Fault is inferred by Crossing (1991) to be oblique-slip, consisting of sinistral and normal displacement (northern block down). However, the movement along the West Balstrup Fault is inferred to have been reverse with no strike-slip component (Crossing, 1991).

Stereographic projection analysis by Crossing (1991) of poles to fault surfaces along the two faults indicate they are a conjugate pair (Fig. 3.6). The principle fault set A relate to surfaces on the Balstrup Fault, set B relate to the surfaces on the West Balstrup Fault. These conjugate sets A and B indicate a principle stress direction (σ_1) for the fault system plunging 45 degrees NW, and having oblique slip displacement (Crossing, 1991) (Fig. 3.6).

The other major WNW trending fault in the Sylvester prospect is the Sylvester Fault. The fault has an average dip of 55 degrees NE and an average trend of 120 degrees AMG. The displacement on the fault is very similar to that for the Balstrup Fault; sinistral and northern block down (Crossing, 1991).

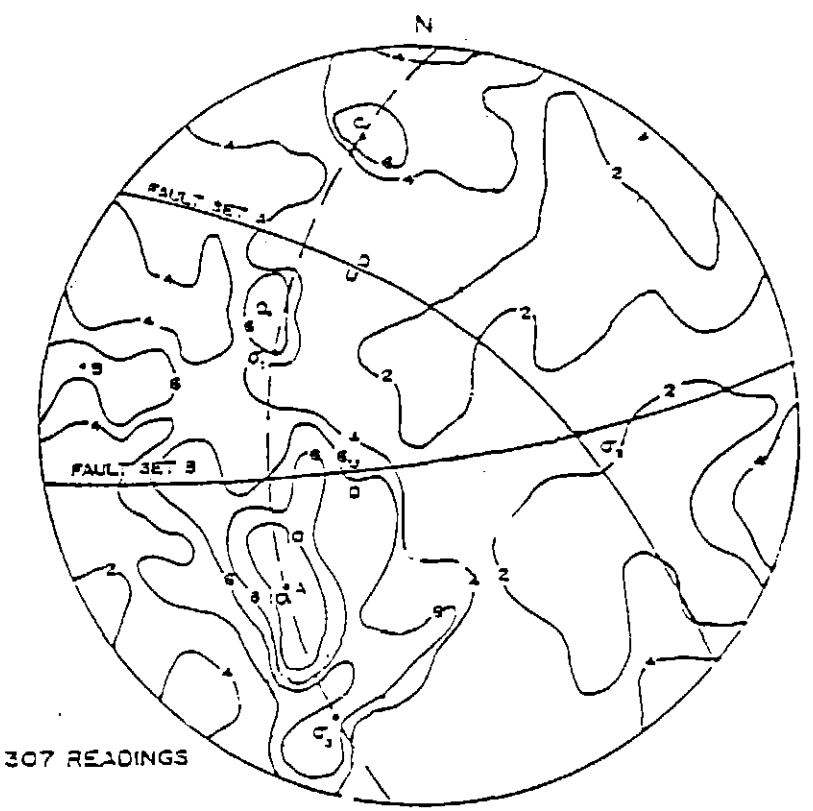

Figure 3.6 Poles to faults-fractures. Fault set A 58 126° AMG (NE)
B 87 260° AMG (S)
σ_1 principal stress direction of conjugates A and B (after Crossing, 1991).

3.3.3.1 Structural history

The composite nature of the Balstrup Faults indicates a complex structural history. The following history is based on the interpretation of Crossing (1992).

(a) Early ductile and brittle deformation producing cataclasite. The cataclasite is only present in the Upper Oonah Formation and along the contact with the Crimson Creek Formation, indicating the earliest deformation event occurred before the mid-Devonian Tabberabberan Orogeny (Crossing, 1992). This also indicates that the Tenth Legion Fault, which is also characterised by cataclasite in its fault zone, may also be a pre mid-Devonian structure.

(b) Main brittle deformation involving oblique-slip displacement. This stage is attributed to the early phase of NE-SW compression associated with the mid-Devonian Tabberabberan Orogeny. This event was also responsible for the formation of the Sylvester Fault.

(c) Minor post-mineralisation displacement as evidenced by fracturing and deformation of sulphide mineralisation (ref, Chapter 5).

CHAPTER FOUR

SKARN PETROLOGY

4.1 INTRODUCTION

Skarn formation in the Sylvester prospect can be divided into three stages or events:

1. A contact metamorphic stage which produced hornfelsing of the sandstone and siltstone units of the Upper Oonah Formation and extensive recrystallisation of carbonates of the Upper Oonah Formation.
2. A early metasomatic stage that formed localised areas of fine-grained pyroxene skarn and minor garnet-pyroxene skarn in Upper Oonah Formation carbonate units.
3. A late metasomatic stage that formed extensive areas of serpentine-magnetite skarn and brucite-serpentine-magnetite skarn in the Upper Oonah Formation carbonate units.

This chapter describes the mineralogy and textures of the three skarn formation stages present in the Sylvester prospect, as inferred from the distribution of skarn types and specific textural age relations. The occurrence of skarn types observed in the diamond drill core of the prospect is shown in Fig. 4.1 (map pocket).

4.2 CONTACT METAMORPHIC STAGE

Contact metamorphism of Upper Oonah Formation carbonate resulted in widespread recrystallisation and patchy bleaching of the dolomitic carbonate units to dolomitic marble and minor limestone units to bleached coarse-grained marble. The dolomitic marble is typically pale- or dark- grey in colour, fine- to medium-grained, consisting of 80 to 90% dolomite, 5 to 10% calcite, and >5% magnesite (Plate 4.4). Despite the presence of minor amounts of original quartz in the marble, no wollastonite is formed.

Metamorphism of the Oonah Formation siltstone and sandstone lithology's resulted in the formation of massive brown biotite hornfels. The occurrence of biotite hornfels in the study area is restricted to two intersections underlying early stage skarn zones in diamond drill core from holes SY014 and SY010 (Fig. 4.1). In drill core, the hornfels is mauvish brown in colour, fine- to medium grained, with bedding defined by interbeds of finer-grained, darker brown green laminae. The main constituents of the hornfels are a quartz, quartzo-feldspathic matrix, biotite, which occurs as abundant fine-grained flakes throughout the matrix. Small amounts (<5%) of irregularly distributed patches of sericite and chlorite and minor amounts of disseminated pyrrhotite and ilmenite are also present (Plate 4.5).

Numerous thin quartz ± epidote and amphibole veinlets crosscut the hornfels, along these veinlets the hornfels becomes grey over a few millimetres in width, owing to the distruction of biotite (Plate 4.5). This veining becomes more common as the overlying skarn is approached.

Separating the biotite hornfels from the overlying skarn is a zone of lime green hornfels (Plate 4.6). The main constituent of the hornfels are quartz, tremolite and lesser plagioclase. The tremolite occurs as fine-grained flakes intergrown in the matrix in a manner similar to that of biotite in the biotite hornfels.

4.3 EARLY METASOMATIC STAGE

Early metasomatic stage skarn formation is observed only in drill core from hole SY014 (Fig. 4.1). The skarn is situated in a unit of Upper Oonah Formation dolomitic marble, between underlying hornfelsed Upper Oonah Formation and overlying Upper Oonah Formation sandstone (Fig. 4.2). The skarn intersection can be divided into three distinct skarns; a garnet-clinopyroxene skarn, a clinopyroxene skarn and a tremolite-talc-calcite skarn.

Garnet-clinopyroxene skarn: The garnet-clinopyroxene skarn is less well developed in comparison to the clinopyroxene skarn and tremolite-talc-calcite skarn. In drill core it is less than 1 m in total thickness, and bound on both sides by hornfels (Fig. 4.2). The skarn is a massive, fine-grained greyish-brown rock with scattered small dark green and white patches. Garnet is present in highly variable amounts, although overall pyroxene is always subordinate. Accessory minerals include interstitial calcite and quartz.

Two types of garnet are recognised in thin section. One is yellow in colour and optically isotropic, its texture varies from fine-grained anhedral aggregates to coarse-grained sub- to euhedra. The second garnet is coarser grained, euhedral, and exhibits weak anisotropic zoning sub parallel to crystal faces (Plate 4.7). The anisotropic garnet tends to occur as rims

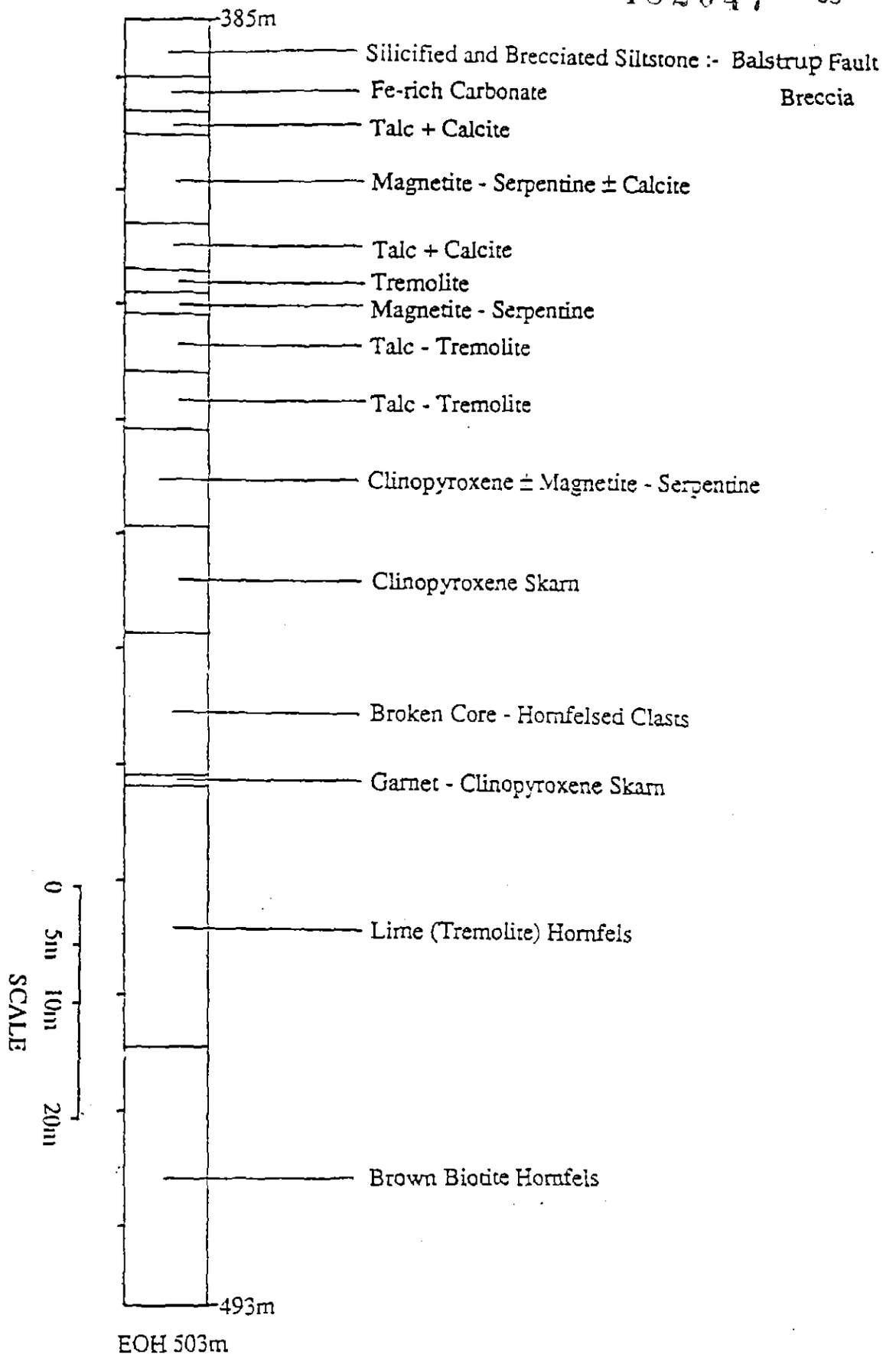

Figure 4.2 Schematic diagram showing the distribution of skarn in drill hole SY014.

surrounding aggregates of isotropic garnet, in a texture that seems to indicate the outer anisotropic zones formed by recrystallisation of the fine-grained isotropic garnet. Clinopyroxene is intimately associated with the isotropic garnet, occurring as colourless, coarse (<1mm), an- to subhedral grains intergrown with isotropic garnet. The pyroxene commonly displays textures that indicate the replacement of isotropic garnet by pyroxene (Plate 4.8). Conversely, pyroxene inclusions in garnet are extremely rare.

Clinopyroxene skarn: The clinopyroxene skarn is the largest of the two calc-silicate skarn zones (Fig.4.2). It is typically white to cream in colour, although commonly pale green (Plate 4.9). The skarn predominantly consists of fine-grained clinopyroxene with only trace amounts of calcite. Garnet is totally absent from the skarn. The texture of the pyroxene ranges from relatively fine-grained (< 0.1mm) subhedral grains, to polycrystalline aggregates of coarse-grained euhedral grains (Plate 4.10). In the upper portions of the skarn, toward the contact with the tremolite zone, the texture of the clinopyroxene is marked by large (up to 2mm), coarse-grained radiating and bladed grains (Plate 4.11). Calcite occurs as minor intergrowths with fine-grained pyroxene.

Tremolite-talc-calcite skarn: Tremolite-talc-calcite skarn occurs between the clinopyroxene skarn and sandstone of the Upper Oonah Formation (Fig. 4.2). The tremolite-talc-calcite skarn is composed of two sections; one that consists of massive tremolite, and a second that is composed of talc, calcite and chlorite. The tremolite section is white to pale green in colour, and is contact with the clinopyroxene skarn. Because the clinopyroxene skarn and the tremolite section are very similar in appearance, and have been extensively overprinted by magnetite-serpentine skarn developed in the late metasomatic stage, it is difficult to identify a boundary between them. The tremolite portion is composed mainly of tremolite accompanied by small amounts of

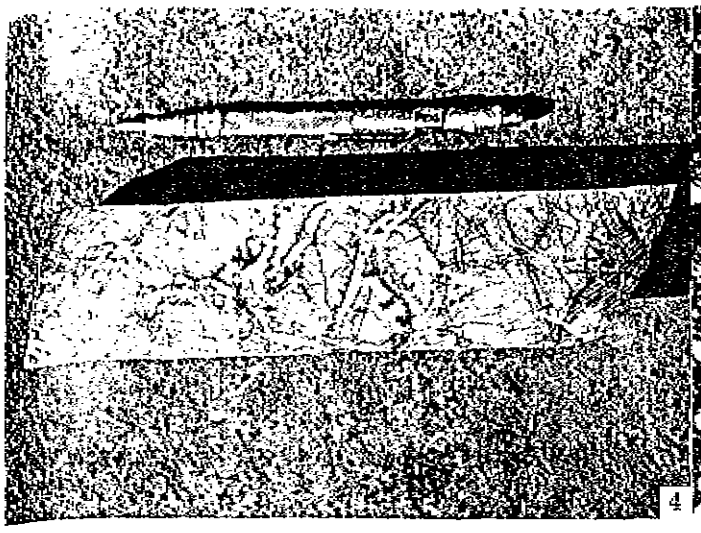

4

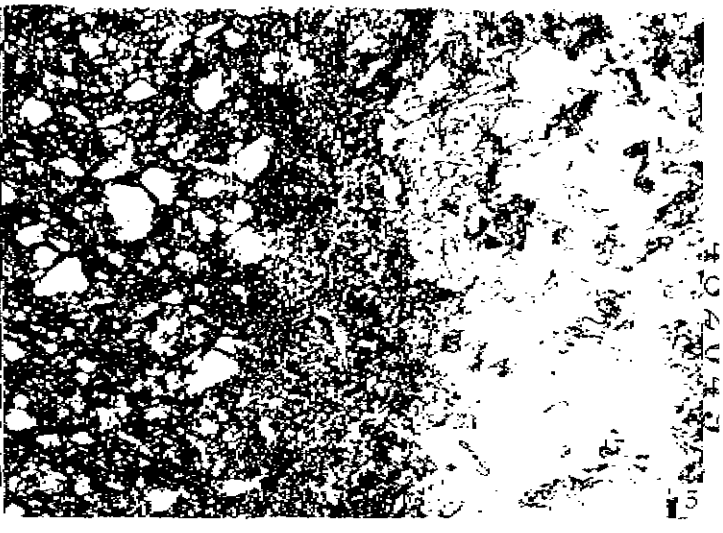

5

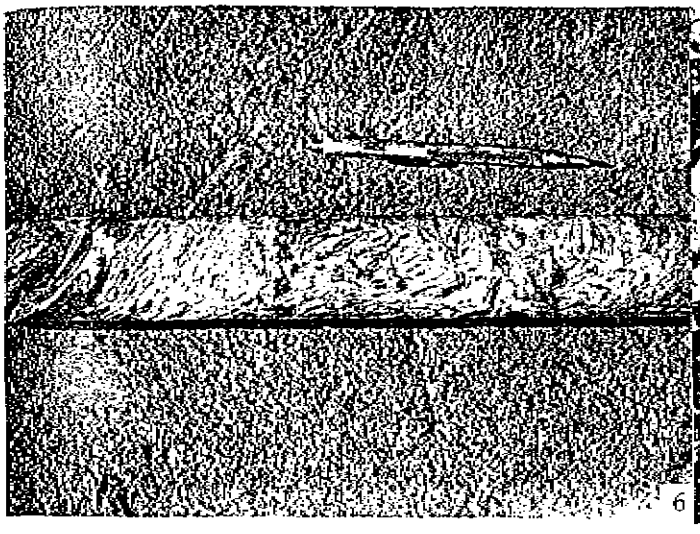

6

7

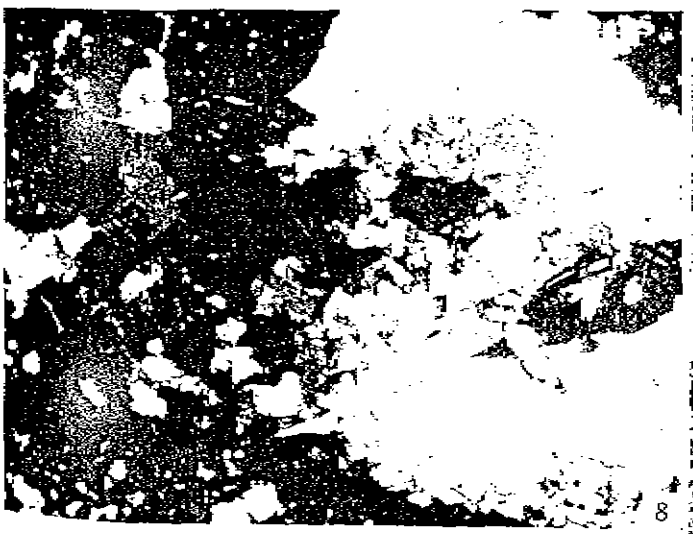

8

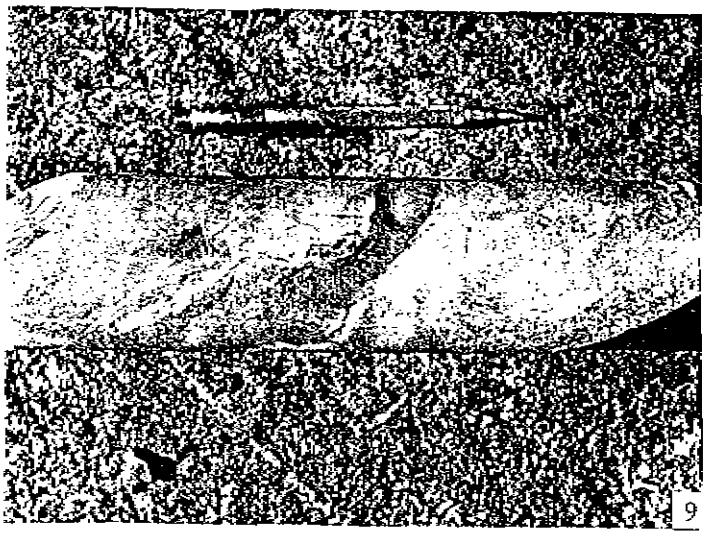

9

10

11

calcite and talc. Sphalerite and pyrrhotite occurs rarely. In thin section the tremolite occurs as randomly orientated, aggregates of an- to subhedral bladed crystals that range in size from very fine-grained (<0.1mm) up to 2mm.

The talc, calcite and chlorite section is characterised by complex textural patterns. Typically the talc occurs as irregular patches that are intergrown with, and occasionally rimmed by calcite and less rarely chlorite (Plate 4.12). The contact between talc-calcite section and the tremolite section somewhat obscured by the development of magnetite-serpentine skarn. In thin section the talc is fine-grained commonly containing small (<0.2mm) aggregates of anhedral chlorite grains (Plate 4.13). Calcite occurs as coarse, euhedral grains.

4.3.1 Mineral Compositions

Mineral analyses of the main calc-silicate skarn minerals, clinopyroxene, garnet, tremolite were done at the University of Tasmania on a CAMECA 50 electron microprobe. Operating conditions were: an accelerating voltage of 15Kv, a beam current of 20 $x10^{-9}$ amps, and a beam area of 5 by 3µm. The recalculation of ferrous and ferric iron was preformed using the MinTabv1.1 mineral recalulation and tabulation computer program by G Carroll (1990).

The individual analyses of each mineral are listed in Appendix A and B.

Garnet: Garnets (12 analyses) in the Sylvester prospect are predominantly andraditic in composition (Appendix A). Expressed as the end members andradite (An: $Ca_3(Fe^{+3},Ti)_2Si_3O_{12}$), calderite (Ca: $Mn_3(Fe^{+3})_2Si_3O_{12}$), hydrogrossular (Hy: $(Ca_3\ Al_2Si_3O_8\ (SiO_4)_{1-m}(OH)_{4m}$, and pyrope (Py:

$Mg_3Al_2Si_3O_{12}$), garnets have mol per-cent end member compositions in the ranges of An_{73-99}, $Ca_{0.5-8}$, Hy_{0-24}, Py_{0-5}.

Compositional zoning is evident in the garnets, particularly in those garnets that are optically anisotropic. An electron microprobe traverse across one garnet, from an optically isotropic core to anisotropic rim is shown in Figure 4.3. The traverse illustrates a general fluctuation in the elements iron, manganese, aluminium, but most notable is the increase in magnesium. Magnesium progressively increases from zero in the isotropic garnet up to ~1 wt% in the outer zones of the anisotropic garnet. This increase in Mg in the outer zones of the anisotropic garnets may indicate possible contemporaneous formation with the relatively Mg-rich clinopyroxenes that, like the anisotropic garnets, in thin section appear to replace the isotropic garnets.

Pyroxenes: Clinopyroxenes (25 analyses) are magnesium rich and manganese poor (Appendix B). Expressed as the end members diopside (Di: $CaMgSi_2O_6$), hedenbergite (Hd: $CaFeSi_2O_6$), johannsenite (Jo: $CaMnSi_2O_6$), pyroxenes have end-member compositions in the ranges Di_{45-99}, Hd_{1-52}, $Jo_{0.1-5}$. There are two compositional populations; one diopsidic and the other more hedenbergitic, both populations have only minor components of johennsenite. Pyroxenes of the diopsidic group occur exclusively in the clinopyroxene skarn, whereas those of the second group are prevalent in the garnet-clinopyroxene skarn (Fig. 4.4).

Amphiboles: The composition of amphiboles analysed (4 analyses) occur within the compositional ranges of tremolite, based on the classification of Leake (1978) (Table 4.1). The $Mg^{2+}/(Mg^{2+}+Fe^{2+})$ values of the 4 amphiboles analysed are all 0.93 (Table 4.1).

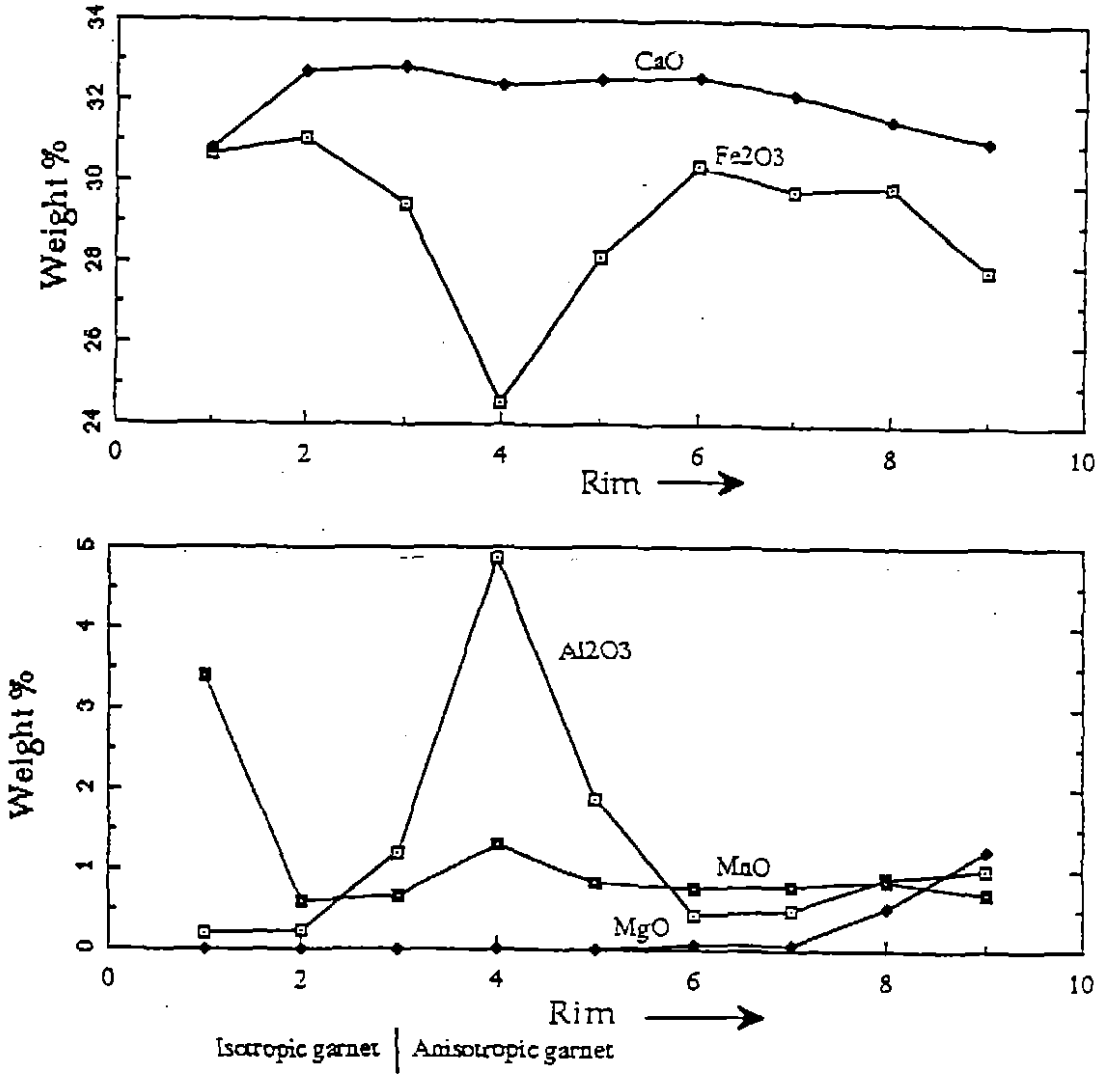

Figure 4.3 Compositional zoning from core to rim across a garnet crystal (T35571 (ring 2); Appendix A) from the garnet-clinopyroxene skarn.

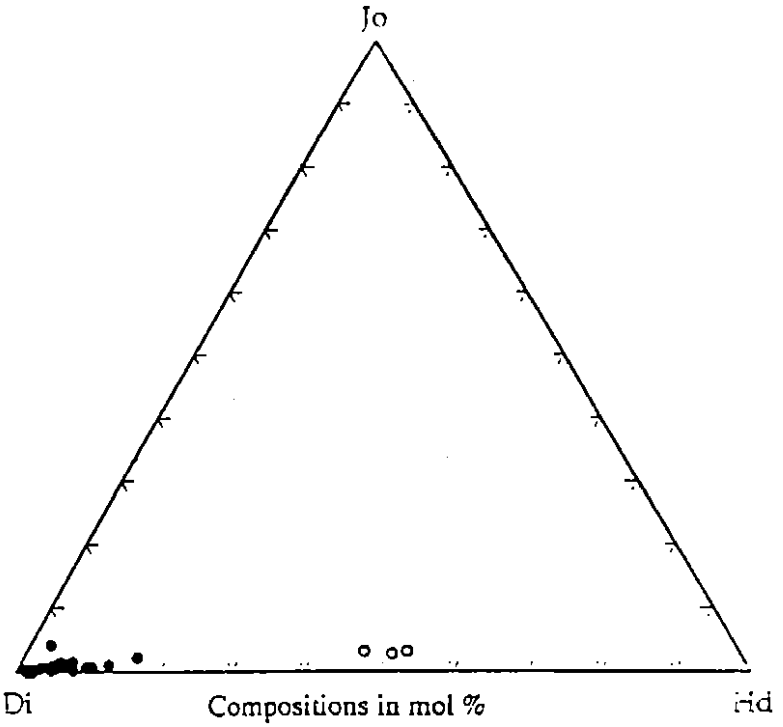

Figure 4.4 Composition of clinopyroxenes from the clinopyroxene and garnet-clinopyroxene skarn zones. Solid circles- clinopyroxene skarn. Open circles- garnet-clinopyroxene skarn. Di= diopside, Jo= johannsenite, Hd= hedenbergite.

Sample No	T3557 R1	T3557 R1 A2	T3557 R3	T3557 R4
SiO2	56.913	57.314	57.047	56.787
TiO2	0.000	0.000	0.000	0.000
AL2O3	0.072	0.051	0.036	0.043
Cr2O3	0.000	0.000	0.013	0.000
MgO	22.085	22.687	22.234	22.681
CaO	13.550	13.417	13.291	12.517
MnO	0.060	0.162	0.142	0.150
FeO	3.263	2.482	3.391	2.852
Total	96.254	96.671	96.542	95.375
CATIONS				
Si	7.961	7.964	7.965	7.994
Ti	0.000	0.000	0.000	0.000
Al	0.012	0.008	0.006	0.006
Fe3+	0.048	0.028	0.046	0.000
Fe2+	0.334	0.260	0.350	0.358
Mg	4.607	4.698	4.627	4.758
Ca	2.031	2.018	1.988	1.888
Mn	0.007	0.019	0.017	0.018
Mg/Mg+Fe2+	0.093	0.930	0.093	0.093

Table 4.1 Electron microprobe analyses of tremolite from the tremolite-talc-calcite skarn.

4.4 LATE (HYDROUS) METASOMATIC STAGE

The late metasomatic stage produced the largest extent of skarn within the Sylvester prospect. The late period of metasomatic alteration is most evident in the massive dolomitic marble, where large areas were converted to massive magnetite-serpentine skarn. Late metasomatic alteration in the dolomite can be divided into two categories: (1) massive serpentine-magnetite skarn; and, (2) carbonate-serpentine-magnetite± brucite skarn. Both types of skarn are located in Upper Oonah Formation dolomite in the footwall of the Balstrup Fault zone, over a strike distance of approximately 1000 metres (Fig. 4.1).

Massive serpentine-magnetite skarn: Massive serpentine-magnetite skarn constitutes the larger of the two skarn zones. The skarn is intersected in four drill holes; SY014, SY010, SY005 and SY009. In SY014 and SY010 the skarn is located in the imediate vicinity of the Balstrup Fault zone (e.g. Fig. 4.2). In holes SY005 and SY009, where the skarn is more extensively developed, it is located further into dolomitic marble, at a distance from the fault zone (Fig. 4.5-4.6).

The skarn is generally yellow to dark green in colour, consisting mainly of serpentine, magnetite and calcite in highly variable proportions, and only minor amounts of talc. The typical texture of the skarn varies from massive serpentine (Plate 4.14), to mottled and banded serpentine and magnetite (Plate 4.15-4.16), to massive magnetite (Plate 4.17).

Serpentine is the dominant phase in the skarn. In thin section serpentine is rarely observed as plates with crystalline contours. More often it forms fine-grained fibrous aggregates, occasional intergrown with talc, very fine-grained

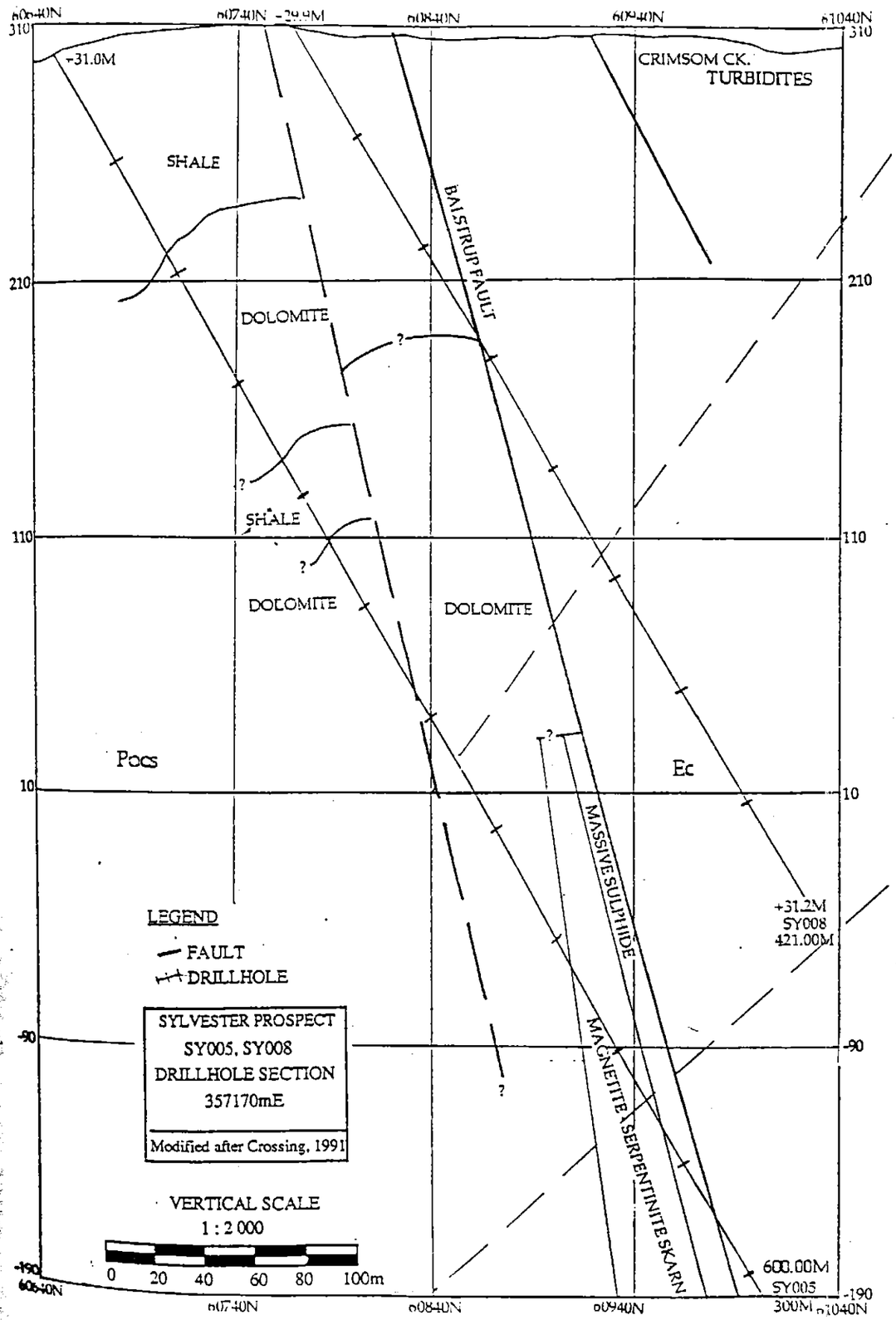

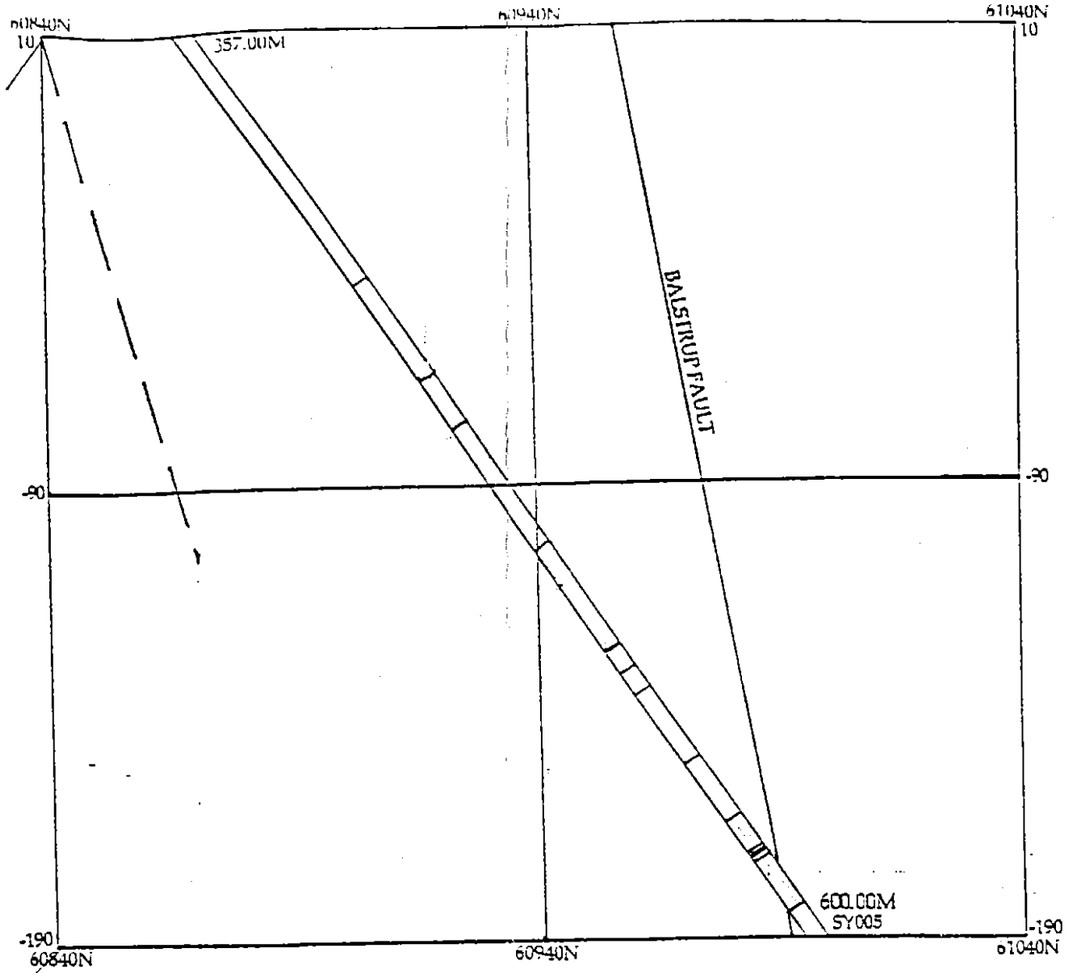

VERTICAL SCALE
1 : 1000
0 10 20 30 40 50m

5 cm

KEY

- Dolomite
- Fault Rock
- Massive Sulphide
- Carbonate-serpentine-magnetite-brucite skarn
- Massive serpentine-magnetite skarn

Figure 4.5 Drillhole sections of SY005 and SY008

Insert - Distribution of late stage skarn assemblages

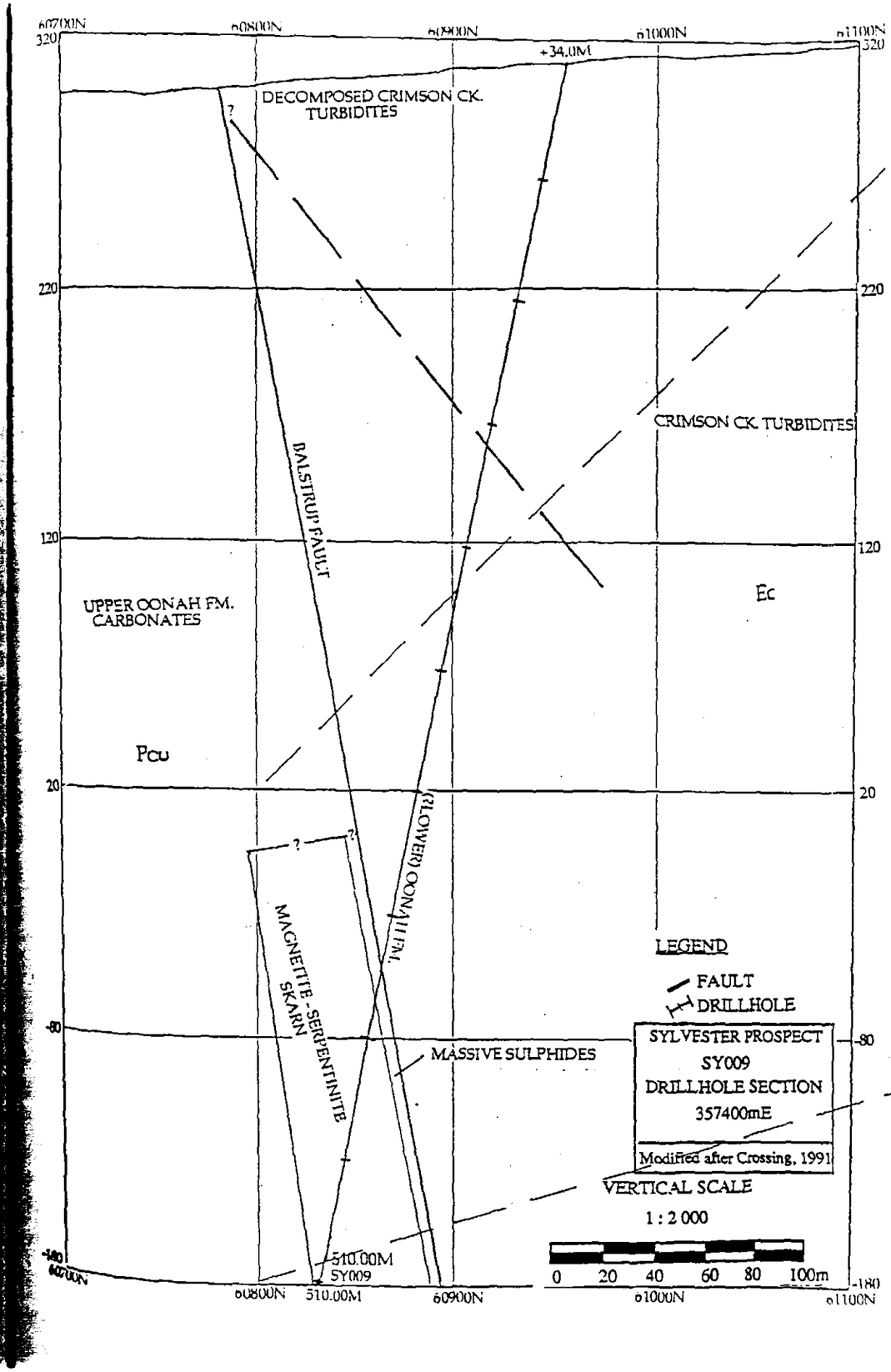

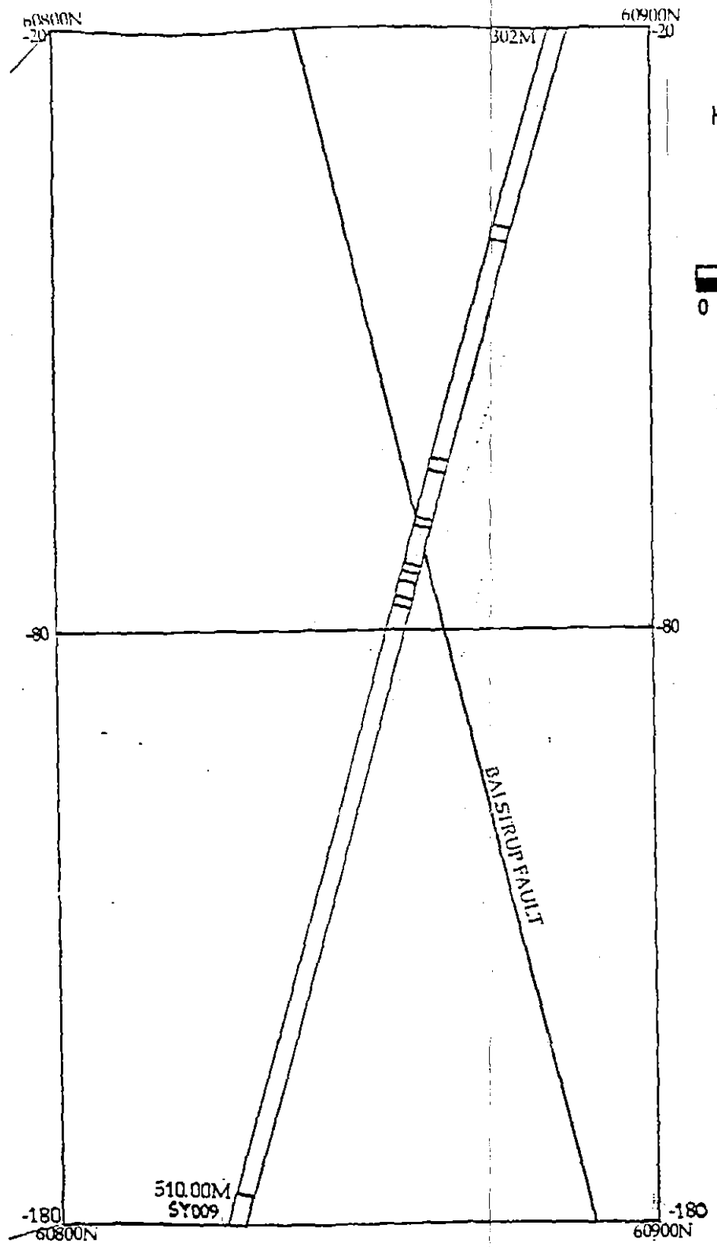

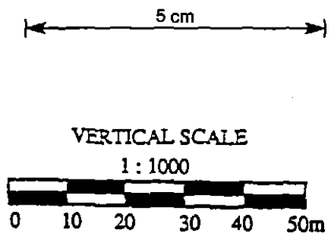

Figure 4.6 Drillhole sections of SY009

Insert - Distribution of late stage skarn assemblages.

(<<0.1mm) serpentine that gives the appearance of being isotropic under cross polarised light (Plate 4.19), and less commonly as serpentine pseudomorphs of euhedral dolomite crystals (Plate 4.18). Magnetite typically occurs as patches of coarse-grained, hexagonal crystals (Plate. 4.20), or as fine-grained, subhedral to anhedral grains when in massive serpentine. The latter texture seems to indicate that the serpentine is replacing the magnetite (Plate. 4.21).

Three additional phases are present in the massive serpentine-magnetite skarn, these are cassiterite, the stannoborate mineral hulsite $\{(Fe^{2+}, Ca, Mg)_4 (Fe^{3+}, Sn^{4+})_2 B_2O_{10}\}$ and the rare borate szaibetyite $\{MgBO_2(OH)\}$. Cassiterite is extremely rare, being identified in only one sample (T41915) by XRD analyses. The borate phases are relatively minor constituents of the skarn by modal occurrence, typically less than 5%. Both szaibetyite and hulsite occur as microcrystalline, haystack-like mats of short fibres, ragged splinters and wisps of grains (<40μm long and <8μm wide) which are locally aligned (Plate 4.22). Szaibetyite is most prevalent in very fine-grained serpentine, but may extend into isolated carbonate grains and is commonly associated with magnetite. Szaibetyite is colourless to pale yellow-brown with moderate relief, birefringence up to mid second order. Hulsite occurrences are similar to szaibetyite, but more often occurs as acicular fibres forming an aureole around magnetite grains.

Carbonate-serpentine-magnetite± brucite skarn: Carbonate-serpentine-magnetite± brucite skarn comprises the rocks that occur between the Balstrup Fault and the massive serpentine-magnetite skarn in holes SY005 and SY009 (Fig. 4.5-4.6).

PLATE 4.12 Calcite-talc-chlorite skarn (SY014 - 404m). The white irregular patches are calcite, green patches are talc and dark patches in the talc are chlorite. Scale shown by hardness pen.

PLATE 4.13 Photomicrograph of calcite-talc-chlorite skarn (T41986). Talc occupies the lower half of the micrograph (fine-grained pink), and shows inclusions of chlorite (dark green). Coarse calcite occupies the left hand corner (calcite under extinsion). Field of view 2mm, XP, Mag. 5x.

PLATE 4.14 Massive serpentine skarn (SY009 - 526m). Typical texture of massive serpentine, characterised by black, dark green and light green serpentine. Scale indicated by pen.

PLATE 4.15 Serpentine-magneitie skarn (SY005 - 498m). Mottled and banded texture of massive serpentine (yellow, black, and dark grey) with coarse-grainedmagnetite (metallic black - far right corner). Scale indicated by pen.

PLATE 4.16 Massive serpentine-magnetite skarn (SY009 - ~450m). Serpenitine (green and black), magnetite (metallic black- around calcite) and calcite (white). Note distinctive banding in lower core. Scale indicated by pen.

PLATE 4.17 Massive magnetite skarn (SY009 - 454m). Magnetite (black) ranges from coarse-grained to fine-grained and banded. Calcite (white) occurs interstitially and is stained yellow by magnetite. Scale indicated by pen.

PLATE 4.18 Serpentitne pseudomorphing dolomite (T41906A). Serpentine (white) in the shape of a rhombohedral dolomite crystal (lower middle). The opaque phase is pyrite. Field of view 2mm, PP, Mag. 5x.

PLATE 4.19 Serpentine-talc in massive fine-grained serpentine (T41940). Serpentine intergrown with talc forming rounded plates in massive very fine-grained serpentine. Serpentine intergrown with brucite is visable in the left hand corner with magnetite (black). Field of view 2mm, PP, Mag. 5x.

12

13

14

15

16

17

18

19

In SY009, the skarn consists of black brucite ($Mg(OH)_2$), serpentine and minor magnetite in near equal proportions to dolomite. The most common textures of the three main phases in this zone are: (1) patches (<2cms) of brucite, often rimmed by calcite (Plate. 4.23 c); (2) irregular shaped patches of dark green and black serpentine surrounding brucite associated with calcite (Plate 4.24); and (3) dissimenations of black serpentine and magnetite in dolomite in a "chickenwire" texture (Plate. 4.23 a and b).

Brucite occurs as aggregates of fine-grained, bladed to fibrous euhedral grains, either associated with intergrowths of serpentine or as fibrous grains replacing carbonate (Plate 4.25). Individual grains generally exhibit a distinctive tarnish, usually present in the core of the grain. This feature is typical of the majority of the brucite aggregates, and may be the result of the inclusion of Fe during brucite formation (R. Berry pers. comm.). Serpentine and magnetite in this skarn occur in the variety of forms described previously. Similarly, the borate minerals are also present associated with serpentine.

The carbonate-serpentine-magnetite± brucite skarn in SY005 is characterised by the absence of large brucite patches. Brucite is present in the skarn but only as rare fibrous intergrowths with serpentine. The overall texture of the skarn is similar to that of SY009, with the exception of an increase in magnetite which is more abundant, up to 30%, forming irregular shaped veins and patches (Plate 4.26).

A significant feature of the carbonate-serpentine-magnetite ± brucite skarn close to the Balstrup Fault zone is the minor overprint by small irregular

patches and veins of magnetite, light green serpentine and calcite (Plate 4. 27). The zone of overprint is more extensively developed in the sulphide mineralisation (Chapter 5).

Mineral compositions

Serpentine: Serpentine in the Sylvester prospect contains significant amounts of iron and manganese substituting for magnesium (Table 4.2). Data from 8 analyses, expressed as mole percent end members serpentine (Se: $Mg_6Si_4O_{10}(OH)_8$) and greenalite (Gn: $Fe_6Si_4O_{10}(OH)_8$), averages $Gn_{1.5\text{-}3}$ and $Se_{95\text{-}97}$.

Column 1	T41984 R1	T41984 R2	T41984 R2	T41984 R5	T41942 R1	T41942 R2	T41942 R2
SiO2	42.87	43.79	46.22	43.78	44.23	44.00	43.43
Al2O3	0.19	0.18	0.09	0.06	0.03	0.05	0.09
FeO	4.23	3.88	4.08	4.23	3.03	3.15	2.97
MnO	0.28	0.28	0.29	0.16	0.37	0.37	0.28
MgO	38.26	38.67	37.72	38.94	40.13	39.84	39.83
CaO	0.13	0.08	0.07	0.16	0.08	0.09	0.14
Na2O3	0.12	0.01	0.03	0.08	0.02	0.01	0.15
K2O	0.24	0.04	0.04	0.10	0.02	0.03	0.31
H2O	12.56	12.65	13.03	12.81	12.87	12.89	12.71
Cl	0.19	0.04	0.05	0.06	0.02	0.03	0.17
TOTAL	99.03	99.76	101.64	100.36	100.90	100.47	100.22
Si	8.15	8.22	8.41	8.20	8.19	8.18	8.13
Al	0.42	0.04	0.02	0.01	0.01	0.01	0.02
Fe	0.67	0.60	0.63	0.66	0.47	0.49	0.47
Mn	0.05	0.05	0.05	0.03	0.06	0.06	0.04
Mg	10.84	10.82	10.32	10.86	11.07	11.04	11.11
Ca	0.03	0.02	0.01	0.03	0.02	0.02	0.03
Na	0.04	0.00	0.01	0.03	0.01	0.01	0.05
K	0.06	0.01	0.01	0.02	0.30	0.01	0.08
Mole %							
Greenalite	2.62	2.40	2.57	2.57	1.81	1.88	1.80
Serpentine	97.38	97.60	97.43	97.43	98.19	98.12	98.20

Table 4.2 Electron microprobe analyses of serpentine from massive serpentine-magnetite skarn. Compositional results expressed as a percentage of end members greenalite and serpentine.

PLATE 4.20 Coarse-grained magnetite in serpentine (T41912). Hexagonal crystals of magnetite (grey band), in serpentine (dark material). Magnetite being replaced by pyrite occurs in the top half of the photomicrograph. Field of view 4mm, RL, Mag. 2x.

PLATE 4.21 Photomicrograph of serpentine and rounded magnetite (T41940). Two forms of magnetite are present, as rounded magnetite (solid black) and as rounded magnetite (centre) partially altered by serpentine. Field of view 2mm, XP, Mag. 5x.

PLATE 4.22 Szaibetyite fibres in serpentine (T41933). Note szaibetyite fibres (pink fibres) occur in aligned bundles, serpentine occurs as massive very fine crystals and appears almost isotropic. Bottom left corner coarser grained serpentine. Field of view 2mm, XP, Mag. 5x.

PLATE 4.23 Carbonate-serpentine-magnetite ± brucite skarn (SY009 - 389 to 392). (Top to bottom); (a) "chickenwire texture" defined by black serpentine in marble, (b) chickenwire texture grading in o patchy texture ,and (c) patches of brucite (black) intergrown with serpentine (dark green) in marble. Scale indicated by pen.

PLATE 4.24 Patches and ovoid textures of serpentine, brucite and calcite (SY009 - 428). Serpentine (black, dark green and green) associated with brucite (dark grey) and calcite (white). Scale indicated by pen.

PLATE 4.25 Brucite within carbonate (T41927). Brucite displays typical birefringence colours (grey and white), growing in calcite (pink). Black mineral far right is very fine-grained serpentine. Field of view 2mm, XP, Mag. 5x.

PLATE 4.26 Magnetite patches and veins in dolomitic marble (SY005 - 498 to 501). Top core contains minor green serpentine. Scale indicated by hardness pen.

PLATE 4.27 Brucite in dolomitic marble (SY009). T41910= Brucite (black patch) in dolomitic marble. T41911= Brucite in marble overprinted by light green serpentine and calcite (white). T41912= Brucite in marble. Scale indicated by hardness pen.

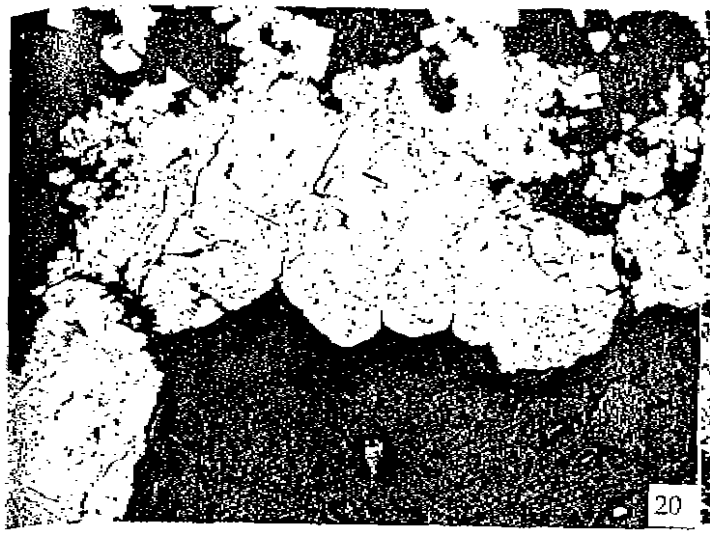
20


21


22

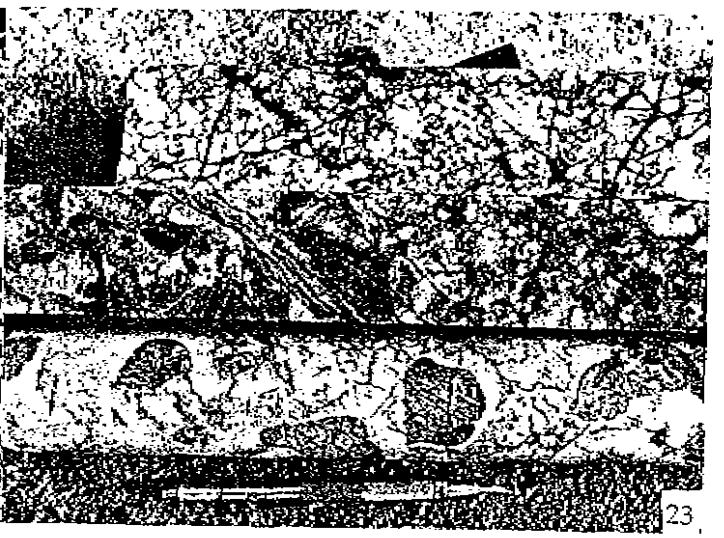
23

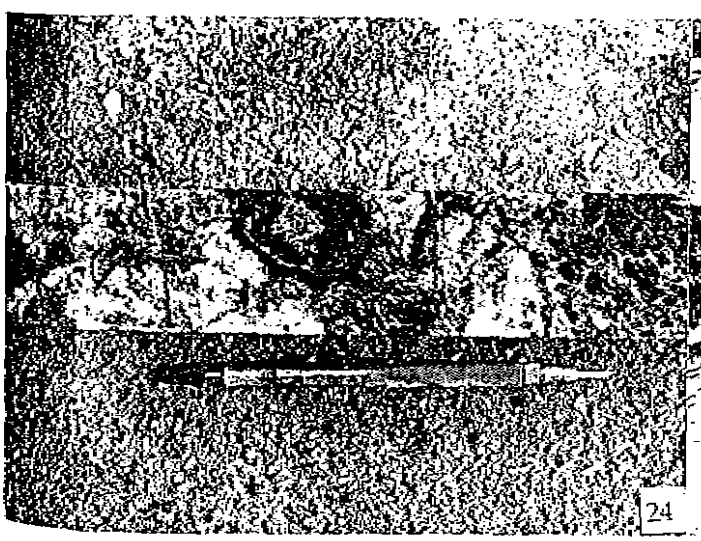
24


25

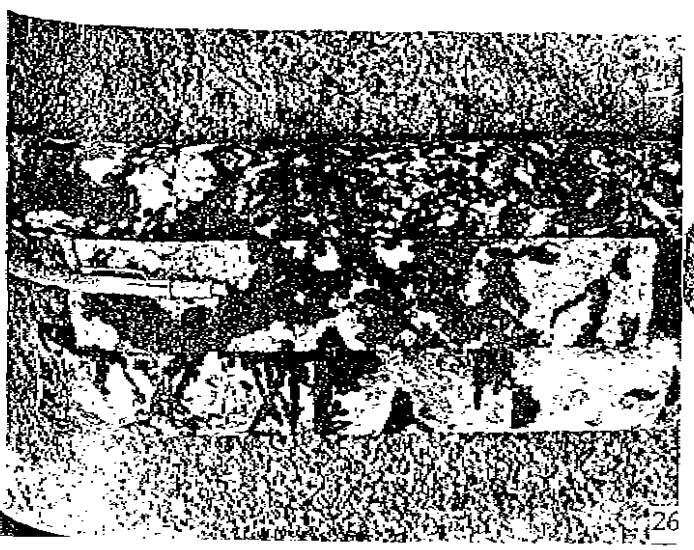
26

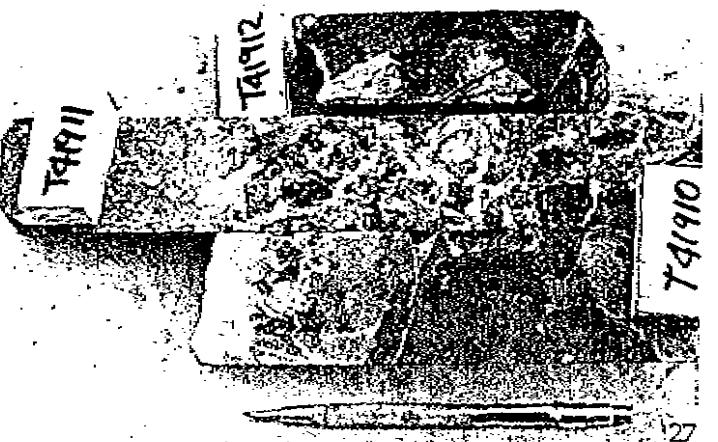

27

4.5 DISCUSSION

The overall sequence of formation of mineral assemblages within the three stages are summarised in Figure 4.7.

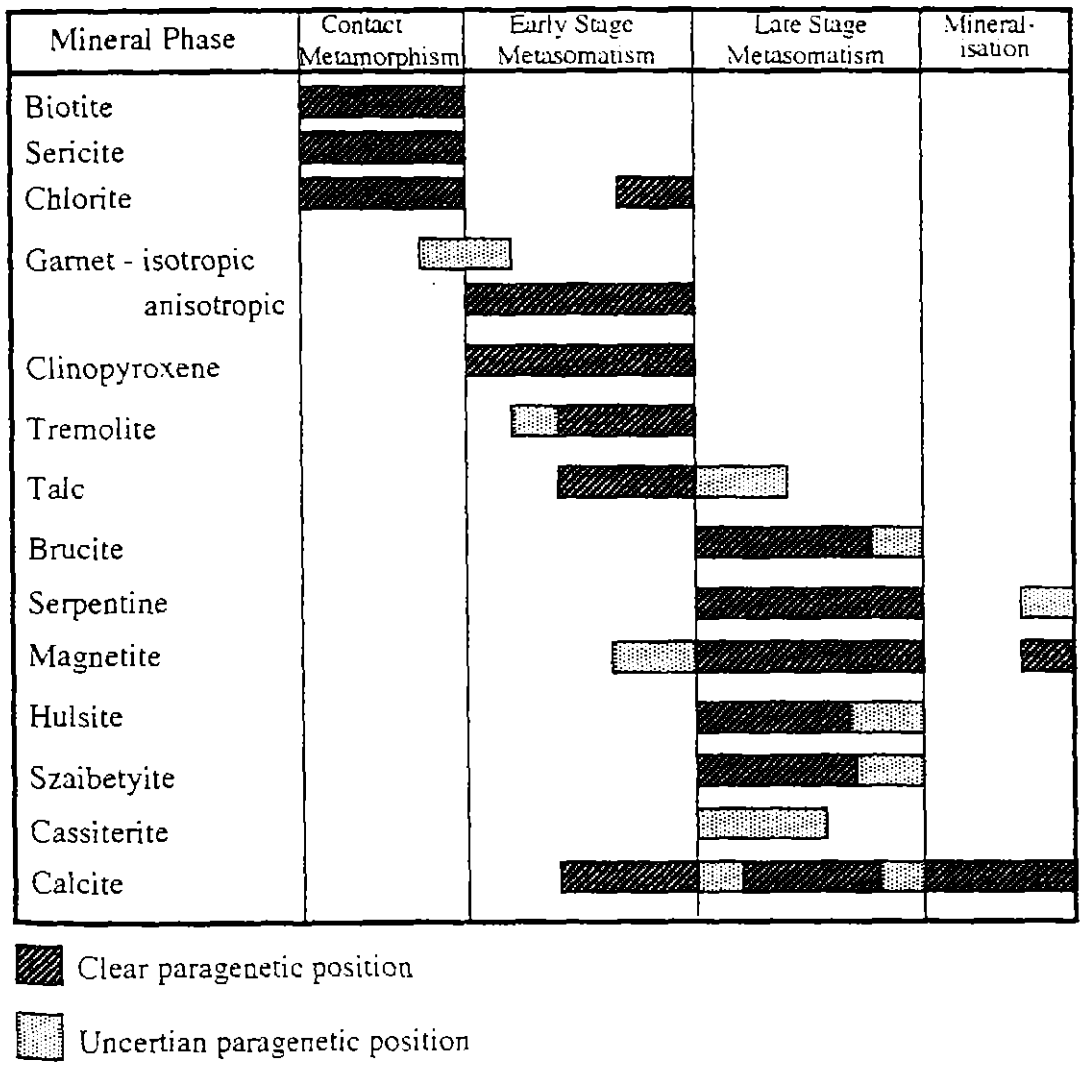

Figure 4.7 Paragenetic sequence of minerals identified in the Sylvester prospect.

Contact metamorphism

The occurrence of biotite hornfels in the two drill holes in the western most part of the prospect represents the outer margin of the contact metamorphic aureole of the Heemskirk Granite. Metamorphism of the pelites of the Oonah Formation to produce assemblages of biotite, sericite and quartzo-feldspathic matrix, although not in equilibrium, is indicative of low grade contact metamorphism (Turner, 1981), most probably relating to the lower temperature and pressure region of the hornblende-hornfels facies. This suggests general metamorphic condition of P= 0.5 to 2 kb and T= 400°C to 500°C (Turner, 1981).

The lime green hornfels situated between the biotite hornfels and the garnet-pyroxene skarn, represents the alteration of biotite hornfels via the replacement of biotite with tremolite. This mineralogical transformation can be viewed as the removal of K and Fe from the biotite hornfels and the addition of Ca, and CO_2. The obvious source of the calcium and CO_2 required for the alteration of the biotite hornfels to tremolite hornfels is from a fluid expelled from a carbonate unit (eg Upper Oonah dolomtic marble) which was concurrently undergoing metasomatic alteration (Dick and Hodgson, 1982). Thus, the lime green hornfels is not purely associated with the contact metamorphic stage but is associated with the early stage metasomatism.

Early stage metasomatism

The formation of garnet and clinopyroxene in carbonate of the Upper Oonah Formation is indicative of early stage metasomatic alteration of carbonate protolith through the reaction of metasomatic fluids, heated by and at least partly derived from the Heemskirk Granite, and the carbonate protolith. The conditions of formation of the skarn can be estimated through relevant reactions and stability fields in the system Ca-Mg-Si-C-O-H at the assumed pressure of fluid of <2kb. Diopside is stable only above a temperature of 400°C and below ~550°C (Fig. 4.8), assuming the mole fraction of CO_2 (XCO_2) in the metasomatic fluid is in the range 0.25 to 0.05 (these assumptions are valid based on studies of typical skarn formation; eg Einaudi et al., 1981). Thus, a formation temperature in the range 400 to 500°C corresponding to XCO_2 values in the range and can be suggested for the garnet-clinopyroxene and clinopyroxene skarns developed in the early metasomatic stage.

Mineral composition analyses of clinopyroxene and garnet-clinopyroxene skarns indicate that the composition of the garnets and clinopyroxenes vary considerably with respect to the wt% of magnesium (Appendix A-B). Garnets display a increase in Mg between isotropic and anisotropic forms, and clinopyroxenes display a difference in Mg values between the two types of skarn. Despite differences in Mg wt% values between clinopyroxenes this data indicates that the fluids that precipitated the clinopyroxene and anisotropic garnets had a high Mg activity. Assuming the fluid with the high Mg activity is the metasomatic fluid, this inturn suggests that the Mg deficient isotropic garnet formed prior to the metasomatic stage. Textural relationships between clinopyroxene and the garnets in the garnet-clinopyroxene skarn indicate that clinopyroxene and anisotropic garnet formed contemporaneously via the partial replacement the isotropic garnet. Thus, it

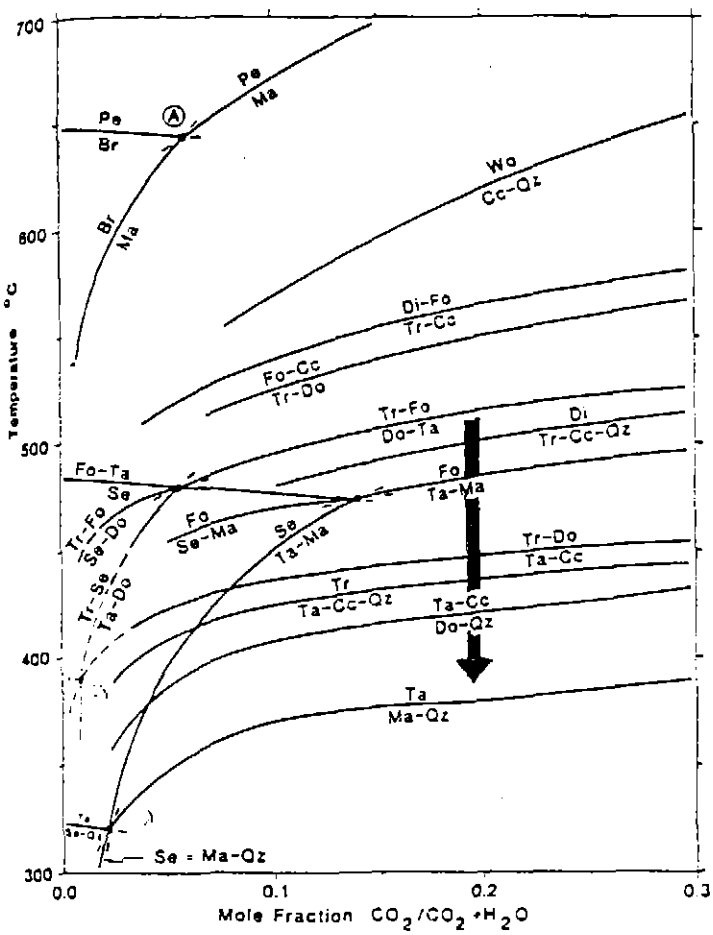

Figure 4.8a Partial T-XCO_2 diagram for water-rich compositions in the system Ca-Mg-Si-C-O-H at 2 kb tot. pressure (after Einaudi et al., 1981). Arrow indicates the behaviour of the early metasomatic stage fluid. Standar abbreviations used.

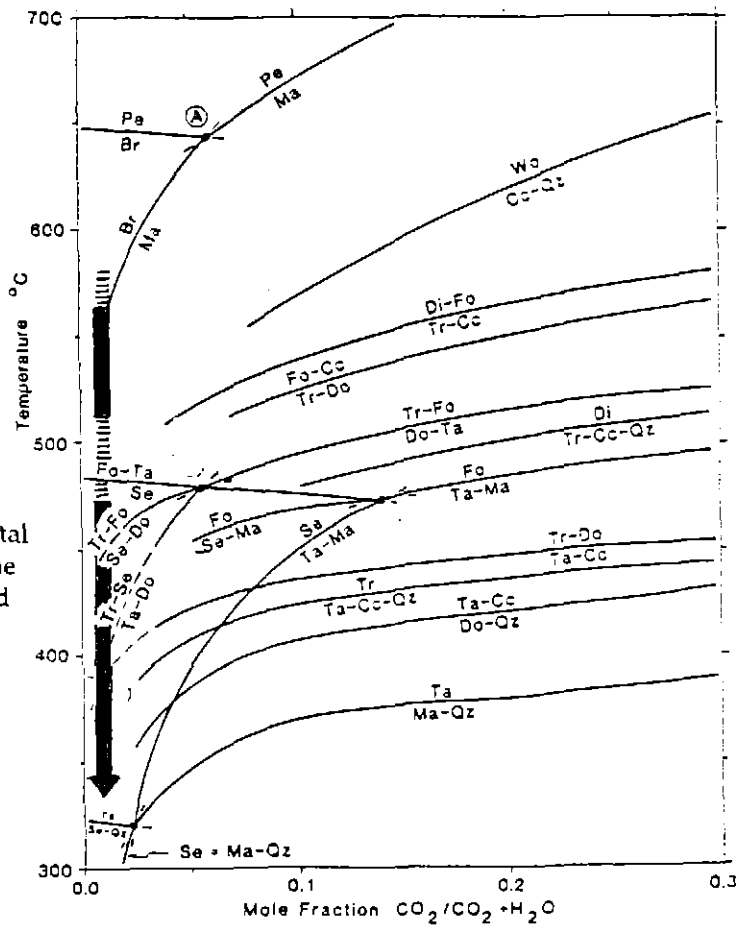

Figure 4.8b Partial T-XCO_2 diagram for water-rich compositions in the system Ca-Mg-Si-C-O-H at 2 kb total pressure (after Einaudi et al., 1981). Arrow indicates the behaviour of the late metasomatic stage fluid. Standard abbreviations used.

seems reasonable to suggest that the clinopyroxene and the anisotropic garnets formed during the metasomatic stage, overprinting the isotropic garnets which formed, most probably, in the metamorphic stage.

The relationship of the tremolite-talc-calcite skarn to the clinopyroxene skarn is largely ambiguous. However, several features of this skarn suggest that in part it may be strongly related to the clinopyroxene skarn, not only spacially but temporally. Skarn typically forms from the reaction of throughflowing metasomatic fluids (infiltration metasomatism) with the carbonate protolith. Progressive reaction of the fluids and protolith results in a mineralogical zonation away from the source of the fluid input (Zharikov, 1970; Einaudi et al., 1981). As metasomatism continues the temperatures of the fluid decreases, and high temperature calc-silicate mineralogy (eg. diopside) becoming no longer stable. In the system Ca-Mg-Si-C-O-H at the pressure and XCO_2 values assumed for the metasomatic fluid above , a decrease in temperature results in the formation of the phases tremolite, calcite and quartz via the break down reaction of diopside (Fig. 4.8a). Further decreases in temperature result in the breakdown reaction of tremolite to talc and calcite (Fig. 4.8a). Thus, by just assuming a decrease in temperature for an externally buffered metasomatic fluid (where by the fluid composition is controlled by the infiltrating fluid, and the reaction sequence on a T-XCO_2 is vertical at the XCO_2 of the infiltrating fluid; Will et al., 1990) it is possible to form the tremolite-talc-calcite skarn from the same fluid system that formed the clinopyroxene skarn (Fig. 4.8a). Other evidence for the tremolite-talc-calcite skarn not being produced during the retrograde stage is suggested by the observation that the clinopyroxene skarn and the tremolite-talc skarn are both overprinted by late stage massive serpentine-magnetite skarn.

Late stage (Hydrous) metasomatism

The late metasomatic stage of skarn formation resulted in the direct replacement of dolomitic marble and early metasomatic stage skarn assemblages by serpentine, magnetite and brucite. The occurrence of brucite suggests that temperatures during late stage skarn formation were, at least initally, relatively high (Fig. 4.8b); at 2kb, brucite is stable between 650 and ~ 400°C. The stablity field of brucite also limits the formation of the late stage skarn to very low XCO_2, as brucite breaks down to form magnesite at values of XCO_2 greater than 0.05 (Einaudi et al., 1981; Fig 4.8b). Serpentine formation at the same XCO_2 conditions as for brucite forms at temperatures below 490°C (Fig. 4.8b). The formation of brucite at higher temperatures than for serpentine results in a similar mineralogical zonation as observed between the clinopyroxene skarn and the tremolite-talc-calcite skarn, where by the higher temperature mineralisation precipitates first closest to the fluid source. In this case the Balstrup Fault is most probably the fluid channelway, with the lower temperature phases form later further from the source (Fig. 4.5-4.6).

4.6 REGIONAL SETTING

Skarn mineralisation in the Sylvester prospect is genetically related to a larger regional skarn complex that extends from the margins of the Heemskirk Granite, along the strike length of the Balstrup Fault to east of the Comstock mine. Figure 4.9 illustrates the distribution of the skarn mineralisation in this zone, based on petrographic work and mapping by RGC (Crossing, 1992) and CRA (Dickson, 1981).

The following broad zones are recognised:

Contact metamorphic aureole: This zone is characterised by intense hornfelsing, resulting in; recrystallisation of pure dolomitic carbonate units to marble, diopside skarn in impure dolomites, and quartz + biotite + feldspar + cordierite hornfels (Crossing, 1992). The outer limit of the aureole at the surface is shown in Figure 4.9. This zone is observed in the Sylvester prospect, represented by the biotite hornfels in drillhole SY014.

Prograde (infiltration) skarns: This a less well defined zone characterised by patchy diopside, garnet ± tremolite calc-silicate mineralisation developed in carbonate units contacting non carbonate units (Crossing, 1992). The outer limit of this zone coincides with western boundary of the Sylvester prospect (Fig. 4.9). The skarn assemblages in this zone corresponds to the early metasomatic stage mineralisation observed in SY014.

Retrograde (hydrous) skarns: These skarns are developed in areas of prograde skarn, in particular the Tenth Legion area, as well occurring further east along the Balstrup Fault in the Sylvester prospect. These skarns are characterised by magnetite-serpentine replacing prograde skarn and carbonate units. These skarns correspond to the late metasomatic stage identified in this thesis.

CHAPTER FIVE

MINERALISATION

5.1 INTRODUCTION

Mineralisation in the Sylvester prospect consists of a narrow, near-vertical, Zn-Pb-Ag sulphide lens hosted by carbonates of the Upper Oonah Formation and late stage skarn mineralisation. The mineralisation is composed primarly of five sulphides; pyrrhotite, sphalerite, galena, chalcopyrite and pyrite, plus minor amounts of arsenopyrite, marcasite and the sulphosalt boulangerite. The sulphide lens, named the Comstock massive sulphide body (Crossing, 1992), occurs in the immediate footwall of the WNW trending Balstrup Fault zone, over a strike length of 1,000 metres. The body has a known vertical extent (down-dip extent) of over 400 metres, and is open at depth below 450 metres over its entire strike length. The body dips 70° toward 010° AMG (NNE), and has a calculated average true thickness of 7.4 metres (Crossing, 1992).

The Comstock massive sulphide body is composed of two distinct styles of mineralisation; medium to coarse-grained massive pyrrhotite replacing magnetite-serpentine skarn in the immediate footwall of the Balstrup Fault, and coarse-grained euhedral massive pyrite replacing dolomitic carbonates at the margins of the sulphide body. In addition there are numerous zones of

pyritic stockwork veins in the Oonah Formation surrounding the massive sulphide body and in portions of the Balstrup Fault zone.

5.2 STYLE OF MINERALISATION

5.2 1 Massive Pyrrhotite

Massive pyrrhotite mineralisation is intersected in three diamond drill holes (SY005, SY009, SY012) (Fig. 4.1, map pocket). In these drill holes the mineralisation is expressed as a number of thin (2-4 m) sulphide intervals separated by 2 to 3 metres intervals of massive serpentine-magnetite skarn and carbonate-serpentine-magnetite-brucite skarn (Fig. 5.1-5.3).

Texturally, the individual intervals of mineralisation are similar, with only minor differences between sulphide intervals closest to the Balstrup Fault and those further away. Sulphide intervals proximal to the Balstrup Fault zone are characterised by granular massive pyrrhotite containing patches (< 10 mm size) of sphalerite and galena (Plate 5.1a). The intervals of mineralisation furthest from the Balstrup Fault zone are consistently more sphalerite and galena rich (10 to 30% visual estimate of total sulphide intersection), and are marked by the presence of milky quartz (Plate 5.1b).

A significant feature of pyrrhotite mineralisation proximal to Balstrup Fault is the overprint of pyrrhotite by pyrite and magnetite. This overprint is characterised by veins, ranging in thickness from 1 mm up to 5 cm, which consist of a core of magnetite and margins of pyrite (Plate 5.2).

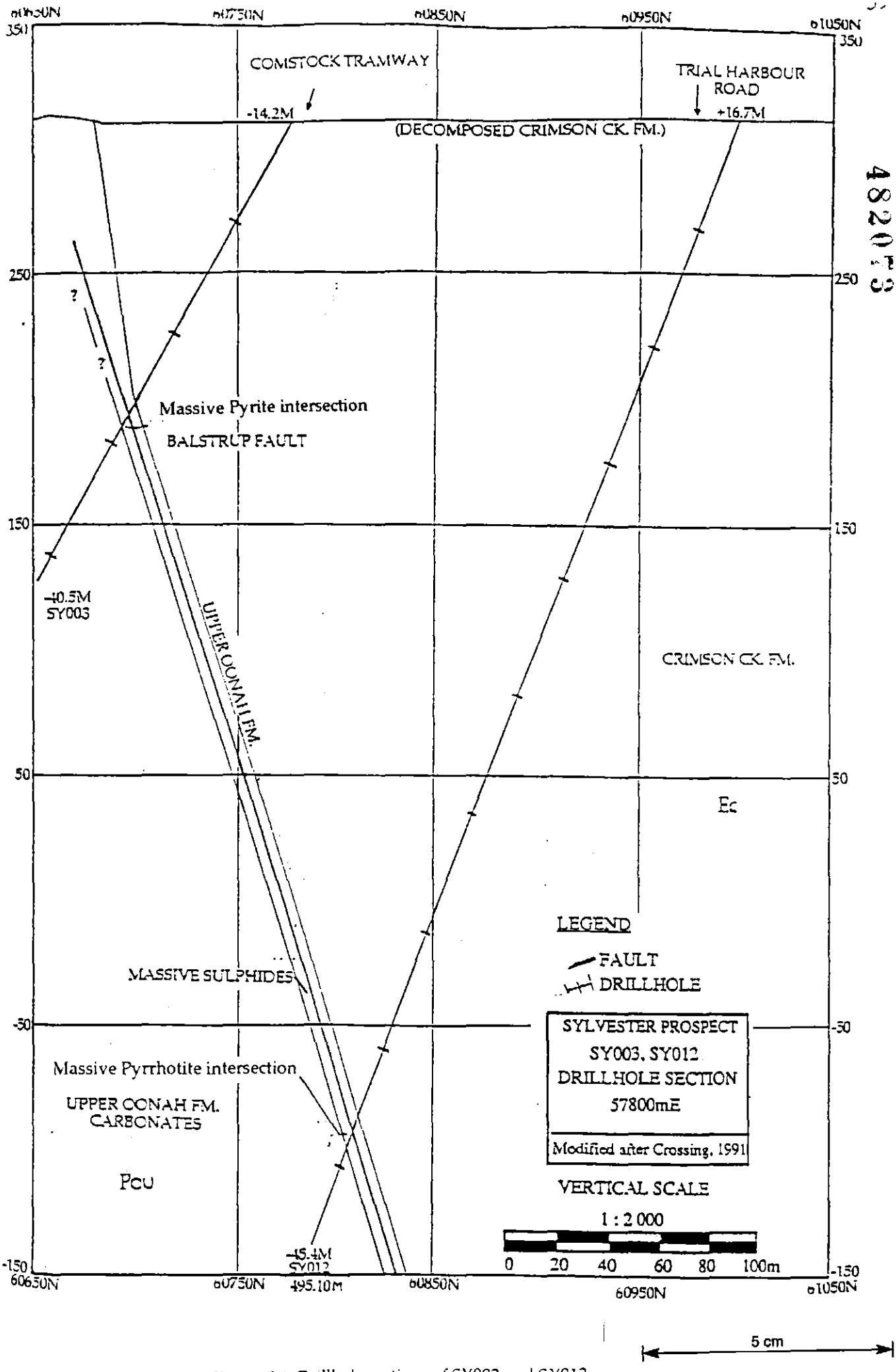

Figure 5.1 Drillhole sections of SY003 and SY012

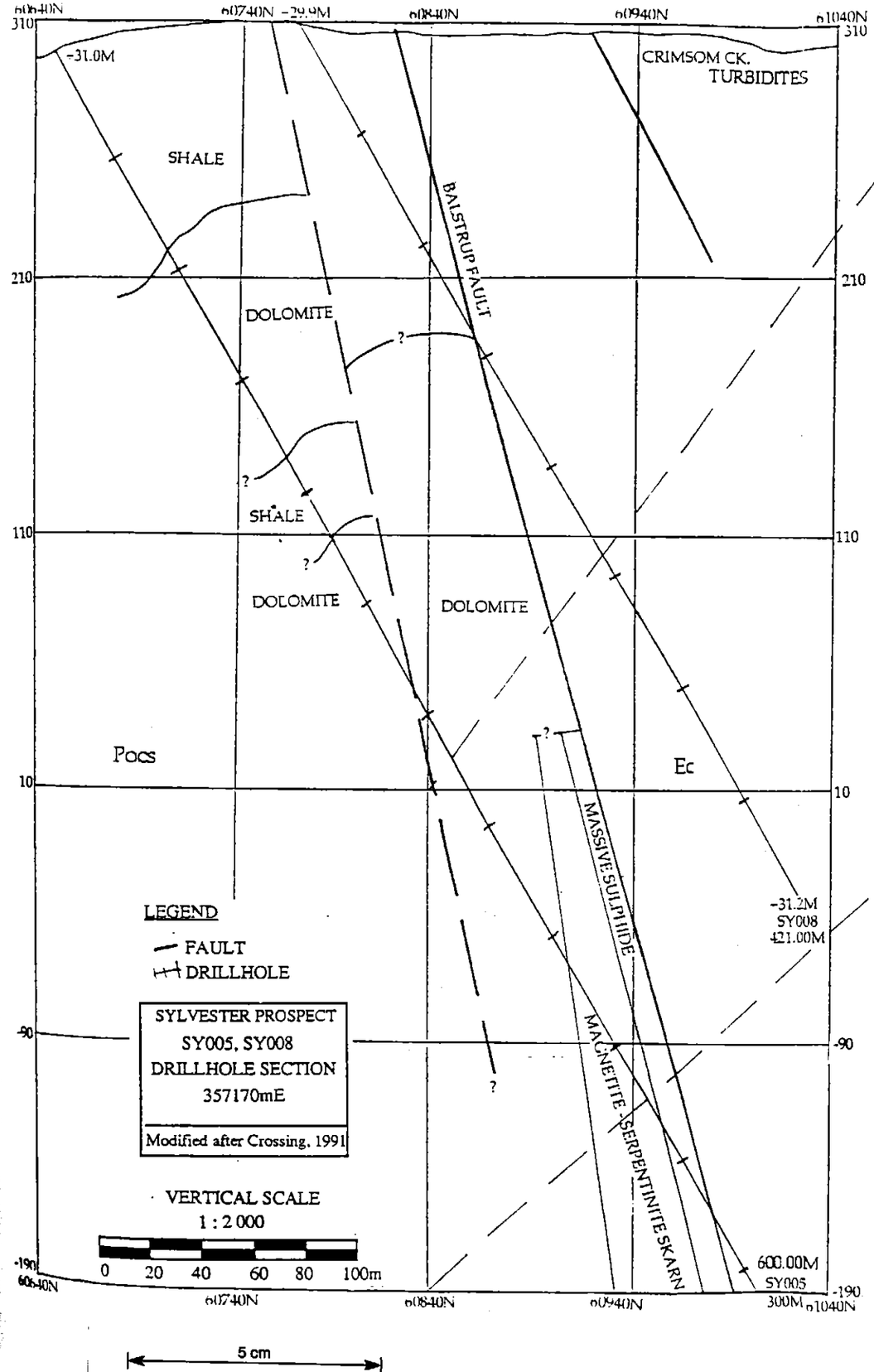

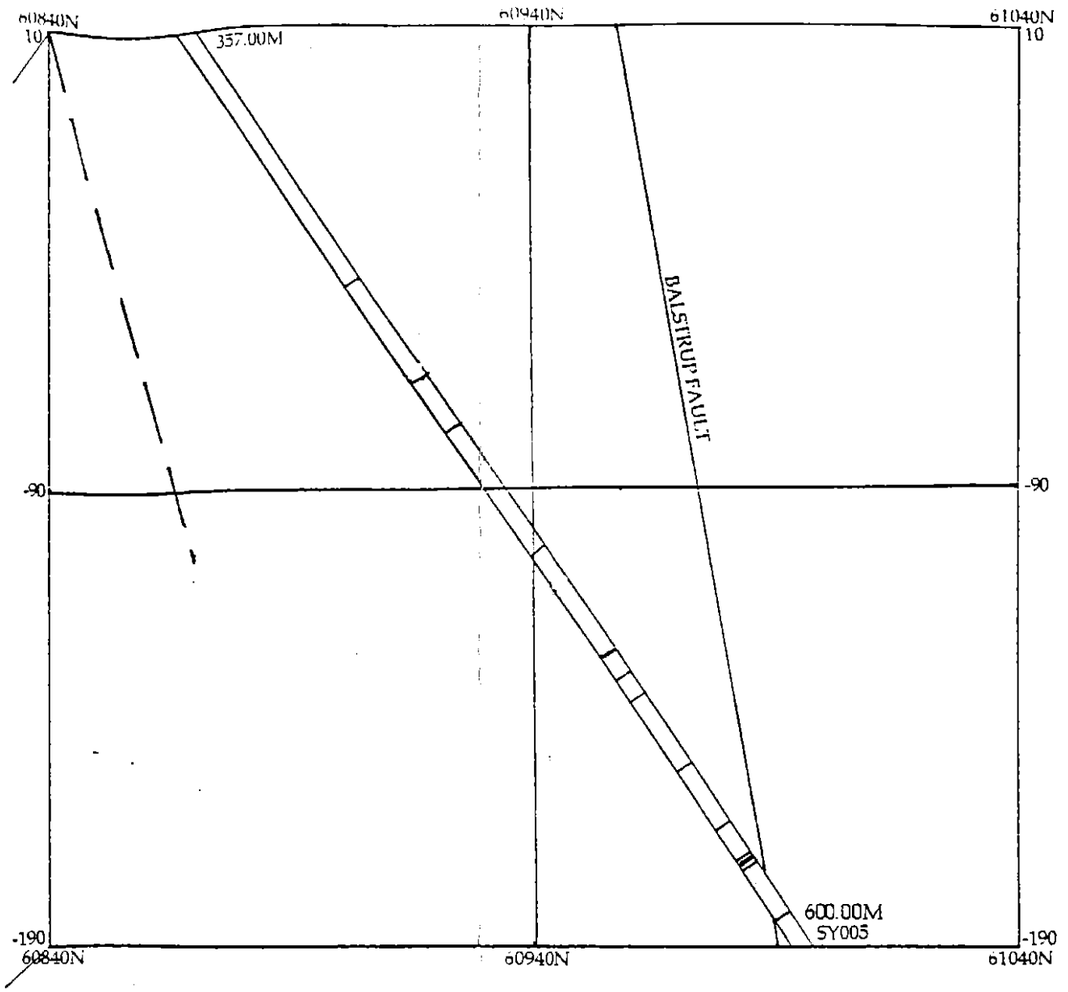

KEY

- Dolomite
- Fault Rock
- Massive Sulphide
- Skarn

Figure 5.2 Drillhole sections of SY005 and SY008

Insert - Sulphide intersections in SY005.

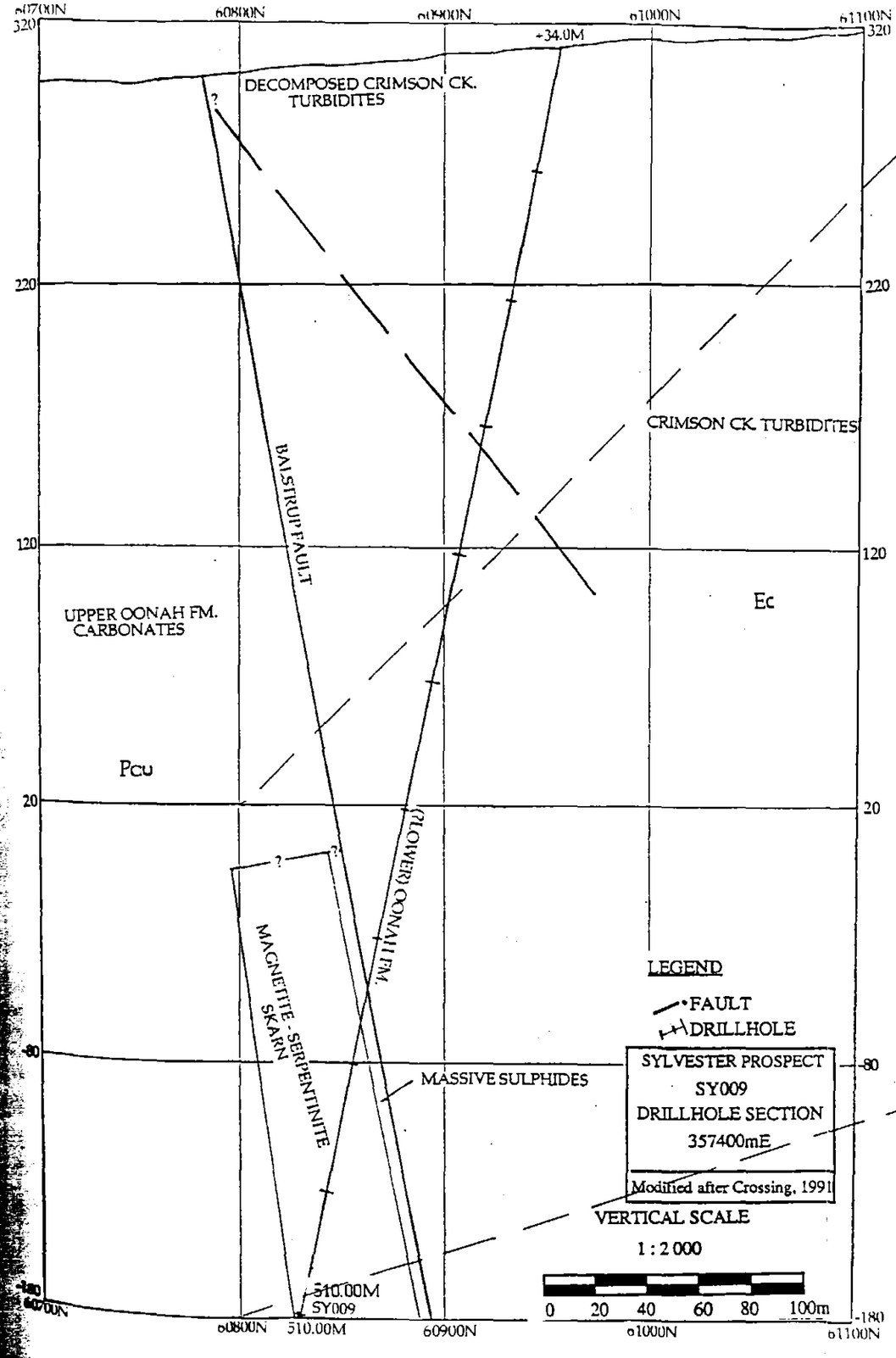

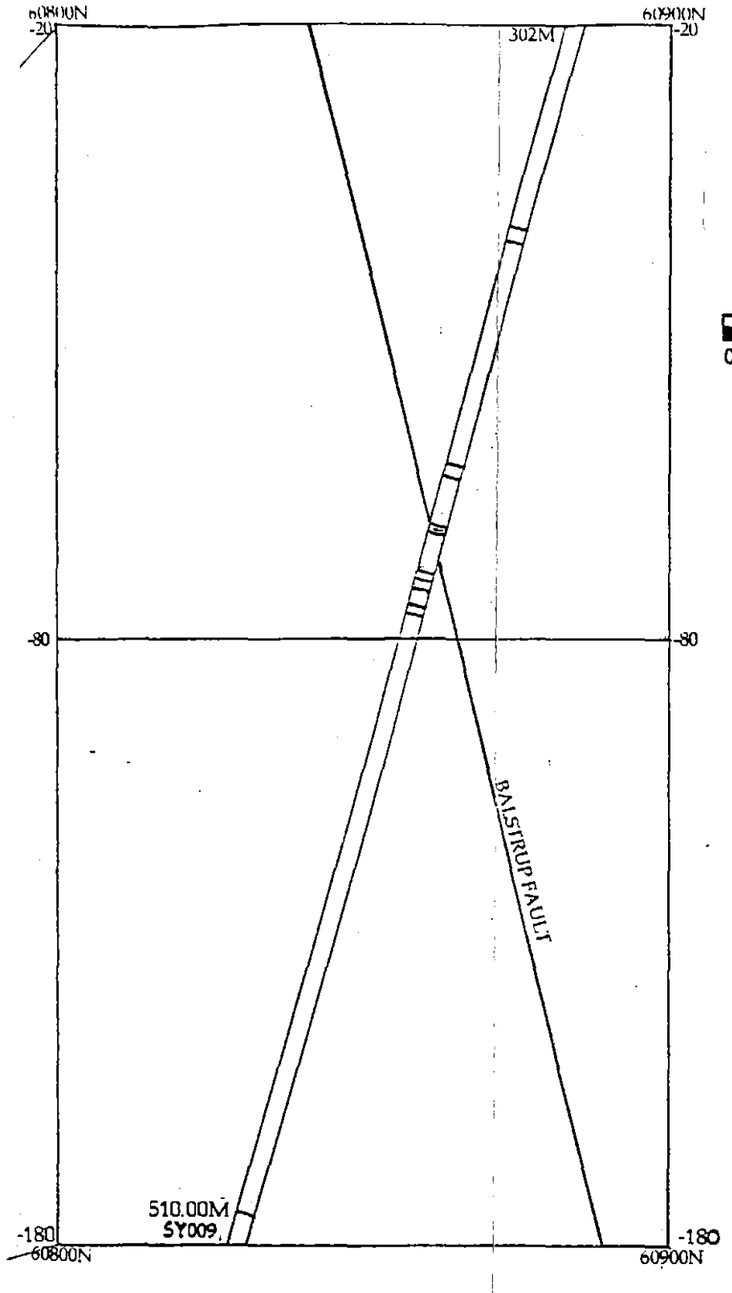

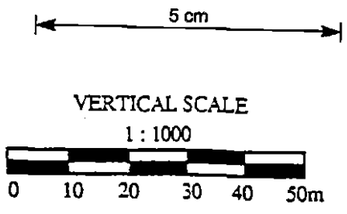

Figure 5.3 Drillhole sections of SY009

Insert - Sulphide intersections in SY009.

5.2.2 Massive Pyrite

Massive pyrite mineralisation is intersected in only one hole, SY003 (Fig. 4.1). The mineralisation is representative of the vertical extention of the massive sulphide intersected in SY012 (Fig. 5.3). It consists of massive to semi-massive coarse-grained euhedral pyrite and aggregates of fine-grained disseminated pyrite. Sphalerite, galena and boulangerite occur as patches and disseminations, and account for 10% of the total sulphide. Quartz is present as irregular veins and patches.

5.2.3 Stockwork Veins

Stockwork vein mineralisation occurs predominantly in zones of fractures and minor faults through out sandstone and siltstone units of the Oonah Formation that occur in areas spatially associated with the Balstrup Fault. The Balstrup Fault zone itself contains numerous stockwork veins. The zones of stockwork mineralisation consist typically of thin veins of fine-grained disseminated pyrite with minor carbonate, quartz and 5% disseminated sphalerite and galena and rare boulangerite.

5.3 MINERALOGY AND TEXTURES

The mineralogy of the massive sulphide body consists predominantly of pyrrhotite, marcasite, pyrite, sphalerite, galena, chalcopyrite and magnetite with minor arsenopyrite and boulangerite .

This study of sulphide mineralogy was undertaken using polished thin sections prepared at the University of Tasmania

Magnetite

Magnetite occurs in two forms. The most common form is as irregular patches ranging up to several cm in size, consisting of anhedral magnetite grains, associated with euhedral pyrite and typically replacing pyrrhotite-marcasite along fractures and grain boundaries. The magnetite grains are marked by numerous inclusions of very fine-grained, unidentifiable gangue (Plate 5.3).

The second form of magnetite is present throught the sulphide body. It occurs as thin veinlets and anhedral grains (<10 μm) intergrown with fine-grained euhedral pyrite along cleavage planes and grain boundaries (Plate 5.6). This form of magnetite is thought to indicate replacement of pyrrhotite-marcasite.

Pyrrhotite

Pyrrhotite is the dominant sulphide mineral in the Comstock massive sulphide body, but is only rare in the stockwork and fault veins. It occurs as either massive aggregates of granular anhedral grains, or as anhedral disseminations. Individual grains range in size from 0.1 to 0.5 mm, and in the massive pyrrhotite mineralisation display approximately 120° interfacial angles at their junctions. Individual grains also displays variations in colour, from grey-brown to yellow-pink, and degrees of anisotropy, marked by strong yellow-grey to weak greyish blue. The majority of the pyrrhotite shows evidence of deformation in the form of late fractures and strain lamellae (Plate 5.4). The massive pyrrhotite is extensively replaced by marcasite, magnetite and pyrite in the sulphide intersection closest to the

Balstrup Fault. A second generation of pyrrhotite occurs as minute exsolution blebs in sphalerite (Plate 5.10).

Marcasite

Marcasite is restricted to the massive pyrrhotite mineralisation were it is relatively common. It occurs as either aggregates or as individual grains, generally <0.1 mm in size. The marcasite grains are very distinctive in their form, being characterised by a marked lamellar texture (Plate 5.5). The sub-parallel lamellae consist of carbonate gangue and minor magnetite, and are intimately intergrown with euhedral fine-grained (100 μm) pyrite grains. Surrounding the marcasite grains are residuals of pyrrhotite which are clearly replaced by the marcasite. The texture of the marcasite and the associated complex intergrowths between gangue, magnetite and pyrite have been observed in a variety of deposits (Edwards, 1957; Buseck, 1967). In these deposits this texture is regarded as forming with the marcasite during the alteration of the pyrrhotite (Edwards, 1957).

Pyrite

Pyrite is ubiquitous in the Sylvester prospect, although its abundance varies substantially between styles of mineralisation. It is subordinate to pyrrhotite in the intersections of massive pyrrhotite mineralisation, but is by far the most common sulphide phase in the massive pyrite mineralisation and stockwork veins. Several varieties of pyrite can be distinguished. In the massive pyrrhotite mineralisation it occurs in two distinct forms. The most common form is as granular aggregates of fine-grained (≤ 0.1 mm) euhedral to subhedral grains intergrown with anhedral magnetite patches and grains in the vicinity of fractures and along crystallographic structures replacing

pyrrhotite (Plate 5.6). The less common form is as individual coarse-grained euhedral pyrite replacing massive pyrrhotite. The grains of pyrite range in size up to 3 mm. This pyrite displays no relationship to magnetite (Plate 5.7).

In the massive pyrite mineralisation pyrite occurs as relatively coarse euhedral crystals, ranging in size from 100 μm to 0.5 mm, associated with sphalerite patches and quartz gangue. The pyrite displays evidence of zoning, marked by trials of very fine (<1 μm) gangue inclusions (Plate 5.8). Some grains of pyrite also contain inclusions of sphalerite, galena and pyrrhotite. There is no evidence of a pyrrhotite precursor.

In the stockwork and fault veins, pyrite occurs as subhedral to euhedral grains, generally <0.1 mm in size. Pyrite is usually intergrown with quartz gangue, and larger grains contain numerous gangue inclusions, which can broadly define a zonal pattern. This pyrite appears to replaced by sphalerite and galena seams (Plate 5.9).

Sphalerite

Sphalerite is present as either individual grains, or as elongate masses of anhedral grains (50 μm up to 15 mm) throughout the massive pyrrhotite and pyrite mineralisation, and associated with pyrite and quartz in the stockwork veins. The masses of sphalerite are extensively fractured and sphalerite grains display strain lamellae. In the massive pyrrhotite mineralisation the majority of sphalerite contains minute inclusions of pyrrhotite and chalcopyrite, these typically range in size from <1 μm grains to 50 μm long lamellae (Plate 5.10). Pyrrhotite inclusions can account for up to 10% of the sphalerite by area. The number of inclusions tend to increase toward the margins of the sphalerite.

PLATE 5.1 Massive pyrrhotite mineralisation (SY005 - 507 to 514m). (Top to bottom); (a) massive pyrrhotite with aggregates of sphalerite (dark patches), (b) massive pyrrhotite with band of milky quartz (quartz is both white and dark green in colour), (c) and massive to semi-massive pyrrhotite associated with serpentine (dark green). Scale indicated by pen.

PLATE 5.2 T41904 (SY009 - 379m) and T41905 (SY009 - 380m) massive pyrrhotite mineralisation crosscut by thin veinlets of pyrite. Note pyrite veins result in staining of pyrrhotite. T41906 (SY009 - 383m) massive pyrrhotite cut by magnetite-pyrite vein. Magnetite (black) occupies the core of the vein, whereas pyrite (yellow) forms a 2cm selvage between the magnetite and the massive pyrrhotite (visible as the darker phase in drillcore below the break). T41907 (SY009 - 384m) massive pyrrhotite.

PLATE 5.3 Magnetite (grey) replacing pyrrhotite (brown) along grain boundaries and along small fractures (T41908). Note the trails of fine-grained gangue inclusions (black dots) in the magnetite. Field of view 1mm, RL, Mag. 10x.

PLATE 5.4 Strain lamellae at the edge of pyrrhotite grain (T41989). The boundary of the grain is indicated by the arrow. Field of view 2mm, RL, Mag. 5x.

PLATE 5.5 Marcasite (T41908). The typical texture of marcasite is characterised magnetite (grey) and gangue inclusions (black) forming parallel lamellae in the marcasite. Small euhedral pyrite grains (bright yellow) are visible in the marcasite grain. The top right of the photomicrograph shows the partial replacement of pyrrhotite (brown) by marcasite. Field of view 0.25 mm, RL, Mag. 40x.

PLATE 5.6 Fine-grained pyrite intergrown with magnetite replacing pyrrhotite (T41907). Note the replacement by pyrite and magnetite occurs strongly associated with fractures. Field of view 1mm, RL, Mag. 10x.

PLATE 5.7 Large euhedral pyrite replacing massive pyrrhotite mineralisation (T41989). Note the lack of associated magnetite. Field of view 4mm, RL, Mag. 2.5x.

PLATE 5.8 Inclusion rich euhedral pyrite in quartz gangue (opaque) (T41977). The grey mineral present is boulangerite. Field of view 1mm, RL, Mag. 10x.


7


5

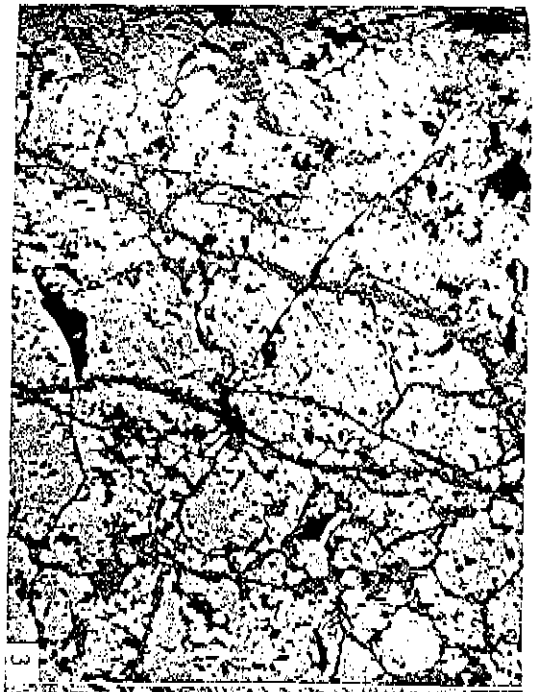
3

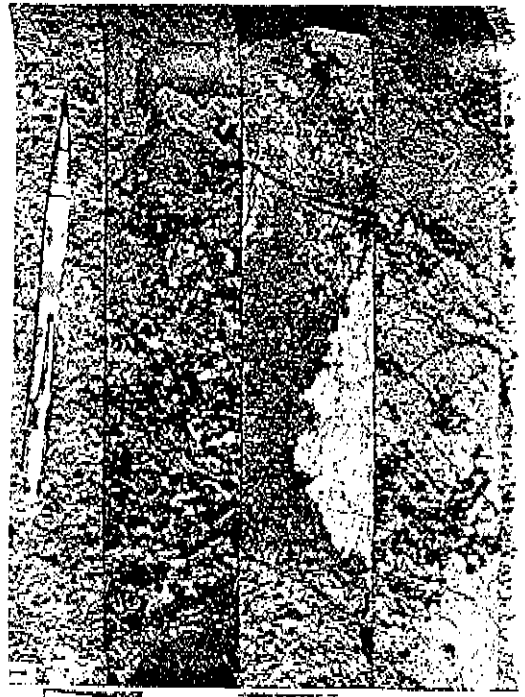
1


8


6


4

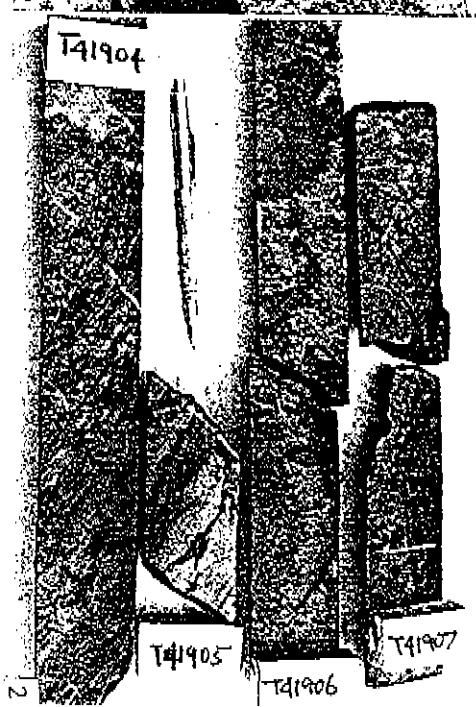
T41904
T41905
T41906
T41907
2

Commonly, the sphalerite contains larger inclusions of pyrrhotite (<0.5 mm) these are unaltered during pyrrhotite alteration.

In the pyrite and stockwork vein mineralisation the sphalerite occurs as anhedral patches interstitial and occasionaly intergrown with the pyrite and quartz gangue

Galena

Galena occurs in a similar distribution to that of sphalerite. It occurs in several textural variations. The main form is as relatively granular intergrowths, up to cm size, with sphalerite, and to a lesser extent pyrrhotite, in massive pyrrhotite mineralisation. The second form of galena is as relatively thick veins along fractures in pyrrhotite, these veins may represent remobilisation during deformation. This galena contains very little entrained material. The third form of galena is as small inclusions (< 20 μm) in sphalerite.

Deformational effect are clearly evident in the galena. Deformation has produced extensive curvature and disruption of linear features in the galena (Plate 5.11).

Chalcopyrite

Chalcopyrite is a relatively minor constituent of the massive sulphide body. It is present as small anhedral patches , usually < 0.1mm, in massive pyrrhotite. Minor amounts of chalcopyrite is also present as numerous small inclusions (<1 μm to 20 μm) in sphalerite patches.

Arsenopyrite

Arsenopyrite is a minor sulphide phase. It occurs as euhedral phenocrysts, up to 0.5mm in size, within massive pyrrhotite mineralisation and less commonly pyrite mineralisation strongly associated with sphalerite and galena.

Boulangerite

Boulangerite is a rare mineral phase, observed only in a relatively small section of massive pyrite mineralisation. Here, it formed anhedral patches and irregular seams of up to cm size interstitial to euhedral pyrite and quartz gangue. Boulangerite also occurred as small inclusions within the outer zones of zoned pyrite crystals (Plate 5.12).

5.4 GANGUE MINERALOGY

Quartz is the dominant gangue mineral. In the sulphide mineralisation it occurs as granular aggregates of interlocking subhedral grains less than < 0.5 mm size, or as large (2 mm) individual euhedral grains with well developed terminations. In the massive pyrite mineralisation the quartz tends to become larger around pyrite grains on which they appear to have nucleated. Quartz is also present as small inclusions in pyrite, sphalerite and boulangerite. A late stage milky quartz is present in numerous fractures and vugs through the sulphide intersections.

Carbonate is a relatively common gangue mineral. It occurs in two major forms. The most common is as thin veins (0.1 to 1 mm), composed of euhedral

PLATE 5.9 Coarse euhedral pyrite replaced by inclusion rich spahlerite (T41990). The inclusions in the sphalerite (grey) are predominantly quartz. Field of view 0.5 mm, RL, Mag. 20x.

PLATE 5.10 Pyrrhotite, chalcopyrite ± galena inclusions within sphalerite in massive pyrrhotite mineralisation (T41913). Note the pyrrhotite (cream), and chalcopyrite (yellow) inclusions increase toward the grain boundary of the sphalerite (brown). Massive pyrrhotite is visible in the top of micrograph. Field of view 1mm, RL, Mag. 10x.

PLATE 5.11 Galena displaying curvature of cleavage (T41913). Sphalerite is visible in the upper right corner. Field of view 1 mm, RL, Mag. 10x.

PLATE 5.12 Euhedral pyrite associated with boulangerite (T41977). Note the boulangerite inclusions in the pyrite. Black material is quartz gangue. Field of view 0.5 mm, RL, Mag. 20x.

PLATE 5.13 Rossetts of tremolite in pyrite (opaque),and strongly associatedwith inclusion rich quartz (T41913). Field of view 0.5mm, XL, Mag. 20x.

9

10

11

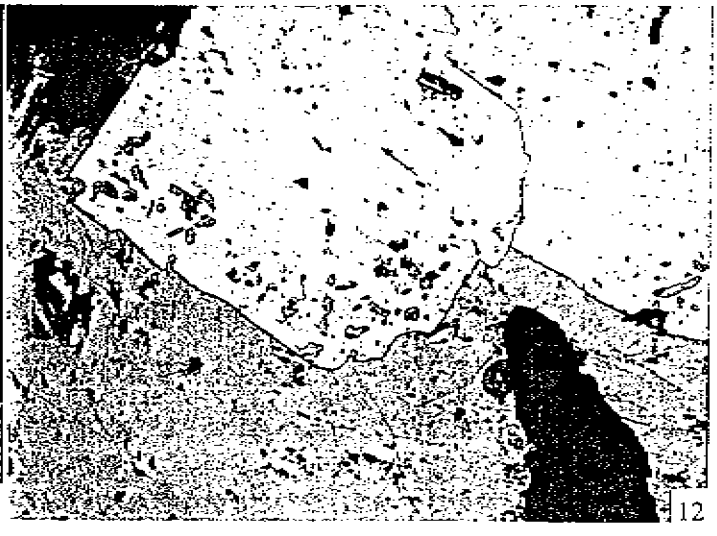

12

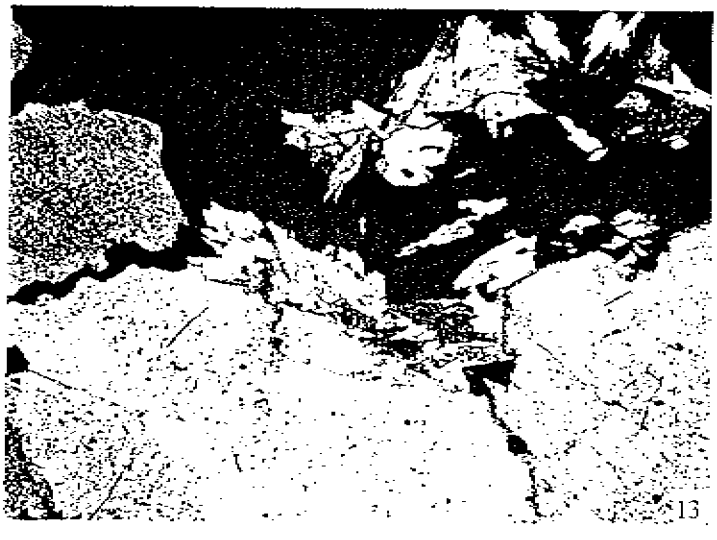

13

crystals that replace along deformational related small scale fractures in the massive pyrrhotite mineralisation. The second form is as a late stage vug fillings mineral in the Balstrup Fault, and in minor fault and vugs occurring in the sulphide mineralisation.

Tremolite is a rare gangue mineral observed only in one thin section. The amphibole forms small rosettes that appear to have nucleated on large quartz grains (Plate 5.13).

5.5 MINERAL PARAGENESIS

On the basis of textural relationships and mineralogical associations the following paragenetic sequence for sulphide and gangue minerals has been established. The paragenetic sequence is presented in Figure 5.2.

The paragenesis table (Fig. 5.2) has been divided into three stages. The earliest stage of mineralisation is characterised by the deposition of pyrrhotite relatively soon after the development of the late stage serpentine-magnetite skarn (ref. Chapter 4). The pyrrhotite replaced dominantly carbonate of the carbonate-serpentine-magnatite skarn in the immediate footwall of the Balstrup Fault.

The pyrrhotite mineralisation is associated with anhedral patches of sphalerite, galena, chalcopyrite and arsenopyrite. Textural relationships between the four sulphides and pyrrhotite, particularly the inclusion of unaltered pyrrhotite suggests their formation was co-eval with that of pyrrhotite. Concurrent with the deposition of massive pyrrhotite replacing skarn in the footwall of the Balstrup Fault, was the deposition of massive pyrite, sphalerite, galena, and chalcopyrite replacing carbonate at the margins

of the sulphide lens. The relationship between the massive euhedral pyrite and the massive pyrrhotite mineralisation is based primarly on the location of the pyrite mineralisation (Fig. 5.1). However, the lack of a pyrrhotite precursor strenghtens this interpretation. The gangue mineral quartz was also deposited in this stage.

The sulphosalt boulangerite is present in the massive pyrite mineralisation, and appears to post date the euhedral pyrite (Plate 5.12). However, some of the pyrite crystals contain inclusions of boulangerite, although deformation has somewhat obscured the exact textural relationship between the pyrite and boulangerite.

The second stage of mineralisation resulted in the replacement of a large proportion of the massive pyrrhotite mineralisation by marcasite. The formation of marcasite was followed by the replacement of both unaltered pyrrhotite and pyrrhotite altered by marcasite by intergrowths of fine-grained pyrite and magnetite along the grain boundaries of the crystals (Plate 5.6).

The final stage of mineralisation resulted in the replacement of pyrrhotite± marcasite by coarse-grained euhedral pyrite. The lack of magnetite in the vicinity of the pyrite suggests this form of pyrite is probably the result of supergene processes (Plate 5.8). This stage also resulted in the Balstrup Fault and fractures being replaced by milky quartz and calcite, and vughs in the massive sulphide body being filled by carbonate.

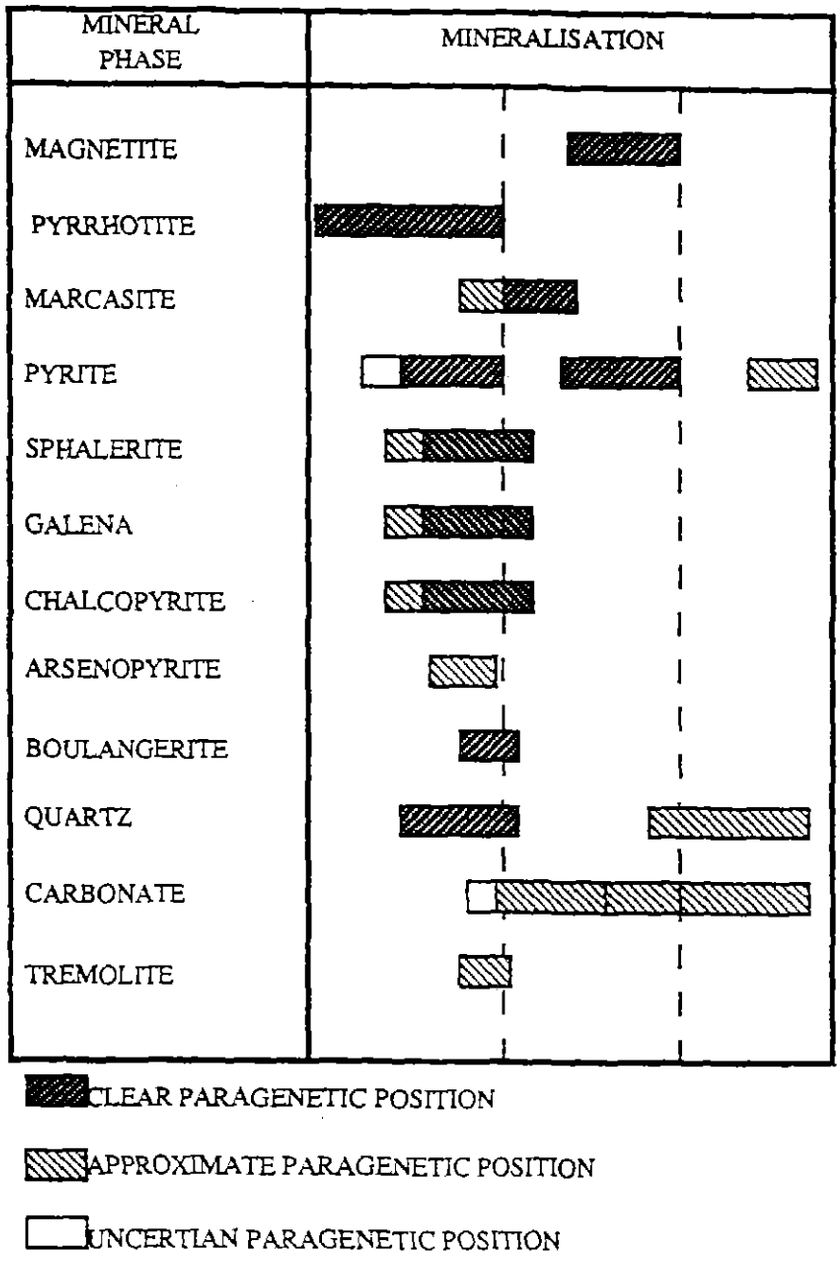

Figure 5.4 Paragenetic sequence of sulphide minerals in the Sylvester prospect.

5.6 OTHER MINERALISATION IN THE SYLVESTER PROSPECT

A number of old mines and open cut workings occur within the Sylvester prospect. These mines were developed to work fissure vein style sulphide mineralisation (ref 2.4) that occur in a belt of Oonah Formation between the Tenth Legion and Sylvester Faults (Fig 4.1). The largest of these mines, the South Comstock, Comstock and Boss mines have been extensively studied by Both and Williams (1968), and the following description on the mineralogy of the veins worked in these mines are based on their work.

The mineralogy of the fissure veins are relatively homogeneous, consisting of sphalerite, galena, chalcopyrite and minor amounts of boulangerite and tetrahedrite in a gangue of pyrite, quartz and minor siderite, marcasite and pyrrhotite (Both and Williams, 1968). Pyrite in the fissure veins is typically coarse-grained, and is characterised by a zonal pattern marked by intergrowths of quartz, similar to the pyrite in the Comstock massive sulphide body. Marcasite is extremely rare in the Zeehan field but is relatively common in the veins in the Sylvester prospect. Here, the marcasite replaces pyrrhotite, and is marked by a lamellar textures similar that of marcasite replacing pyrrhotite in the massive sulphide body. The sphalerite, galena, tetrahedrite and boulangerite occur as patches partially replacing pyrite. All four ore minerals are intimately associated, and are parageneticaly related to the same mineralisation stage (Both and Williams, 1968).

Spatially, the pyritic veins are closely associated with the Balstrup and Tenth Legion Faults, with the majority of the veins occurring in the shales and carbonates of the wedge of Upper Oonah Formation between the two faults.

Thus, based on mineralogical and textural similarities between the pyritic fissure veins and the Comstock massive sulphide body, and the close spatial association the Balstrup Fault, it is reasonably to suggest the pyritic veins and the massive sulphide body are genetically related.

CHAPTER SIX

METAL DISTRIBUTION, ASSOCIATIONS AND GRADE

6.1 INTRODUCTION

Metal assay data obtained from diamond drill-holes intersecting the skarn and sulphide mineralisation (SY003-SY014) are used in this chapter to determine; (1) the distribution of metal abundance with respect to skarn and massive sulphide mineralisation, (2) the associations between metals Cu, Zn, Pb, Sn, and W, and (3) the overall grade and resource of the Comstock massive sulphide body.

Diamond drill-holes SY002-SY014 were assayed by R.G.C. Exploration for the elements Cu, Pb, Zn, Ag (AAS-method 101), Sn, W (XRF-method 401), Au, As and Sb (FA/ASS -method 309). Each assay represents the average metal content over one metre. All assay data of selected drill-holes is presented in Appendix C.

6.2 SPATIAL ASSOCIATION OF METALS

Figures 6.1-6.5 illustrate the distribution of metal abundance in selected drill holes SY003, SY005, SY009, SY012 and SY014. This type of plot shows the occurrence of each metal with respect to the different lithology's, skarn assemblages and sections of massive sulphide mineralisation.

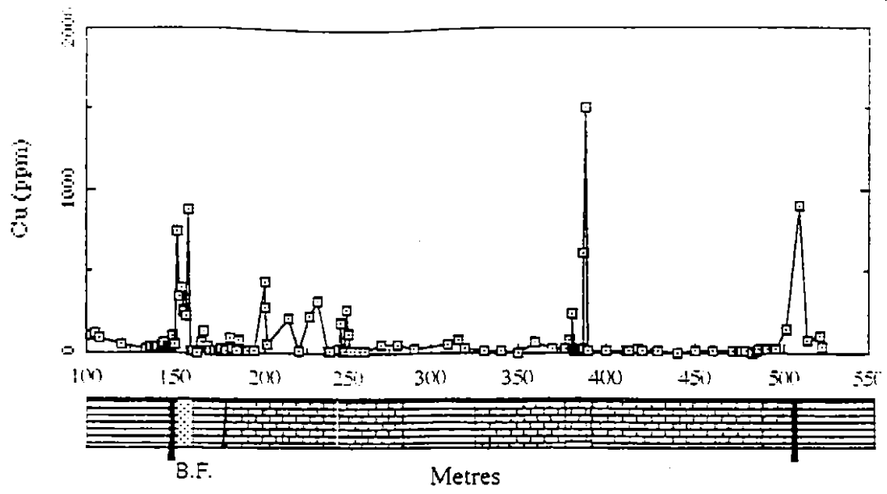

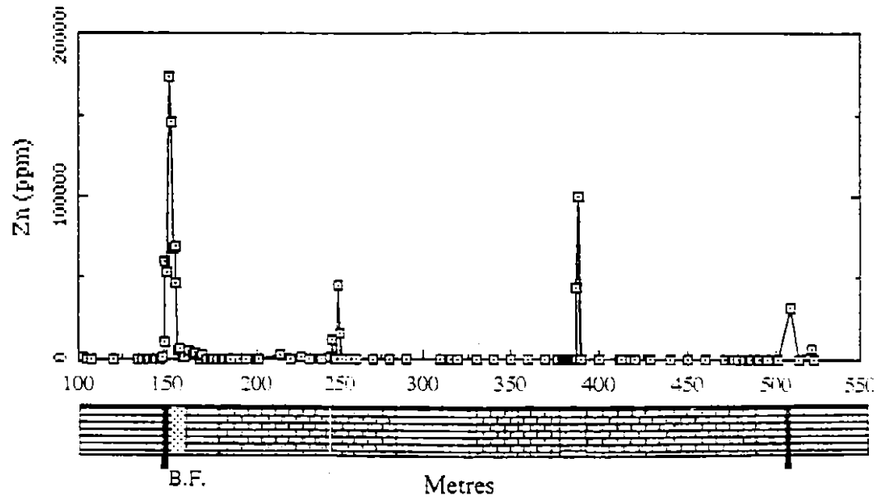

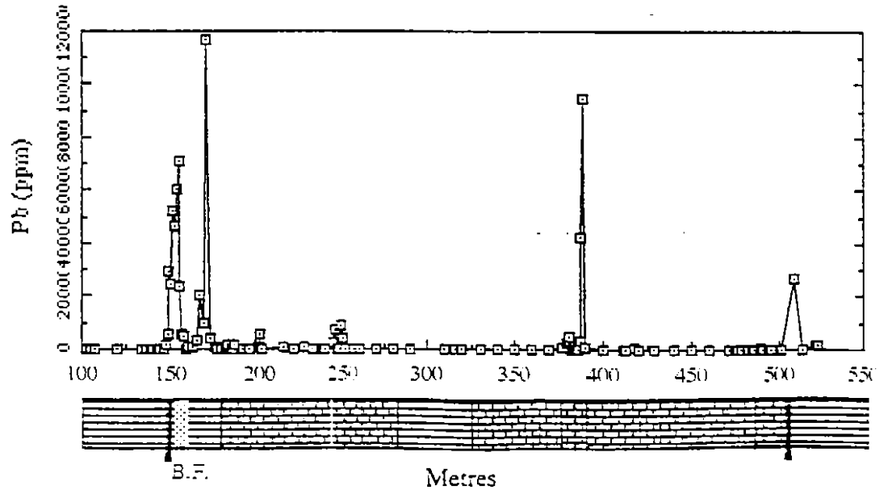

Figure 6.1 Metal distribution in drillhole SY003

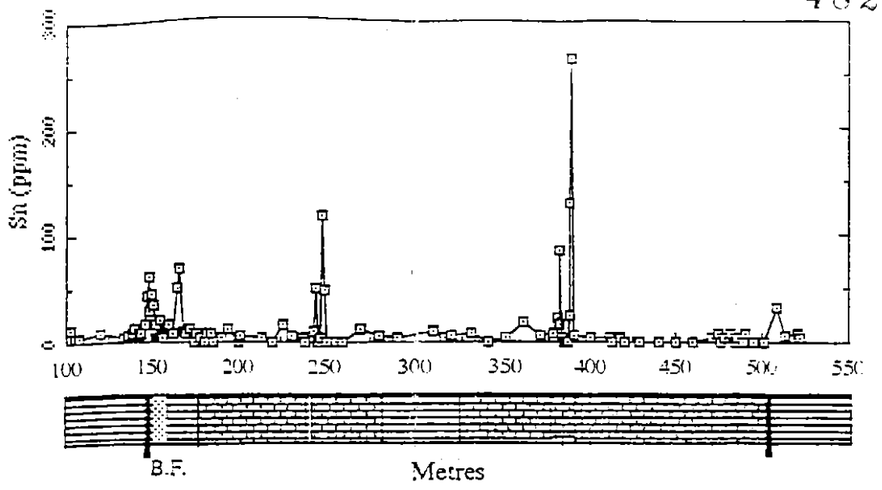

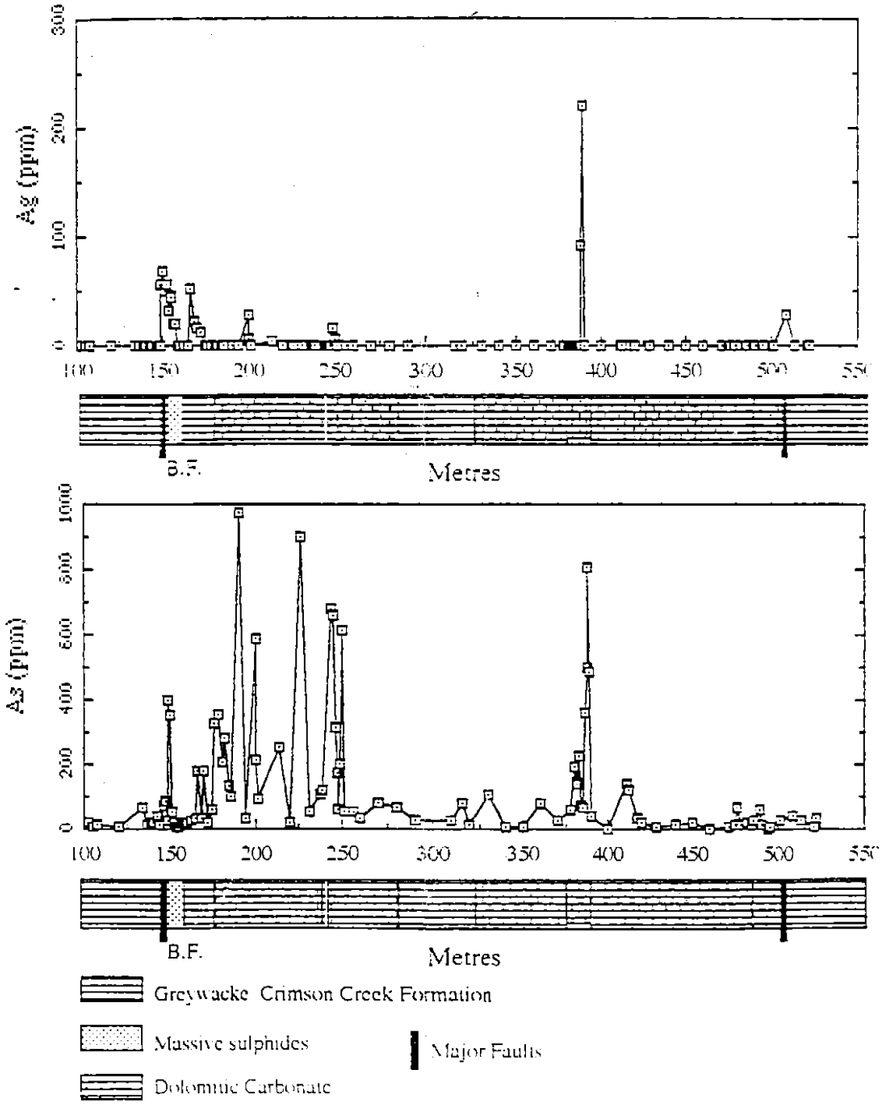

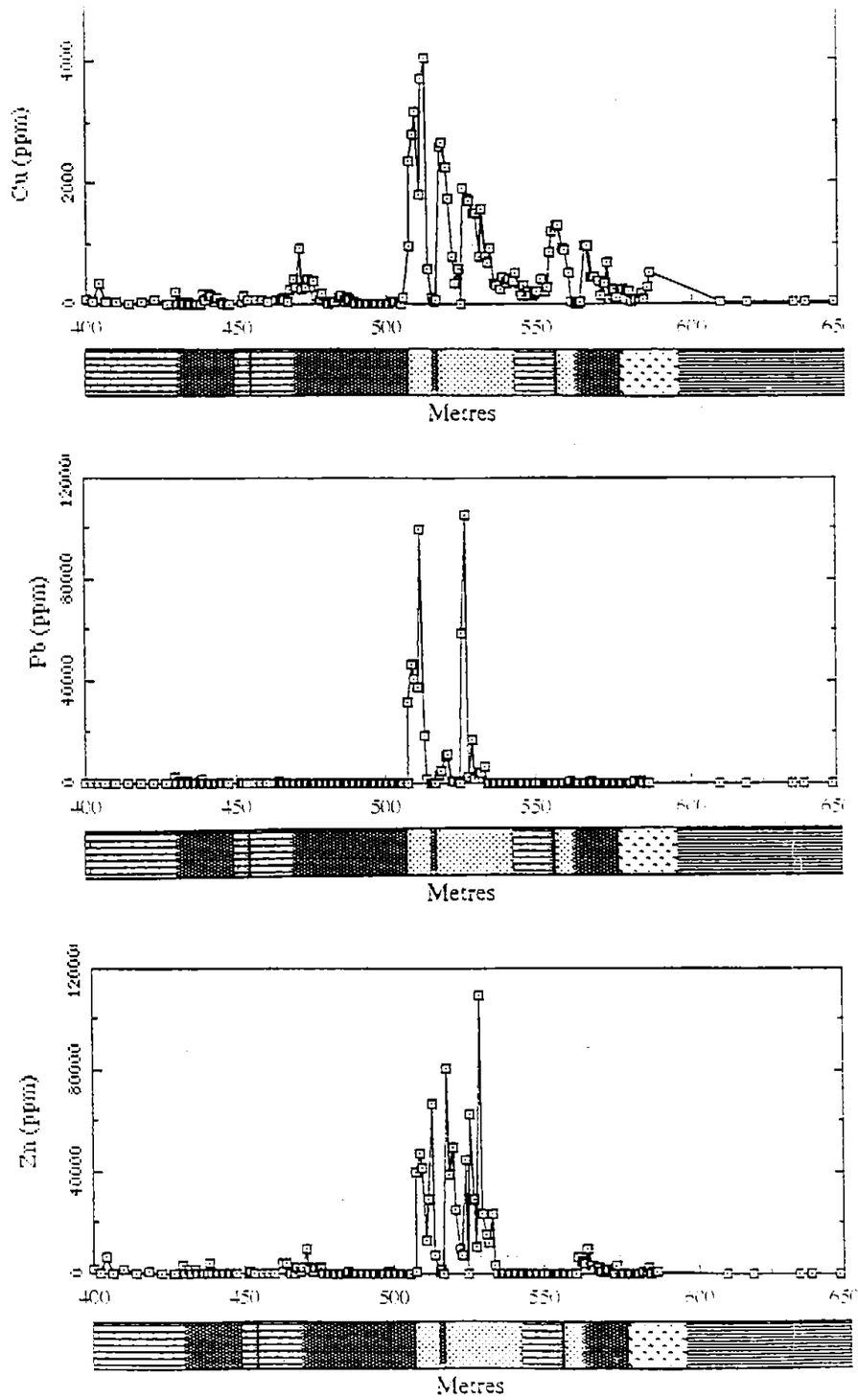

Figure 6.2a Metal distribution in drillhole SY005

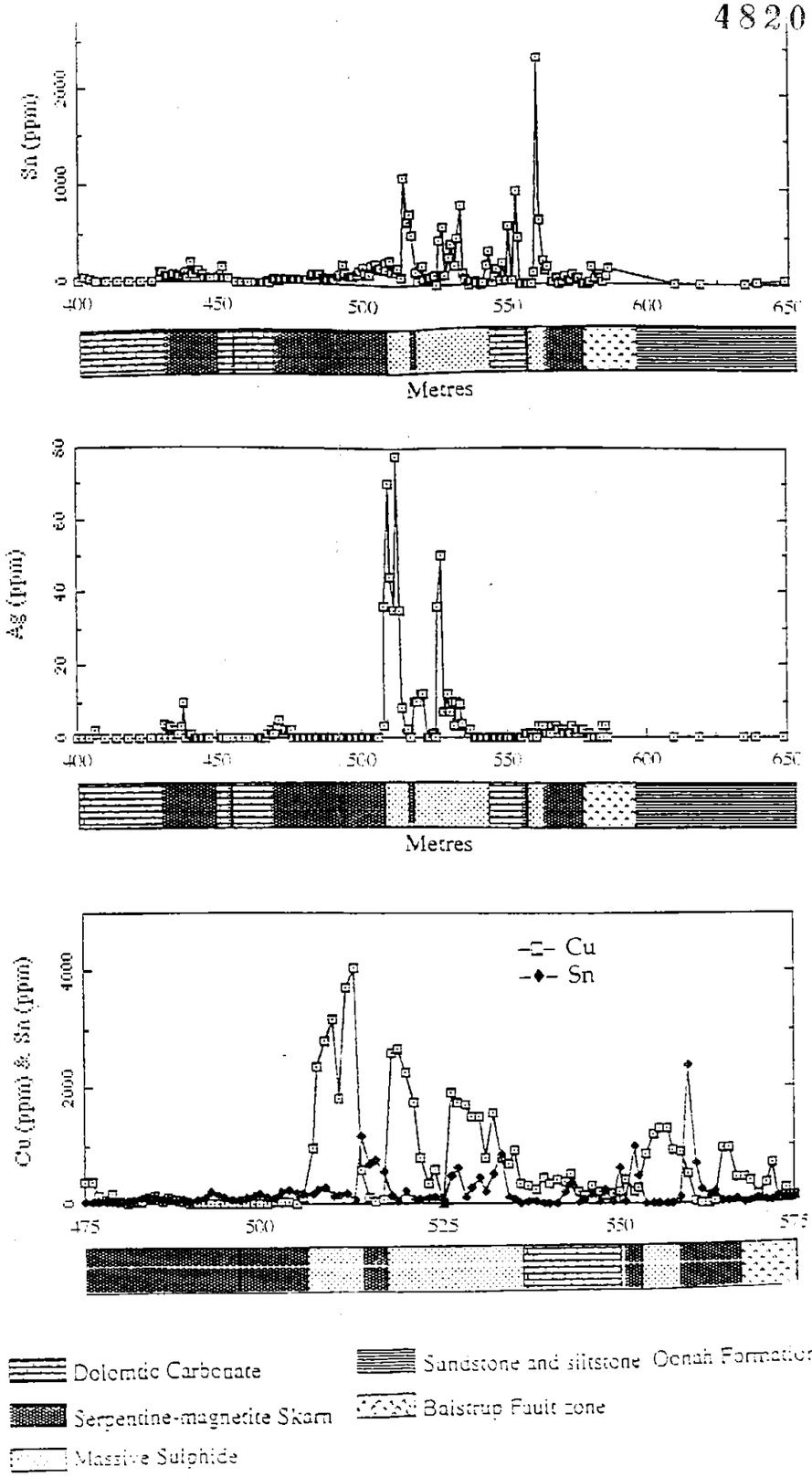

Figure 6.2b Metal distribution of Cu and Sn in the skarn-sulphide interval of drillhole SY005

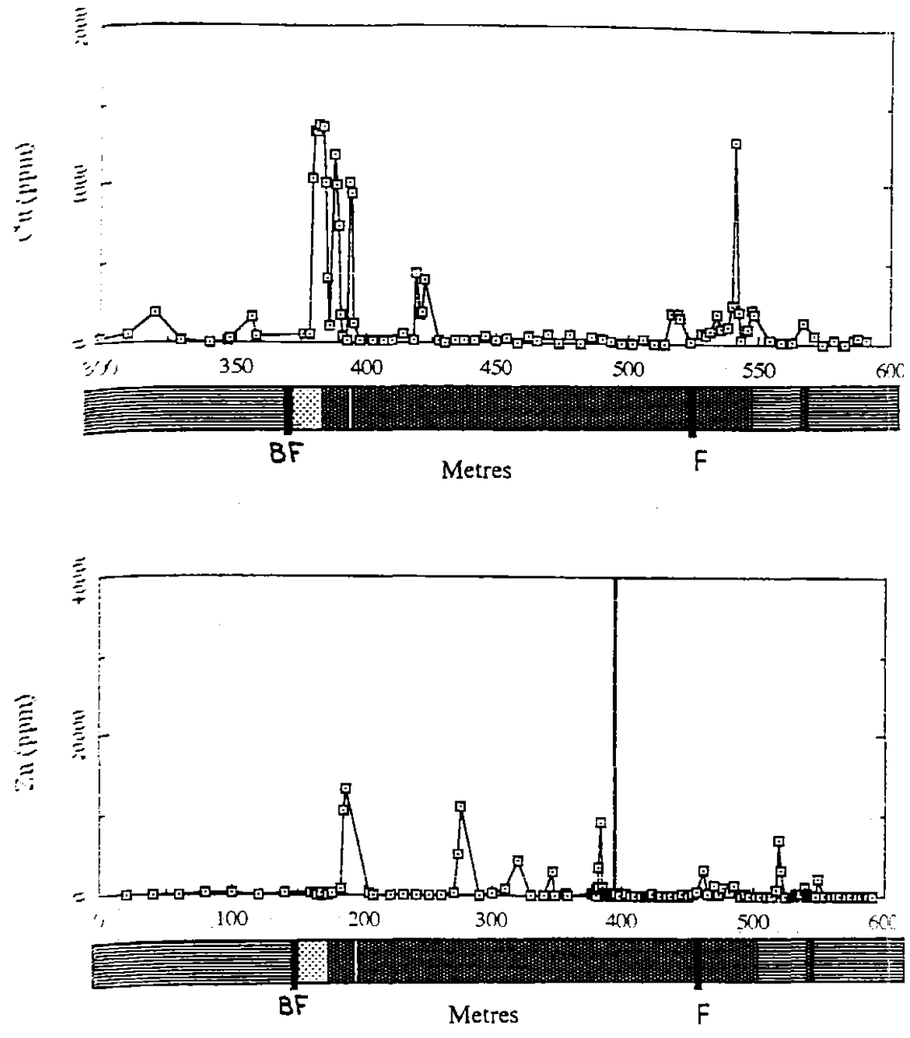

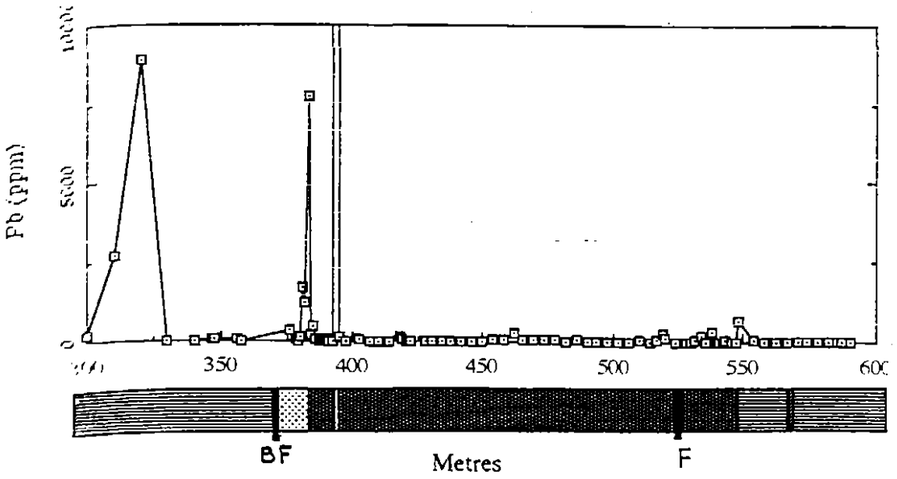

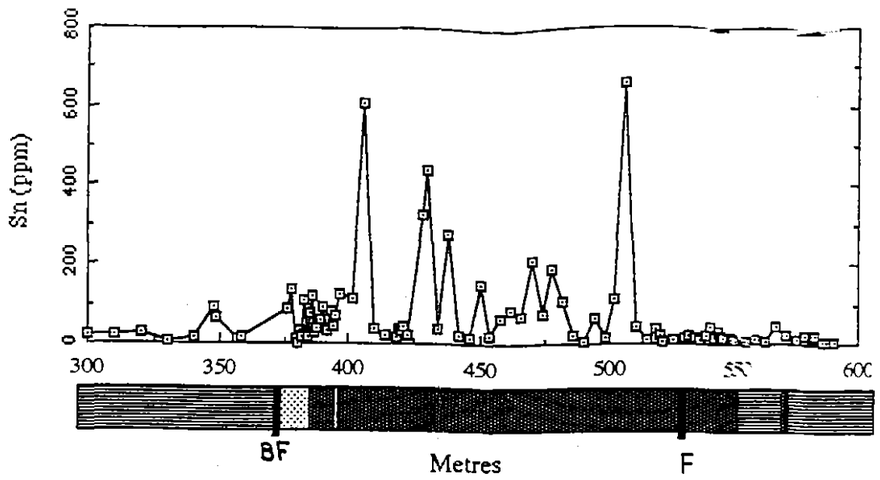

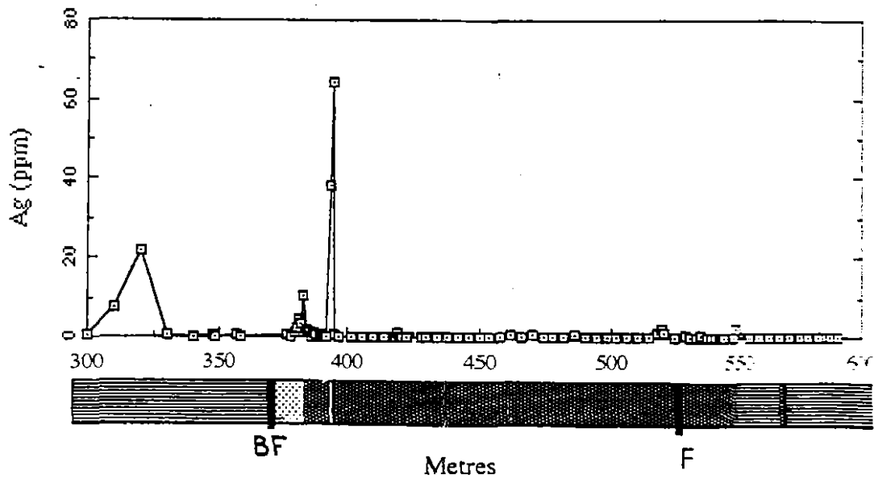

Serpentine-magnetite Skarn

Massive Sulphide

Sandstone and siltstone Oonah Formation

Balstrup Fault zone

Figure 6.3 Metal distribution in drillhole SY009

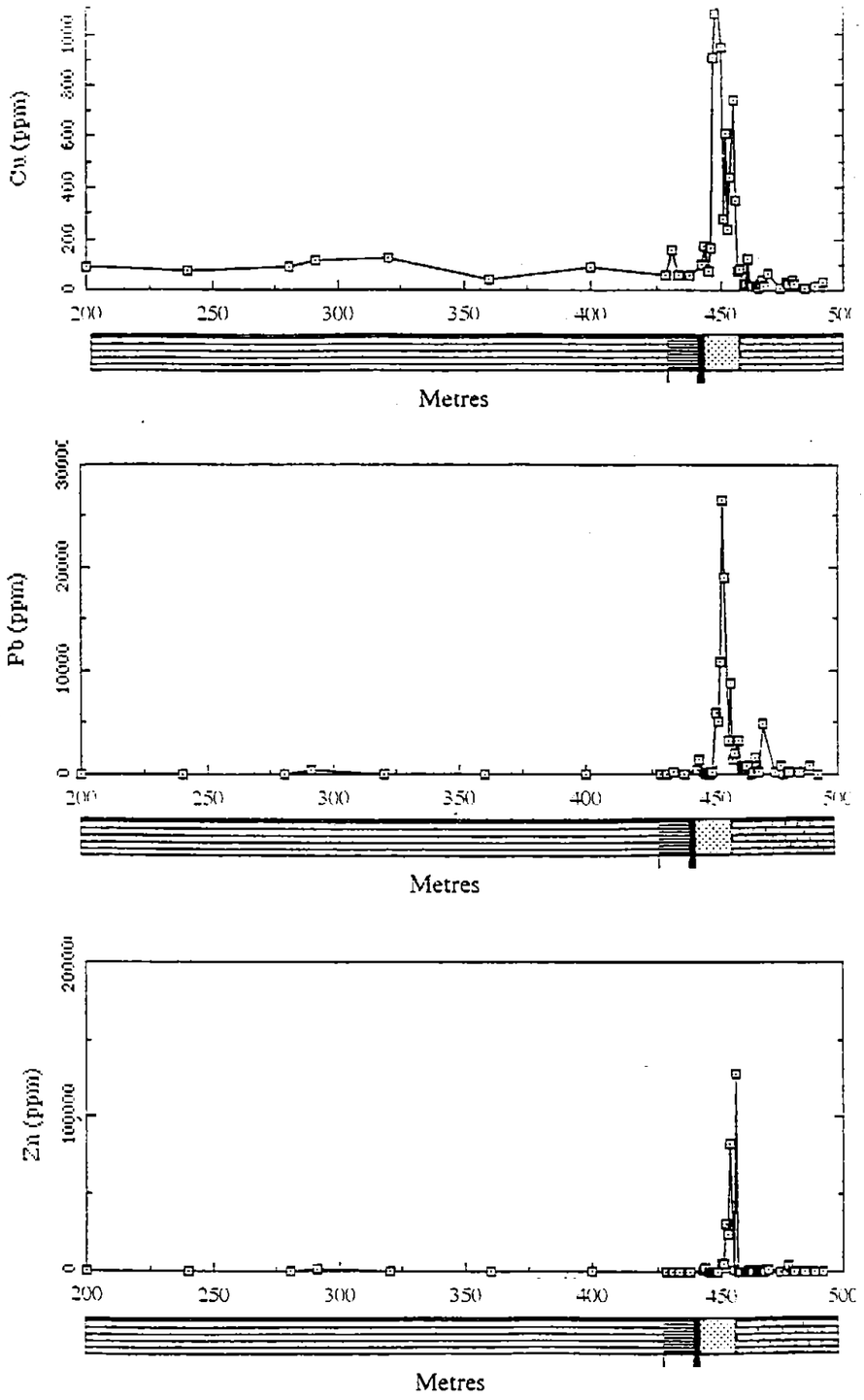

Figure 6.4 Metal distribution in drillhole SY012

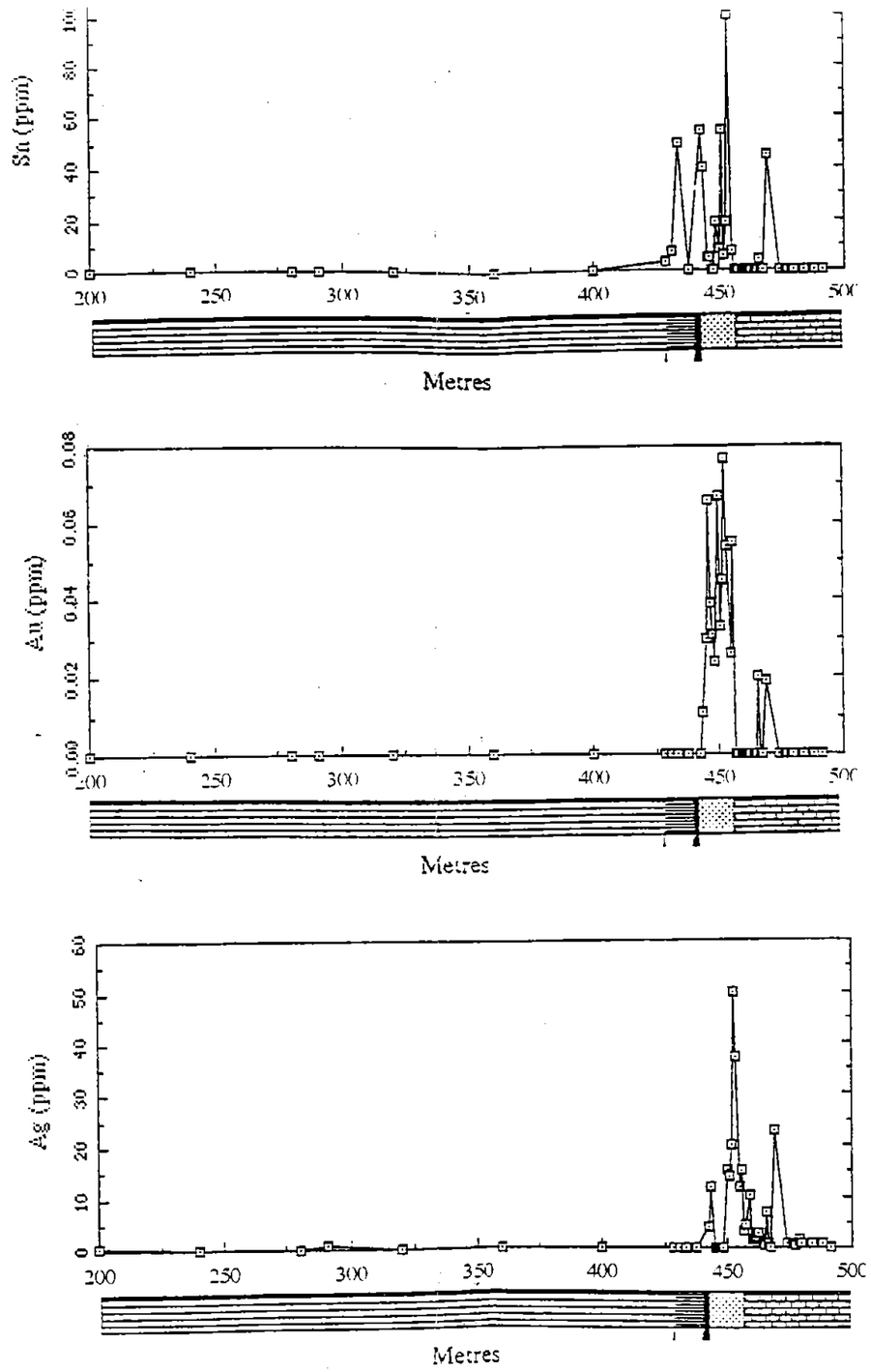

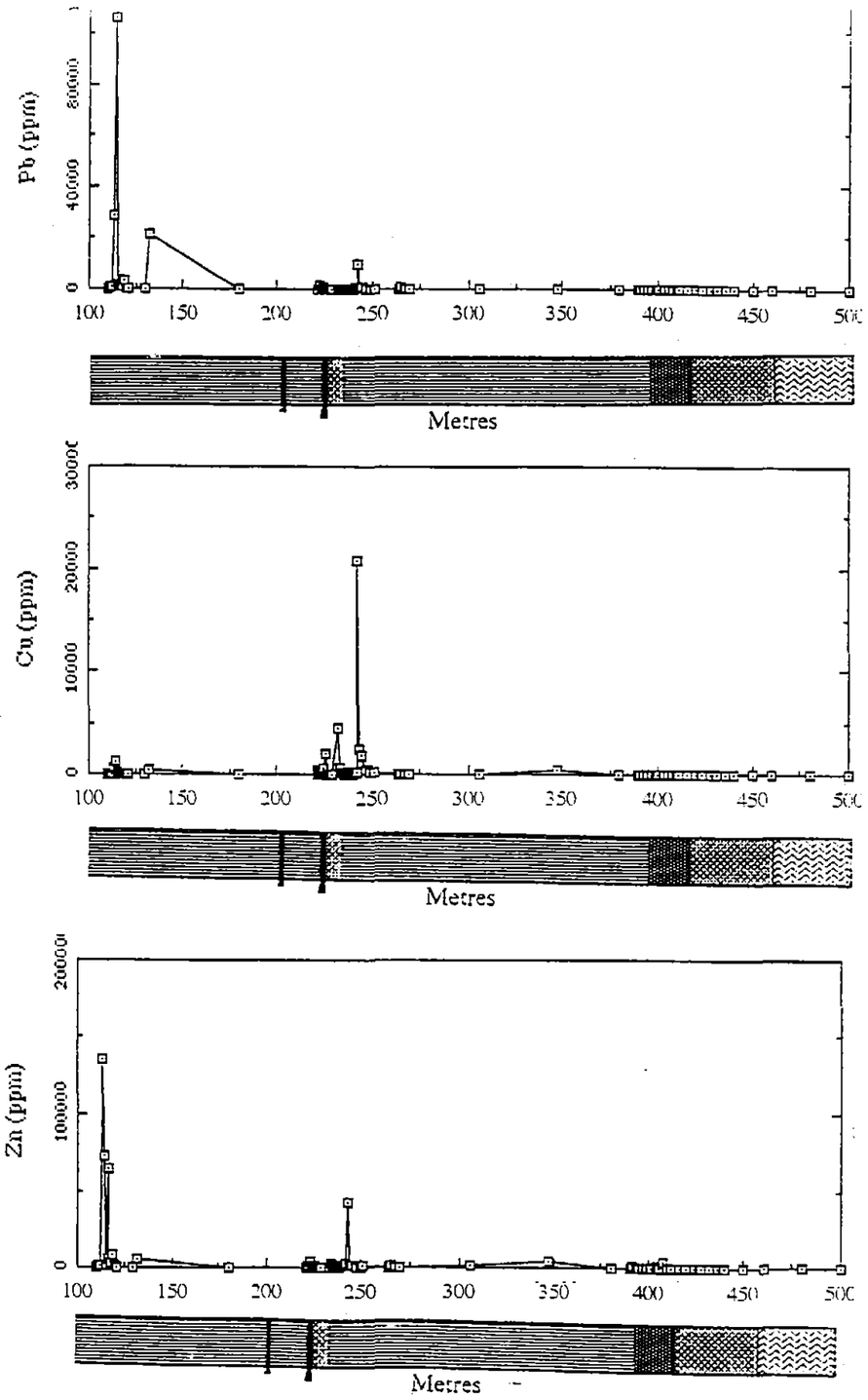

Figure 6.5 Metal distribution in drillhole SY014

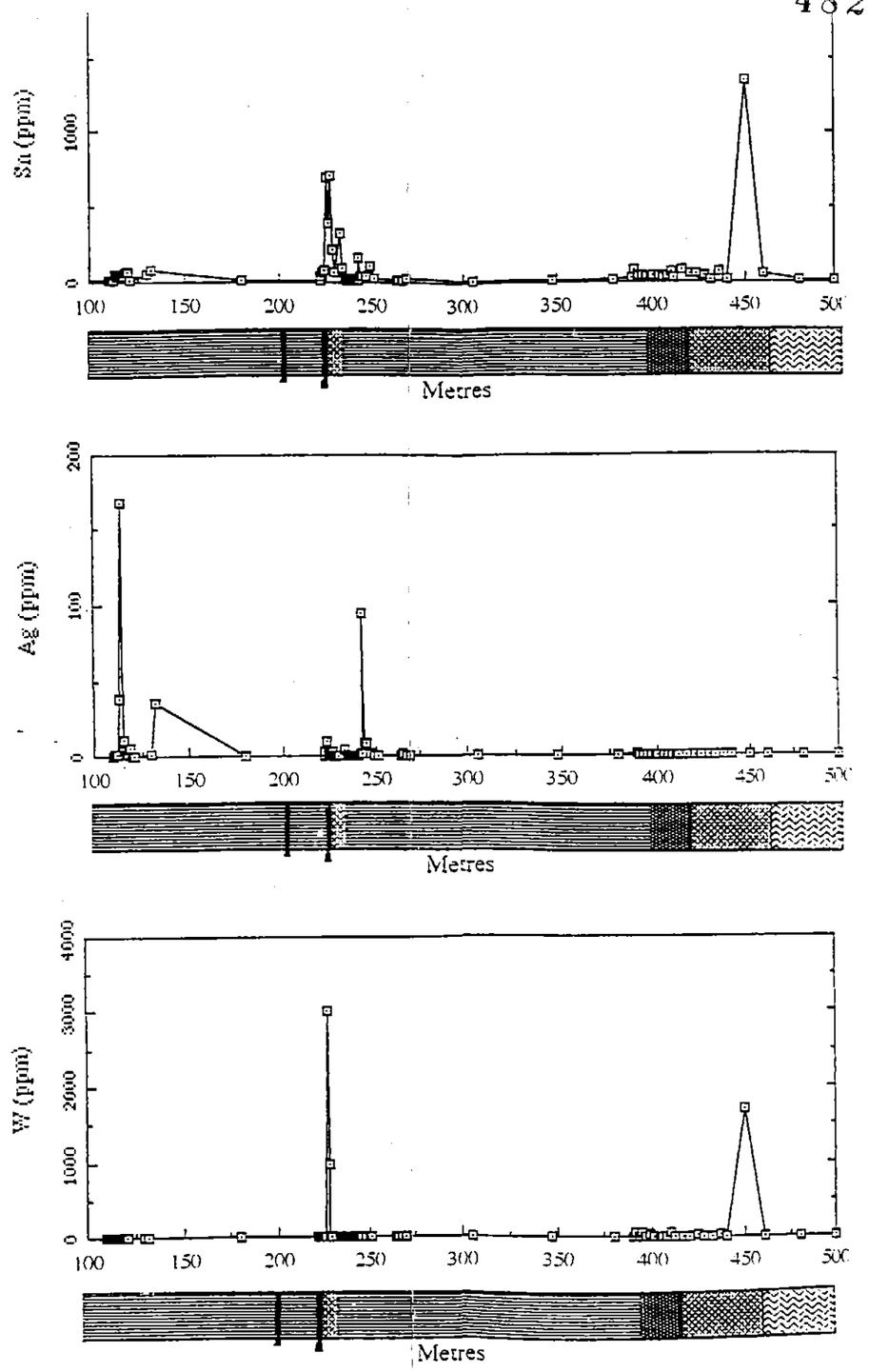

Copper predominantly occurs in the intersections of massive sulphide mineralisation (both massive pyrrhotite (Figures 6.2-6.4) and massive pyrite mineralisation (Figure 6.1)), were it has a strong spatial association with the elements Pb-Zn-Ag. Within intersections of massive pyrrhotite mineralisation copper grades reach a maximum almost ubiquitously toward the outer margins, where the pyrrhotite contacts either carbonate or skarn (eg. Fig. 6.2b). This feature is also prevalent in the distribution of the other major metals Zn, Pb, and Ag. Minor copper grades (<0.005%) occur in sporadic patches throughout dolomitic marble (Fig. 6.1) and Oonah sandstones (Fig. 6.4-6.5). These grades correspond to minor zones of pyritic stockwork veins.

Lead abundances are considerably higher than those of copper, but spatially the two elements are strongly associated. The highest lead grades correspond to the massive pyrite mineralisation (Fig. 6.1), which averages approximately 3% Pb, and stockwork vein which vary between ~0.5% to 3% Pb. The average concentration of lead in the massive pyrrhotite mineralisation varies from 0.6%, reported in SY009 (Fig. 6.3) and SY012 (Fig. 6.4), to 2% reported from SY005 (Fig. 6.2; Table 6.1). Lead occurs only in trace amounts in the skarn mineralisation.

Zinc displays a distribution similar to that of lead. The highest concentrations of zinc correspond with those of lead, but the grades of zinc are consistently double that of lead. In intersections of massive pyrite mineralisation and stockwork zones Zn values can exceed 10%, but on average are around 4 to 6%. The average grades in the massive pyrrhotite zone range from 1.2% (SY009) to 3% (SY005) (Table 6.1). Zinc is also developed to a greater extent in both the early stage and late stage skarn. Although, values in the skarn rarely exceed 0.02%.

LOCATION			ETT CALCULATIONS				AVERAGE GRADES			
Hole	From	To	HT	HD	HB	ETT	Cu	Pb	Zn	Ag
SY003	148.0	158.0	10.2	50.8	187.5	8.76	0.90	3.25	6.41	40.4
SY005	507.4	535.8	28.4	57.0	353.0	5.75	0.15	1.90	2.97	18.3
SY008	129.0	139.9	10.9	52.0	000.5	3.28	—	3.68	5.81	25.0
SY009	378.7	397.1	16.4	73.0	197.3	9.83	0.075	0.60	1.06	8.5
SY012	443.8	457.0	13.2	63.0	204.5	9.47	0.042	0.64	1.31	14.8
OVERALL AVERAGE						7.42		2.02	3.51	21.4

Table 6.1 Grade and thickness calculations for massive sulphide mineralisation. HT = (down) Hole Thickness, HD = Hole Dip, HB = Hole Bearing, and ETT = Estimated True Thickness. (modified after Crossing, 1992).

Tin grades are consistently low, with only peaks of relatively high grades restricted to the late stage skarn mineralisation. Figure 6.2b illustrates the distribution of tin in the large intersection of skarn and massive pyrrhotite. Clearly, the peaks of highest Sn grades correspond to the areas of late stage serpentine-magnetite skarn. Cassiterite has been identified in thin-sections from serpentine and magnetite skarn but typically cassiterite is rare. The majority of tin is in the form of the tin borate (hulsite, ref section 4.3), which has been identified in thin sections in modal concentrations up to 20%. Minor concentrations of tin are also present in the certain zones of the early stage skarn, in particular the garnet-pyroxene skarn (Fig. 6.5). Kwak and Askins (1981) reported garnets from the Moina area containing up to 0.7wt% Sn in

solid solution. Therefore it is possible that Sn grades in the skarn zone correspond to Sn incorporated in the andraditic garnet, however, Sn was not included in the microprobe analysis of garnets in this study.

Silver grades are highest in the massive pyrite mineralisation where values average around 40 ppm. Silver abundance in the massive pyrrhotite mineralisation is generally lower, around 15 to 20 ppm. The distribution of silver follows closely that of lead.

Gold abundance is generally low, averaging only 0.1 ppm, with the exception of 20 ppm recorded in SY003. Although, these values must be viewed with caution as Au grades where generally below detection limits.

Only two holes were assayed for tungsten; SY005 and SY014. The distribution of tungsten in SY014 is identical to that of tin, occurring predominantly in the garnet-clinopyroxene skarn, indicating W^{4+} may also substitute into the lattice of andraditic garnets replacing Fe^{3+} or Ti^{4+} (Kwak and Askins, 1981). The distribution of tungsten in SY005 is restricted to the massive pyrrhotite mineralisation were relatively high grades of 0.15% W are reached.

Arsenic was only assayed in SY003. The distribution and grades of arsenic followed closely that of copper.

6.2.1 Metal Zonation

A weak metal zonation is apparent with respect to Cu and Sn along the strike length of the late stage skarn and massive sulphide body. Copper grades in drill-hole SY005, located at the western end of the sulphide body (Fig. 4.1), are relatively higher, up to 0.2% Cu, compared to grades from drill holes SY009

SY009 and SY012 further east, which have values as high as 0.01% and 0.04%Cu respectively (Table 6.1). Tin grades in the late stage skarn display a similar decrease, from up to 0.02% Sn in SY014 to less than 0.015% Sn in SY012.

A zonation is not reflected in the Pb-Zn grades of the Comstock massive sulphide body. The grades of these metals remain fairly constant, with the Pb:Zn ratio constant around 1:2 throughout the Comstock massive sulphide mineralisation (Table 6.1).

A regional metal zonation is also apparent along the Balstrup-Tenth Legion Faults. This east-west zonation is defined by magnetite-serpentine skarn that is relatively enriched in tin (0.7 to 1% Sn; Dickson, 1981) in the Tenth Legion area, copper dominant massive sulphides associated with magnetite-serpentine skarn further east in the Kynance area (Crossing, 1990), Zn dominant Pb-Zn-Ag massive sulphides and pyritic fissure veins associated with magnetite-serpentine skarn in the Sylvester prospect, and Pb dominant Pb-Zn-Ag veins in the Spray mine area east of the Sylvester prospect (Fig. 4.9).

6.3 METAL ASSOCIATIONS

The metal distribution diagrams indicate that strong similarities exist, at least spatially, between some metals. In this section metal associations are reviewed further through the use of metal grade-metal grade scattergrams.

Figures 6.6-6.10 show a series of metal-metal correlation scattergrams depicting the interrelationships between Cu, Pb, Zn, Ag, Sn, W, As and Sb, for assay data from drill holes SY003, SY005, SY009 and SY012.

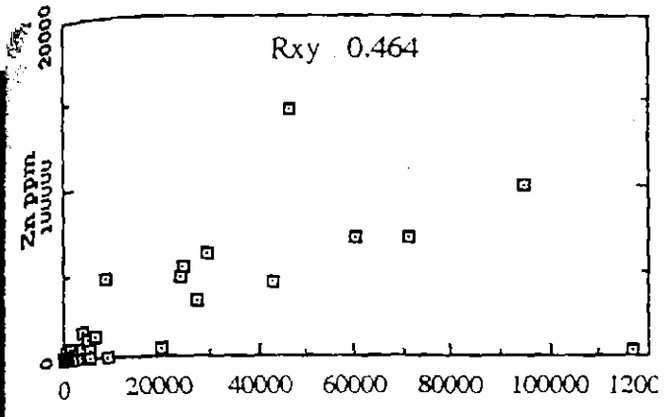

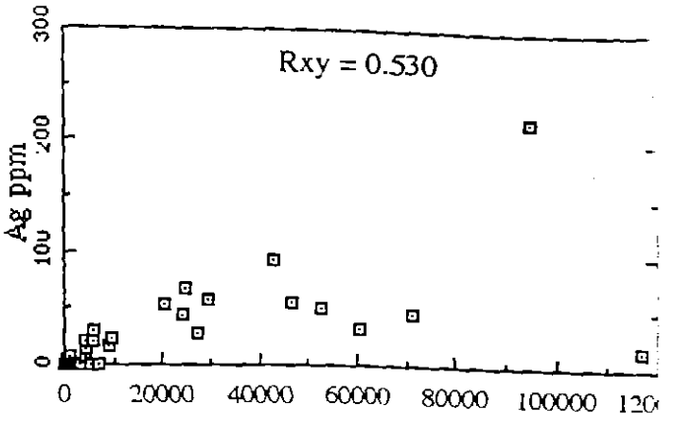

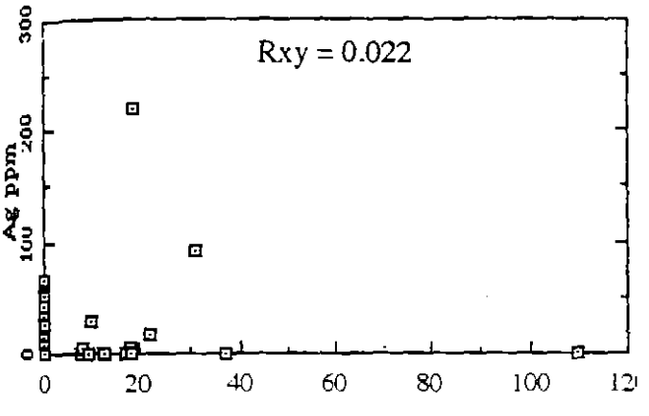

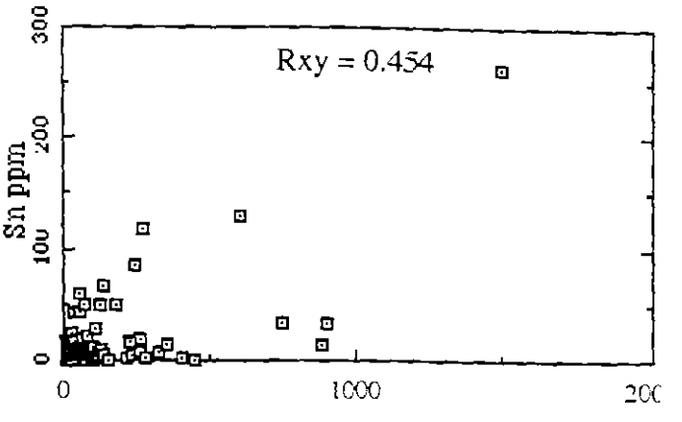

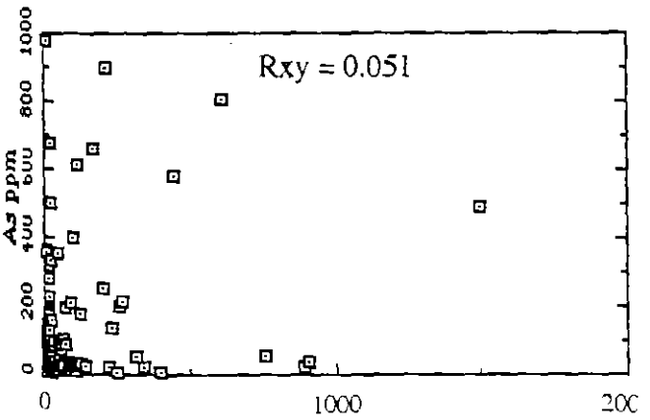

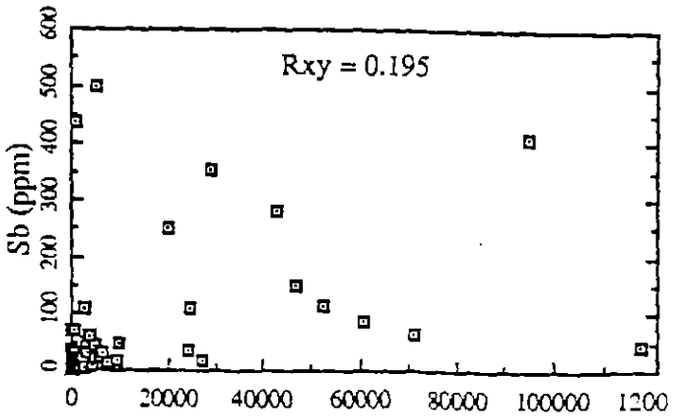

Figure 6.6 Scattergram illustrating the relationships between elements Cu, Zn, Pb, Sn, As, Ag and Au in drillhole SY003. R_{xy} is the correlation coefficent of the axis X and Y.

Above approxiamtely 0.4 indicates a correlation

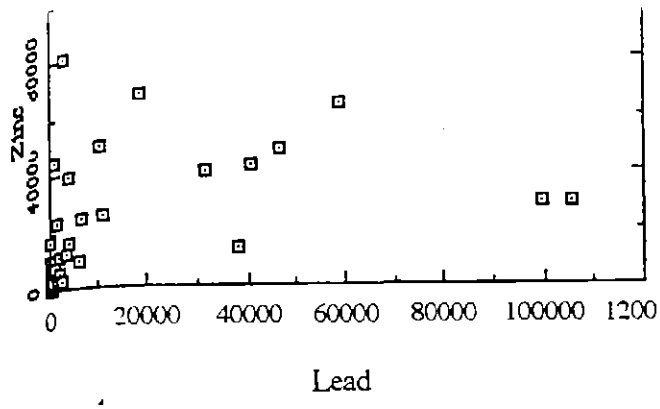

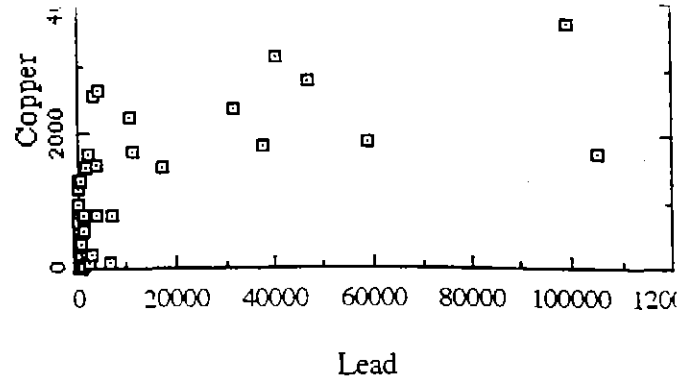

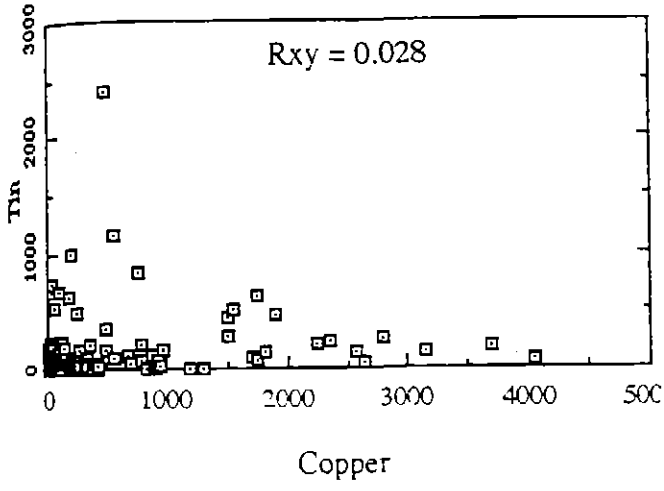

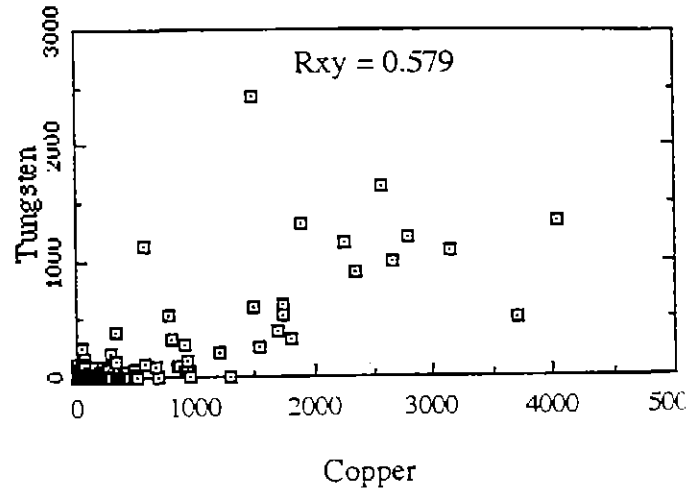

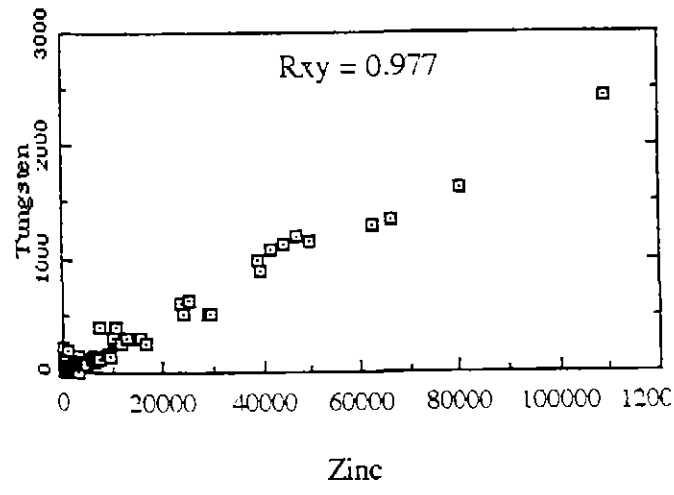

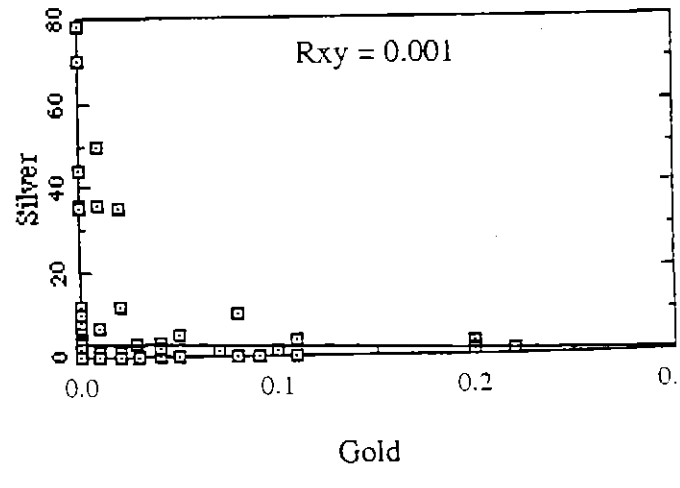

Figure 6.7 Scattergram illustrating the relationships between elements Cu, Zn, Pb, Sn, W, Ag and Au in drillhole SY005. R_{xy} is the correlation coefficent of the axis X and Y. Above approxiamtely 0.4 indicates a correlation

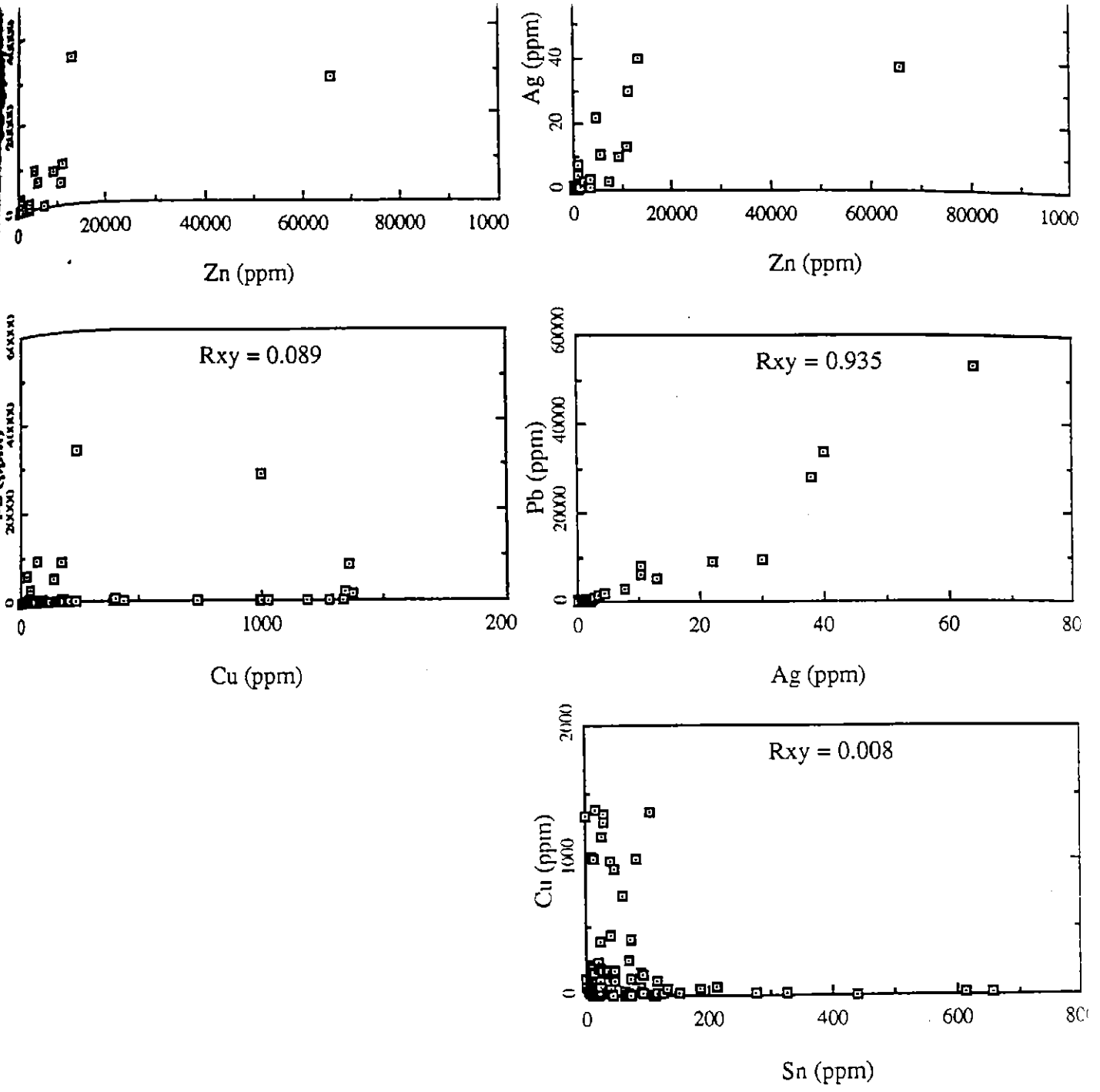

Figure 6.8 Scattergram illustrating the relationship between elements Cu, Zn, Pb, Sn, Ag, and Au in drillhole SY009. R_{xy} is the correlation coefficient of the axis X and Y. Above approximately 0.4 indicates a correlation.

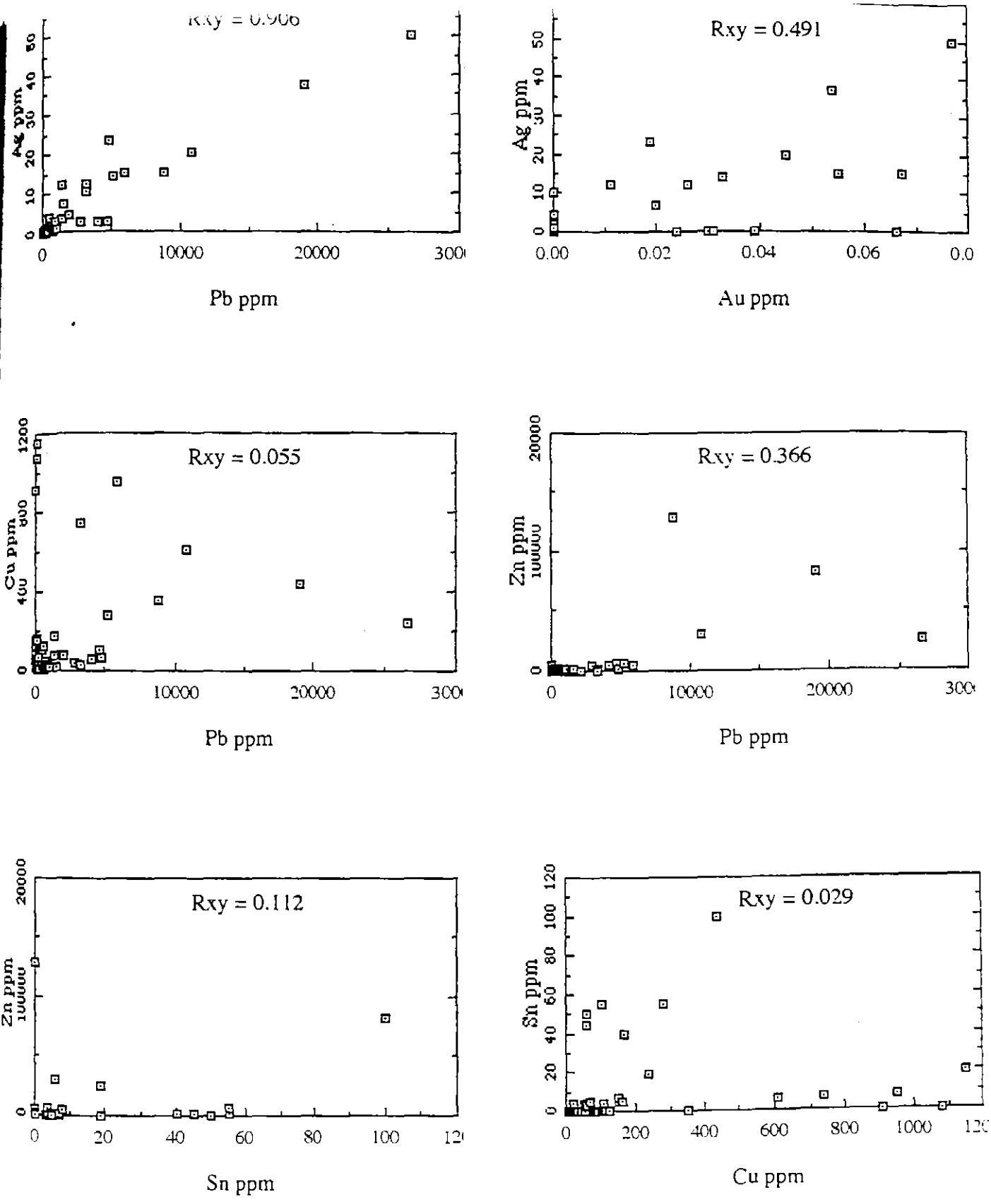

Figure 6.9 Scattergram illustrating the relationships between elements Cu, Zn, Pb, Sn, Ag and Au in drillhole SY012. R_{xy} is the correlation coefficent of the axis X and Y. Above approxiamtely 0.4 indicates a correlation

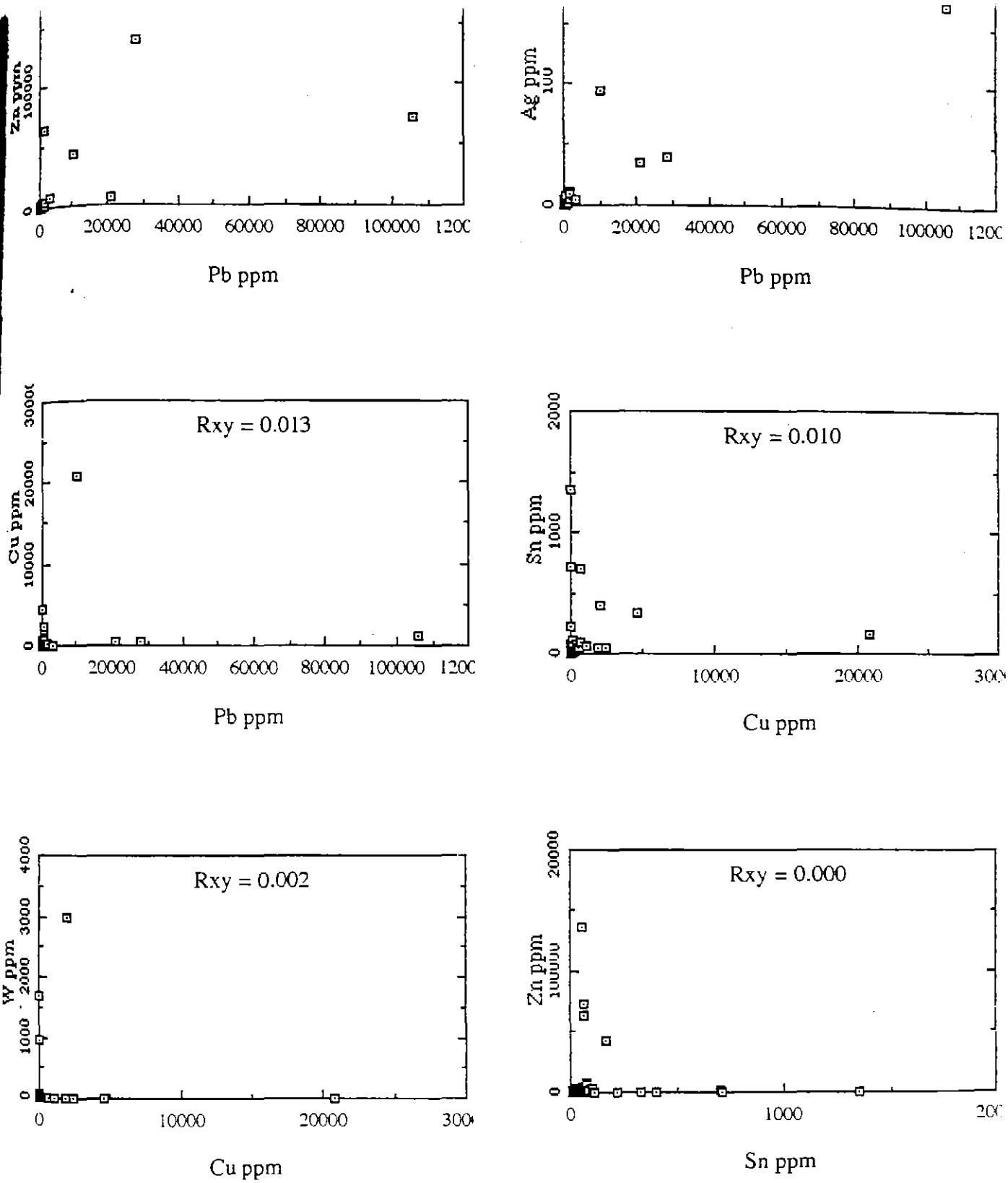

Figure 6.10 Scattergram illustrating the relationship between elements Cu, Zn, Pb, Sn, W, Ag, and Au in drillhole SY014. R_{xy} is the correlation coefficient of the axis X and Y. Above approximately 0.4 indicates a correlation.

Visually, several scattergrams display good to excellent correlation. These being Pb-Zn, Pb-Cu, Pb-Ag, Cu-W, Zn-W (Fig. 6.7 and 6.8), and to a lesser extent As-Cu and Pb-Sb (Fig. 6.6). Conversely, plots of Sn vs (Cu, Zn, Pb, W) and Ag-Au show very poor correlation.

The strong correlation between the metals Cu, Pb, Zn, Ag and As in the massive sulphide mineralisation suggests the sulphide phases chalcopyrite, galena, sphalerite ± arsenopyrite are both spatially and paragenetically strongly associated. This association confirms the close relationship of these phases observed in the ore mineralogical studies of Chapter 5

The very strong association between Ag and Pb is most probably due to the Ag being incorporated in the sulphide galena. Trace element analyses of galena's from other parts of the Zeehan field indicate that up to 0.08% Ag can be accommodated in the galena structure (Both and Williams, 1968). The association between Ag and Sb is similarly as close, indicating that galena may also have a component of antimony. However, the majority of the Sb is likely to be associated with the sulphosalt phase boulangerite ($Pb_2Sb_4S_{11}$), which is observed in the massive pyrite mineralisation. Thus the strong association between the Ag and the Sb is probably due to the close spatial and paragenetic relationship between the galena and boulangerite.

The poor correlation between Sn and the base metals indicates that the majority of tin present in the Sylvester prospect is association with the late stage serpentine and magnetite skarn where it occurs in the form of either cassiterite or tin borates. The poor correlation between Au and Ag indicates that gold is not associated with the main Pb-Zn-Ag mineralisation.

The correlation between W and Zn is unusual. No tungsten bearing minerals were identified in thin section. The form of the tungsten and its close association Zn is unusual. Most likely this close association is due to contamination from a tungsten-carbide mill during commercal sample preperation.

CHAPTER SEVEN

SULPHUR ISOTOPES

7.1 INTRODUCTION

Sulphur isotope analyses were preformed on sulphide minerals from the Comstock massive sulphide body in order to attempt to determine the source of sulphur in the hydrothermal system responsible for the mineralisation, and to identify any isotope variations along the strike length of the sulphide body.

Sulphide samples were selected from drill core that intersected the massive pyrrhotite mineralisation and the pyritic stockwork vein mineralisation. The samples taken from the massive pyrrhotite mineralisation were selected from drillholes along the length of the massive sulphide body.

7.1.1 Procedure

Conventional procedures were employed for the sulphur isotopic analyses. Drilled sulphide mineral separates were combusted with excess CuO in vacuo to produce SO_2 gas (Robinson and Kusakabe, 1975), the gas was then analysed on a VG Micromass 602D mass spectrometer. All anaylsis was preformed in the Central Science Laboratory, University of Tasmania. Results are expressed in terms of conventional per mil deviations ($\delta^{34}S$) relative to the

Cãnon Diablo troilite meteoric standard. The analytical uncertainty is estimated to be ± 0.2 per mil.

7.2 RESULTS

Sulphur isotope analyses for the 15 sulphide samples collected are presented in Table 7.1 and 7.2, and Figure. 7.1. The $\delta^{34}S$ values of the mineralisation fall in the narrow range +3.3 to +7.6‰ . The pyrrhotite and pyrite samples from the massive sulphide body fall in the narrow range +3.3 to +7‰ , with a mode of +6 to +7‰. The 2 pyrite samples from the stockwork vein mineralisation have slightly higher values of +7.5‰ and +7.6‰.

Sample No.	Sulphide	Location	$\delta^{34}S_{CDT}$
T41904	Pyrrhotite	SY009 379.2m	7.0
T41906	Pyrite	SY009 383.5m	6.8
T41913	Pyrrhotite	SY009 394.2m	5.3
T41913A	Pyrrhotite	SY009 394.1m	6.9
T41944	Pyrrhotite	SY009 422.6m	6.9
T41945	Pyrrhotite	SY005 520m	6.8
T41946	Pyrite	SY005 523.3m	6.6
T41947	Pyrrhotite	SY005 539.8m	4.8
T41948	Pyrrhotite	SY005 556.8m	4.8
T41951	Pyrrhotite	SY0010 516m	3.3
T41952	Pyrrhotite	SY012 446.9m	6.6
T41953	Pyrrhotite	SY012 447.9m	6.7
T41954	Pyrite	SY012 460.5m	6.6

Table 7.1 Sulphur isotope analyses of sulphide minerals from massive pyrrhotite mineralsation, Comstock massive sulphide body. All $\delta^{34}S$ values are positive.

Sample No.	Sulphide	Location	$\delta^{34}S_{CDT}$
T41949	Pyrite	SY003 106m	7.6
T41950	Pyrite	SY003 388.5m	7.5

Table 7.2 Sulphur isotope analyses of sulphide minerals from pyritic stock work veins. All $\delta^{34}S$ values are positive.

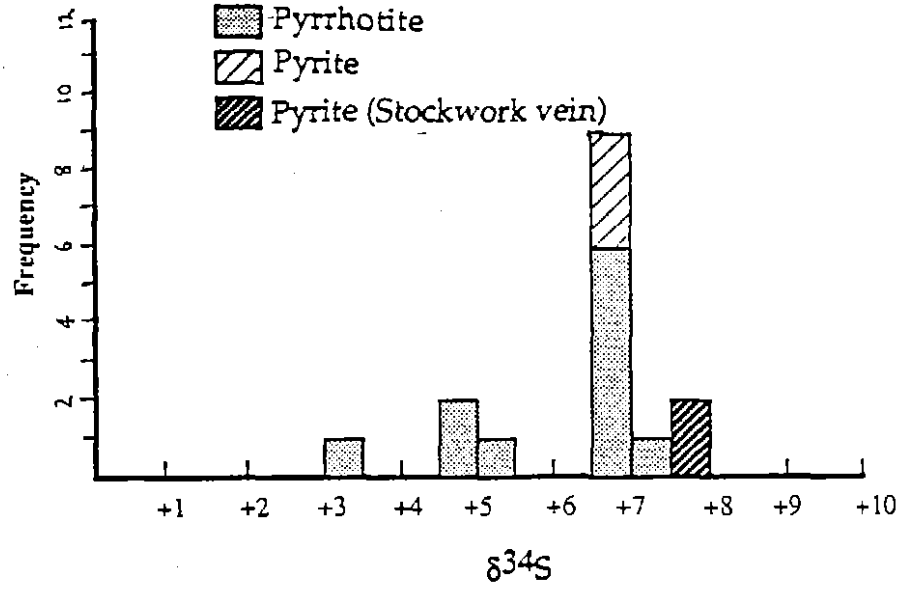

Figure 7.1 Histogram of $\delta^{34}S$ values of sulphides from drill core, Comstock massive sulphide body.

7.3 DISCUSSION

The geographic distribution of $\delta^{34}S$ values along the strike length of the Comstock massive sulphide body is illustrated in Figure 7.2. Even though the $\delta^{34}S$ values from holes SY010 and SY005 are slightly lower than values from holes SY009 and SY012 further to the east, there appears to be no isotopic zonation in the body. This suggests that the sulphur isotopic composition of the mineraliation is uniform, and not influenced by increasing distance from the Heemskirk Granite.

The average $\delta^{34}S$ value of +6 to +7‰ is considerably more positive than for a typical range of $\delta^{34}S$ values encountered in magmatic fluids generated in S-type granites; the typical range being 0±5‰ (Ohmoto, 1986). This implies that the sulphur in the fluids responsible for mineralisation did not orginate from a purely magmatic source. The most likely explaination for the observed values is that the mineralising fluids contained a mixture of sulphur from two sources. One source being magmatic fluids from the Heemskirk Granite and the other source being sulphur leached from the sedimentary pile. Two syngenetic pyrite samples from the Oonah Formation have been analysed by Hijitaheri (1985) and these gave $\delta^{34}S$ values of +18.3‰ and +19.4‰. Thus, mixing of S^{34} enriched sedimentary sulphur with S^{34} depleted magmatic sulphur could conceivably lead to the observed intermediate $\delta^{34}S$ values of +6 to +7‰.

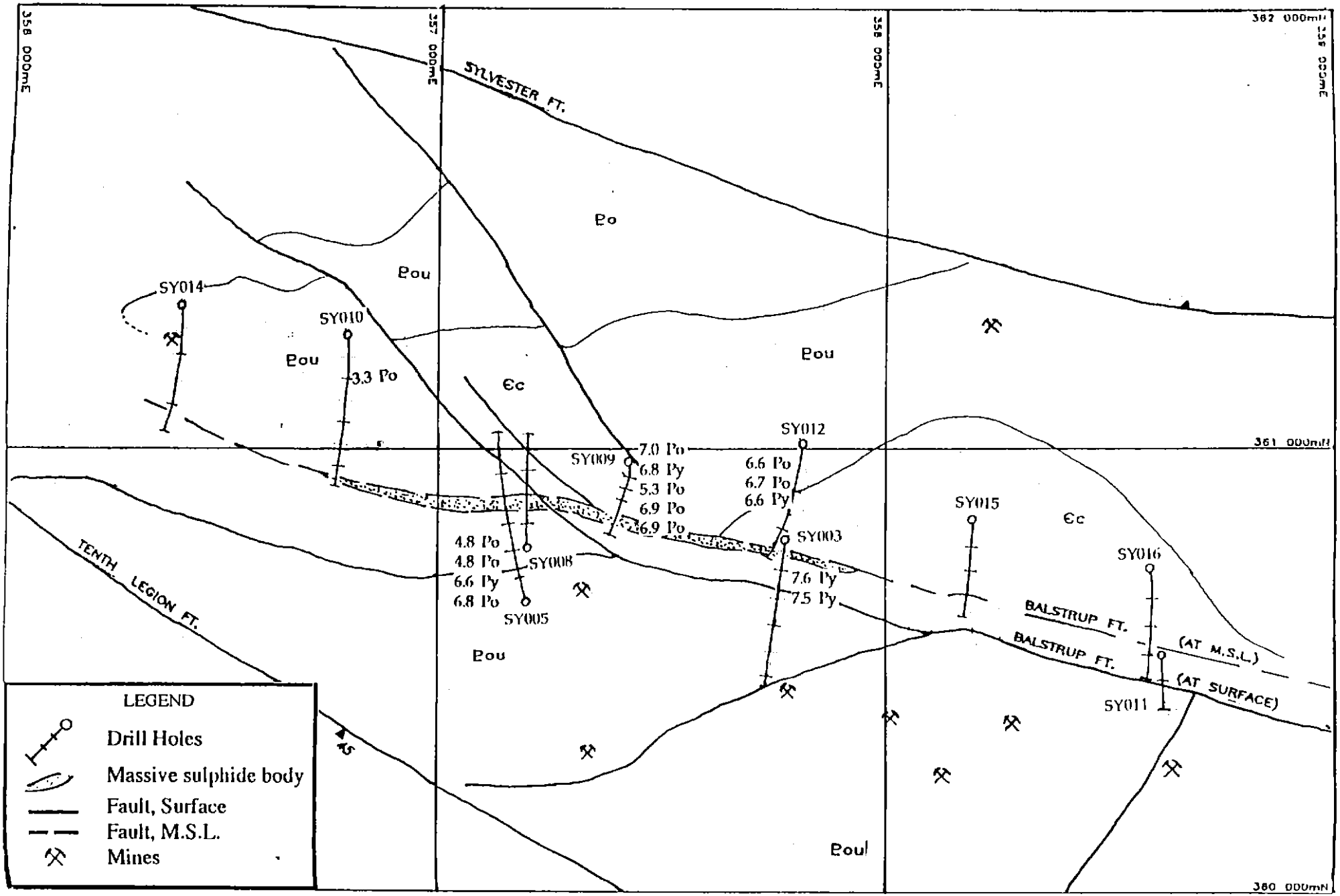

Figure 7.2 Distribution of sulphur isotope values along the Comstock massive sulphide body

The sulphur isotope results are consistent with the hydrothermal system responsible for the mineralisation being generated in the country rock during the emplacement of the Heemskirk Granite, where meteoric fluids, which leached sedimentary sulphur, mix with fluids derived from the underlying granite.

$\delta^{34}S$ values of sulphides from pyritic veins centred on and around the Balstrup Fault (Comstock-Sylvester area) have been analysed by Both et al. (1969). $\delta^{34}S$ values obtained by Both et al. (1969) generally fall in the range of +5‰ to +12‰ . These values correlate well with the $\delta^{34}S$ values for the massive pyrrhotite and stockwork vein mineralisation obtained in this study. Therefore, supporting the suggestion that the veins in the Comstock area are genetically related to the Comstock massive sulphide body.

7.4 SULPHUR ISOTOPE VALUES OF THE ZEEHAN FIELD

A comprehensive analyses of the sulphur isotope compositions of Pb-Zn veins in the Zeehan field has been presented by Both et al. (1969). The distribution of sulphur isotope values in the Zeehan field produced by Both et al. (1969) is shown in Figure 7.3. The distribution of values in the field show a pattern from low values (< 4‰) in the north east, centred on the Queen Hill area, to higher values in the area south of the Balstrup Fault. Both et al (1969) interpretated this distribution of values as "a decline in $\delta^{34}S$ values with increasing distance from a source that lies in the south-west part of the field". Solomon (1981) reinterpreted this data suggesting that the entire field is hydrologically symmetrical, related to fluids that emanated from, and circulated around, a cupola situated below the Queen Hill area. The low $\delta^{34}S$ values representing magmatic dominant fluids. The only anomaly to this

model, according to Solomon (1981), was the relatively high values from deposits in the Comstock-Sylvester area. However, if it is assumed that the Pb-Zn veins centred on the Balstrup Fault are associsated with the Comstock massive sulphide mineralsation, these higher values can be explained as being related to the same hydrothermal system, which leached sulphur from the sedimentary pile and mixed with sulphur from fluids derived from the Heemskirk Granite.

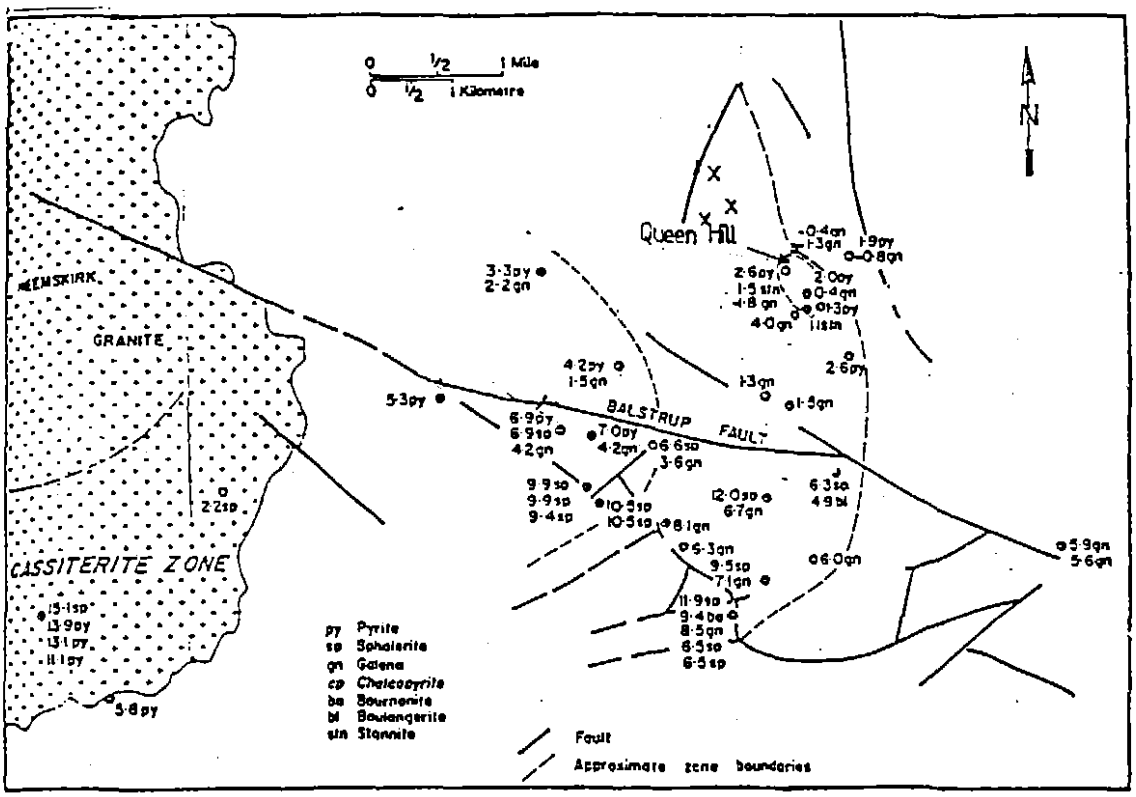

Figure 7.3 Distribution of sulphur isotope analyses in the Zeehan field.

After Both et al. (1969)

5 cm

CHAPTER EIGHT

CARBON AND OXYGEN ISOTOPES

8.1 INTRODUCTION

Carbon and oxygen isotope studies were conducted on a limited number of carbonate samples from the late stage skarn mineralisation and the dolomitic marble, with the principal aims of defining the relationships between the skarn associated carbonate and the dolomitic marble, and the origins of the late stage skarn fluid.

Seventeen carbonate mineral samples were analysed for their carbon and oxygen isotope compositions. Eleven samples were selected from the dolomitic marble. Six samples of calcite were selected from within the massive serpentine-magnetite skarn. Table 8.1 indicates the sample localities.

8.1.1 Procedure

Isotopic analyses were made by standard techniques. Drilled carbonate mineral separates were dissolved to produce CO_2 gas (McCrea, 1950), the gas was analysed on a VG Micromass 602D mass spectrometer in the Central Science Laboratory, University of Tasmania. The carbon isotopes values are reported in the conventional δ expression in per mil unit relative to the PDB standard. The oxygen isotope values are reported in the conventional δ expression in per mil unit relative to the SMOW standard.

8.2 RESULTS

The $\delta^{13}C$ and $\delta^{18}O$ values obtained for the carbonates analysed are presented in Table 8.1 and Figure 8.1. Two zones of values emerge from the data. The $\delta^{13}C$ values in zone A range from -0.8 to +3.5‰ and the $\delta^{18}O$ values, from +11.2 to +24.6‰. In zone B the $\delta^{13}C$ values range from -2.6 to -4.6‰ and the $\delta^{18}O$ values from +3.8 to +8.2‰ (Fig. 8.1).

Sample No.	Style	Location	$\delta^{13}C_{PDB}$‰	$\delta^{18}O_{SMOW}$‰
T41910 A	dolomite	SY009 390.2m	0.020	11.20
T41910 B	calcite	SY009 390.2m	-2.63	6.40
T41910 C	calcite	SY009 390.3m	-2.90	3.88
T41917	dolomite	SY009 413.9m	1.63	15.76
T41922	dolomite	SY009 425.8m	0.98	12.70
T41925	dolomite	SY009 440.5m	1.35	13.67
T41935	calcite	SY014 393.1m	-4.04	13.72
T41956	dolomite	SY009 506.5m	1.75	17.07
T41958	dolomite	SY011 132.1m	-0.095	21.60
T41959	calcite	SY016 333.1m	-3.50	8.17
T41961	dolomite	SY003 244m	3.53	24.68
T41963	dolomite	SY003 470.1m	-0.84	16.57
T41964	dolomite	SY005 460.2m	2.15	16.63
T41965	dolomite	SY005 463.2m	2.32	19.60
T41966 A	calcite	SY010 562.1m	-4.66	7.90
T41966 B	calcite	SY010 562.2m	-3.64	7.405
T41967	dolomite	SY012 448m	-0.04	15.66

Table 8.1 Carbon and oxygen isotopic compositions of carbonates from the Sylvester prospect

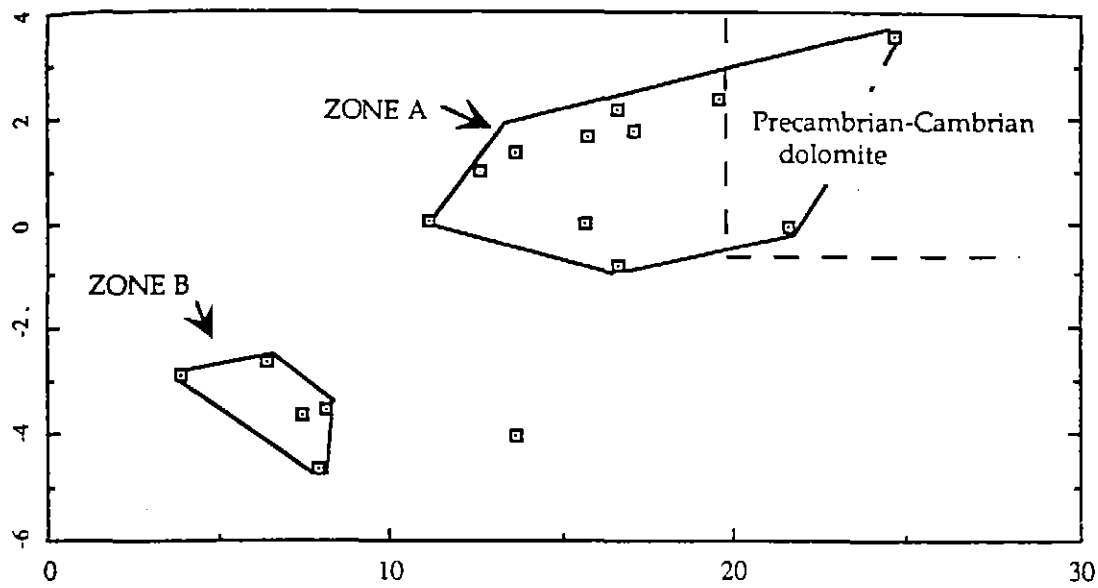

Figure 8.1 Plot of $\delta^{13}C$ vs $\delta^{18}O$ values for carbonates in the Sylvester prospect. Precambrian-Cambrian dolomite box after Viezers and Hoefs (1976).

8.3 DISCUSSION

The isotopic compositions of carbonate samples from the unmetasomatised but contact metamorphosed Oonah dolomite all fall within zone A. The $\delta^{13}C$ and $\delta^{18}O$ values of the dolomite in zone A shows some degree of overlap with the typical $\delta^{13}C$ and $\delta^{18}O$ values of Precambrian-Cambrian dolomites (Viezer and Hoefs, 1976), and overall show slight depletions in ^{18}O and particularly ^{13}C. The isotopic composition of calcites from within the metasomatic skarn (zone B), here after termed skarn calcite, are strikingly different to that of dolomitic marble, being considerably depleted in both ^{13}C and ^{18}O.

Depletions in ^{13}C and ^{18}O of skarn calcite relative to marble have been observed by several workers (Shieh and Taylor, 1969; Taylor and O'Neil, 1977). Such depletions have been ascribed to decarbonation during the

replacement of marble by skarn; whereby carbon and oxygen are removed from the carbonate mineral by evolving CO_2 enriched in ^{13}C and ^{18}O. The progressive depletions in ^{13}C and ^{18}O during decarbonation (assuming Rayleigh distillation) cannot, however, produce the very depleted values of skarn calcite (Ohmoto, 1986). Decarbonation does produce a certain degree of depletion of ^{13}C and ^{18}O in calcite, and this is probably the case for the more depleted values in zone A trending away from the typical Precambrian-Cambrian dolomite values. However, to obtain values as depleted as those of skarn calcite it is inferred that an infiltration of ^{13}C and ^{18}O depleted fluid is nescessary (eg. metasomatic fluid) (Ohmoto, 1986).

Brown et al (1985) demonstrated that values of skarn calcite could be explained by interaction between marble and large volumes of fluid in equilbruim with fluids derived from a igneous source, thus suggesting a magmatic source for the carbon and oxygen. The ^{13}C and ^{18}O values of calcite precipitating from a "so-called" magmatic fluid ($\delta^{13}C$ -5±2.5‰, $\delta^{18}O$ +5~10‰) at various temperatures are shown in Figure 8.2. The values of $\delta^{18}O$ and ^{13}C ($\delta^{18}O$ in particular) from this study show only slight overlap with the range of $\delta^{18}O$ and ^{13}C values expected for magmatic calcites at the temperatures that broadly correspond to late stage skarn formation (assuming a temperature for late stage skarn formation of 400 to 200°C, as presented in Chapter 4), indicating only a tentative correlation for magmatic fluids being the source of calcite .

An alternative explanation for such a ^{18}O depleted skarn forming fluid could be the involvement of meteoric water. Shimazaki et al. (1986) and Layne et al. (1991) have suggested the involvement of meteoric waters, which are equilibriated with dolomite at higher temperature, mixing with igneous fluids to explain the $\delta^{18}O$ values present in hydrous skarns. Thus, given the close

association of late stage skarn formation and sulphide deposition, it would seem resonable to suggest the fluids responsible for both stages had a large component of meteroic water. This conclusion agrees favaroubly with the interpretation from the $\delta^{34}S$ data (Chapter 7).

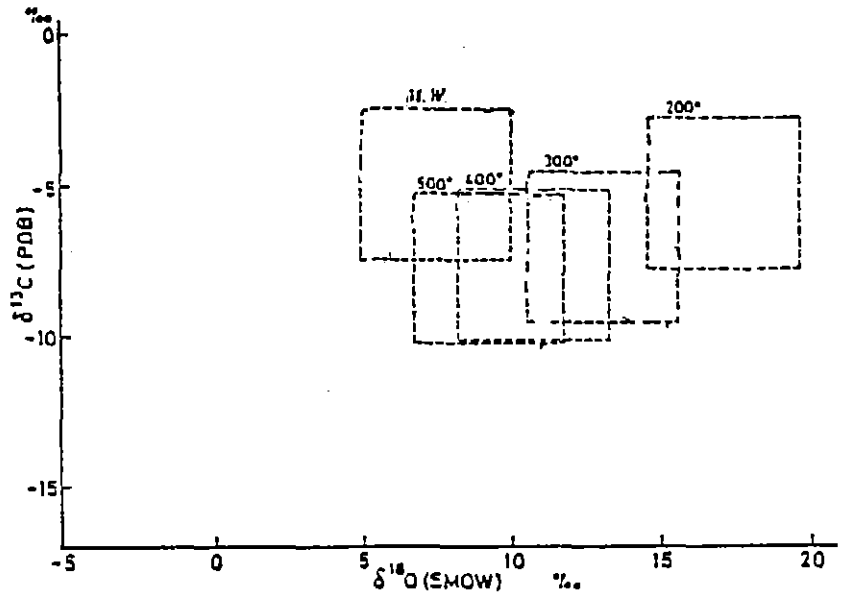

Figure 8.2. Isotopic ranges of calcite expected to precipitate from the magmatic water solution (M.W.) at the indicated temperatures. (modified after Shimazaki etal.,1986).

8.4 CLASSIFICATION

The carbon and oxygen isotopic compositions of skarn calcites may also be used as a means of classification among the major skarn classes (Shimazaki et al., 1986). The isotopic composition of the skarn calcite in the Sylvester prospect fall well within the Pb-Zn zone (Fig. 8.3).

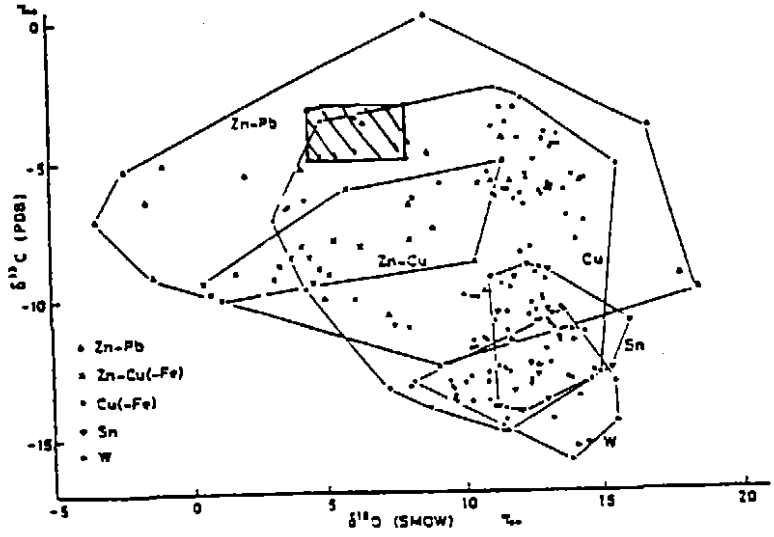

Figure 8.3 $\delta^{13}C$ vs $\delta^{18}O$ values of skarn calcite from the major skarn classes. Based on skarn calcite from Japanese skarn deposits. (after Shimazaki et al., 1986). Calcite from the Sylvester prospect is indicated by a box.

CHAPTER NINE

CONTROLS ON MINERALISATION

9.1 STRATIGRAPHIC CONTROLS

The majority of skarn and massive sulphide mineralisation in the Sylvester prospect, with the exception of scattered occurrences of pyrrhotite mineralisation, is within carbonate beds of the Upper Oonah Formation. This restriction of skarn and sulphide mineralisation to carbonate units indicates the importance of favourable strata as a control on mineralisation.

The favourability within the Upper Oonah Formation is further illustrated by the morphology of the Comstock massive sulphide mineralisation. The subdivision of the body into sulphide lenses (Fig. 9.1-9.2), indicates that deposition of the sulphide mineralisation occurred in selective portions of the carbonate unit. The controlling factors for this selectivity of deposition environment is most probably a function of the composition of the carbonate unit, and the permeability of the unit. These two factors would have the effect of forcing fluids to migrate along bedding planes. Similar selectivity of depositional environment is shown by the late stage skarn, but to a much lesser extent.

The presence of hornfelsic pelites underlying carbonate beds in regions of early stage calc-silicate skarn is another feature of the stratigraphy that

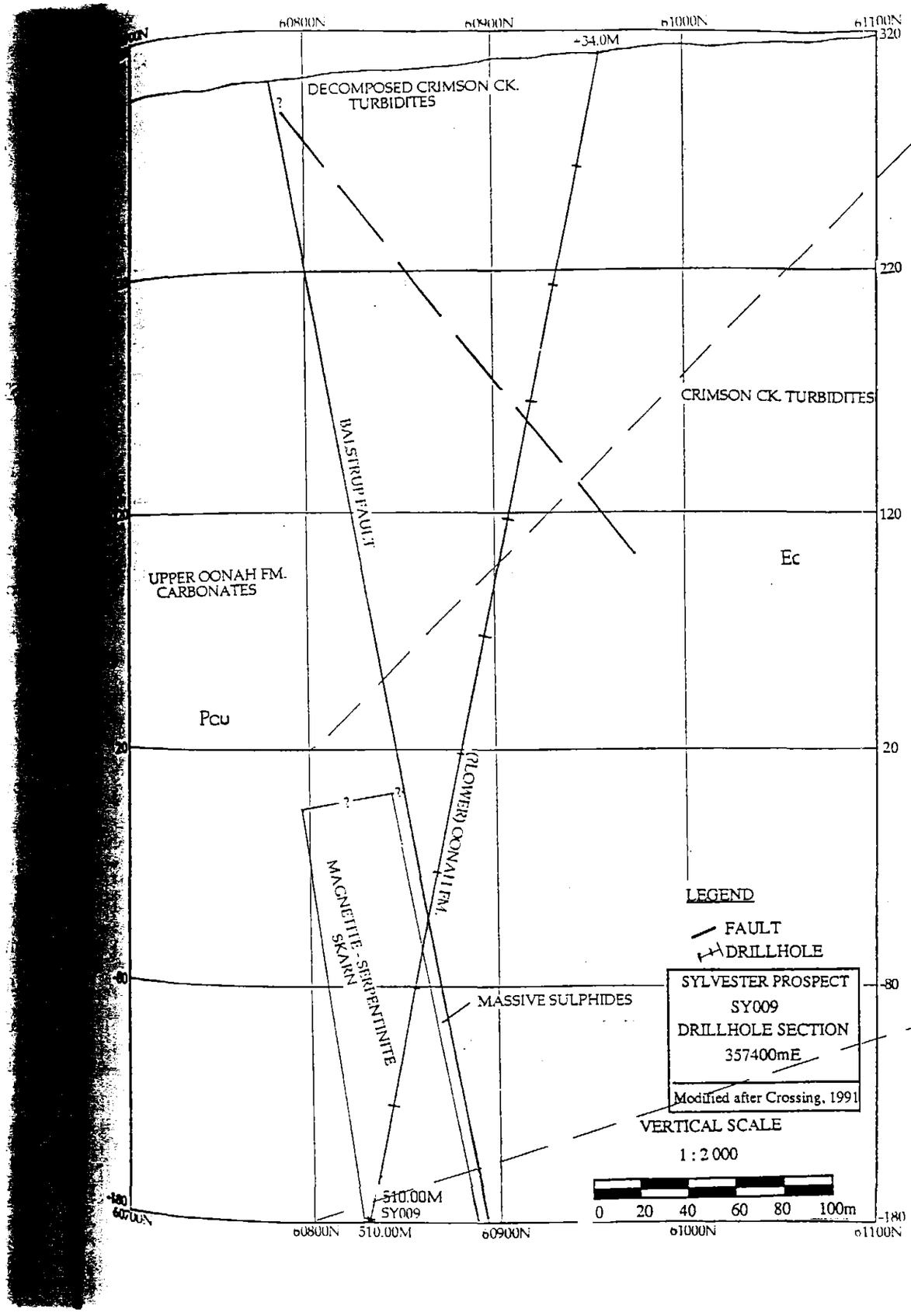

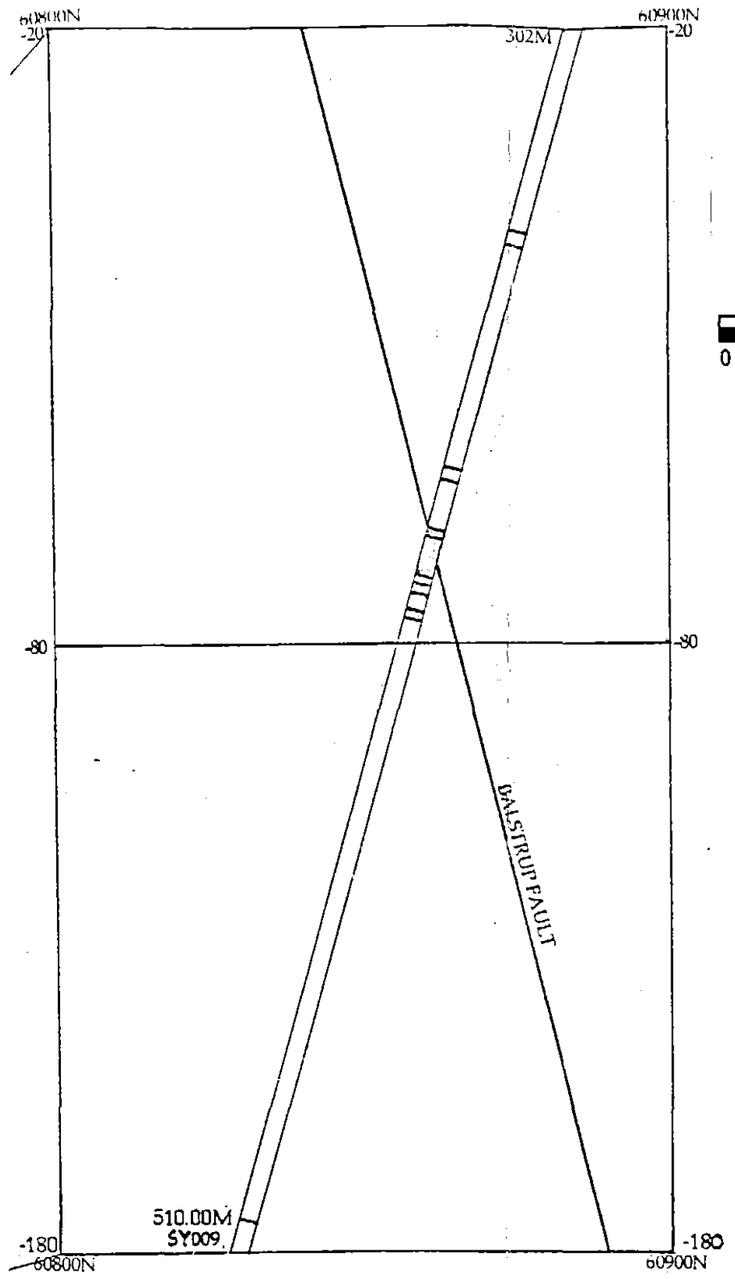

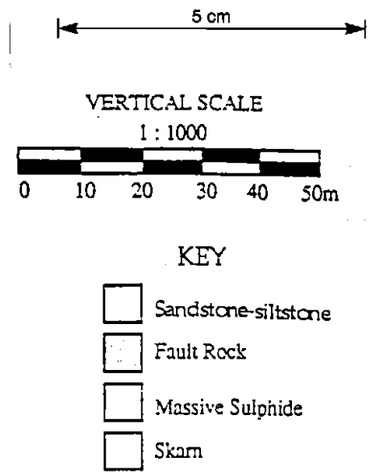

Figure 9.1 Drillhole sections of SY009

Insert - Sulphide intersections in SY009.

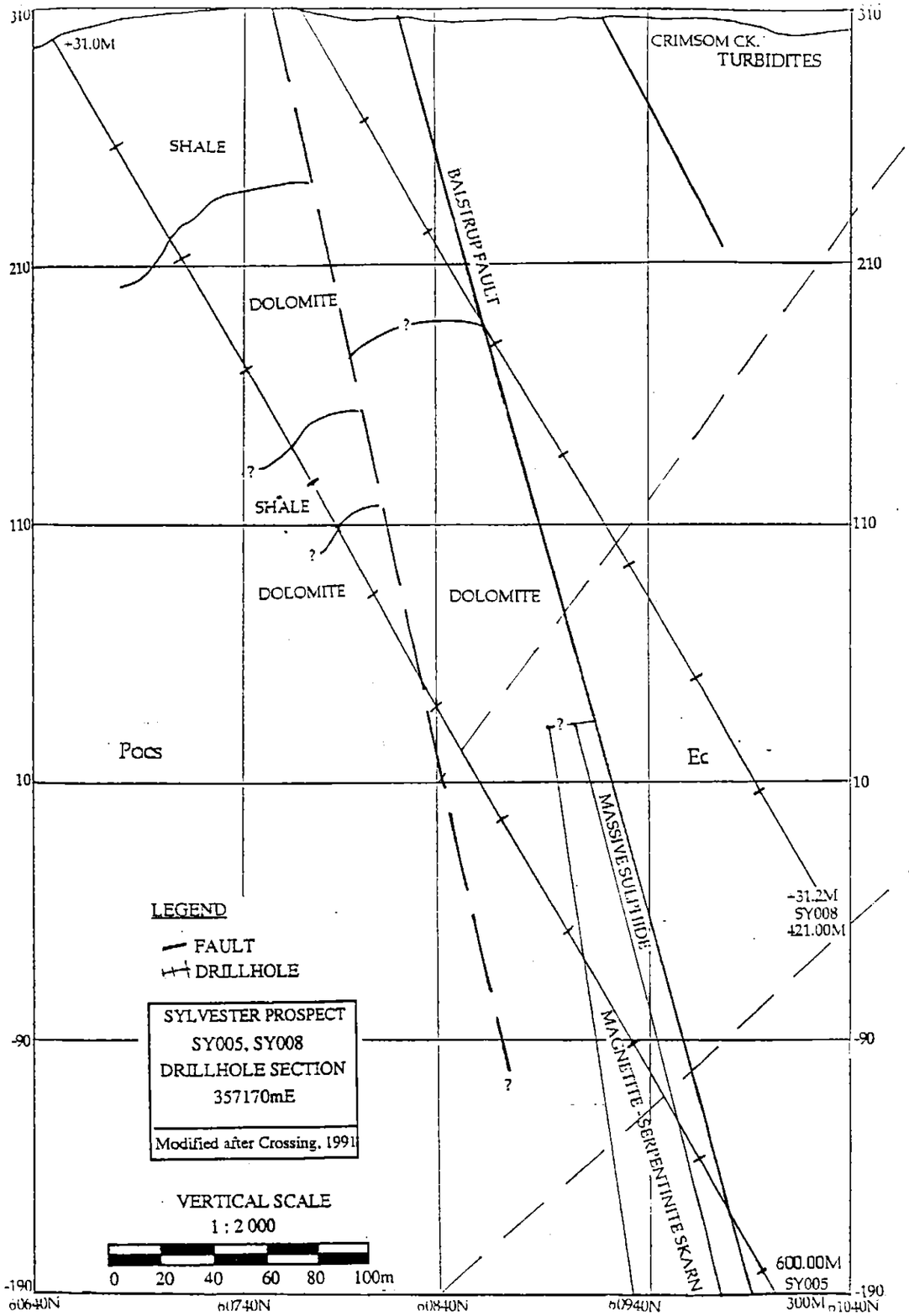

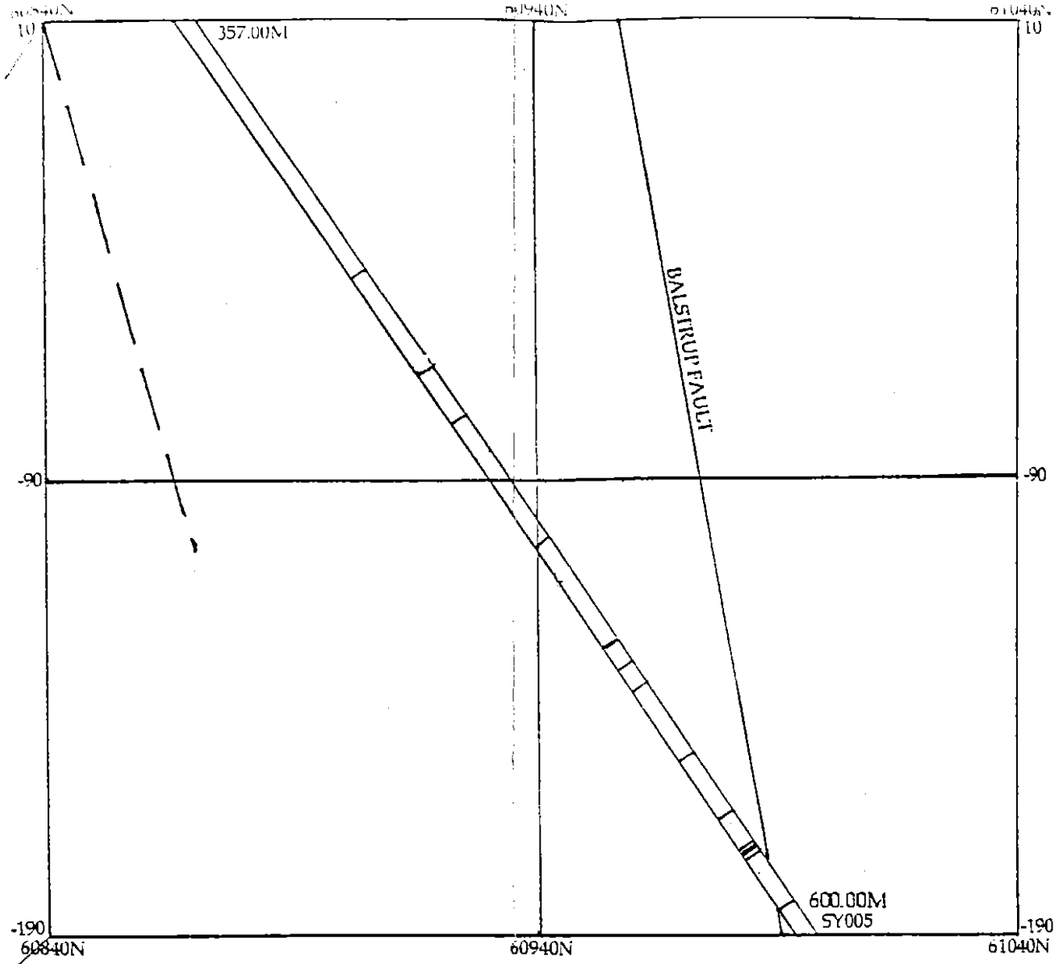

VERTICAL SCALE
1 : 1300
0 13 26 39 52 65m

KEY
- Dolomite
- Fault Rock
- Massive Sulphide
- Skarn

Figure 9.2 Drillhole sections of SY005 and SY008
Insert - Sulphide intersections in SY005.

controls mineralisation. The calc-silicate skarn observed in SY014 (Fig. 9.3) displays a zonation in mineralogy from the contact with the hornfels into the overlying carbonate unit. This mineralogical zonation away from the hornfels suggests that the metasomatic fluids responsible for the formation of the skarn flowed upwards from the lithological boundary of the hornfelsic pelite before moving into the carbonate.

The flow of fluids along lithological boundaries is most probably due to the low permeability of the hornfelsic rocks, which retards the metasomatic fluids from progressing up through the stratigraphy, and instead disperses fluids laterally via permeability barriers such as lithological boundaries and bedding planes. This has the effect of producing patches of calc-silicate skarn in favourable units over a wider area. This effect is documented in the area between the Sylvester prospect and the Heemskirk Granite (Fig. 4.9, map pocket).

9.2 STRUCTURAL CONTROLS

9.2.1 Folding

The carbonate horizon that hosts the serpentine-magnetite skarn and Comstock massive sulphide body is gently folded downward along the strike of the Balstrup Fault (ref Chapter 3). Folding of otherwise shallowly dipping strata in the footwall of major faults associated with skarn deposits has been noted in a number of deposits (Titley, 1961). In these deposits the highest grade of ore and the greatest thickness of skarn mineralisation is located within the crestal portions of the fold. Although the morphology of the skarn and sulphide mineralisation is largely unknown, it would reasonable to assume that folding of strata adjacent to the Balstrup Fault may also have

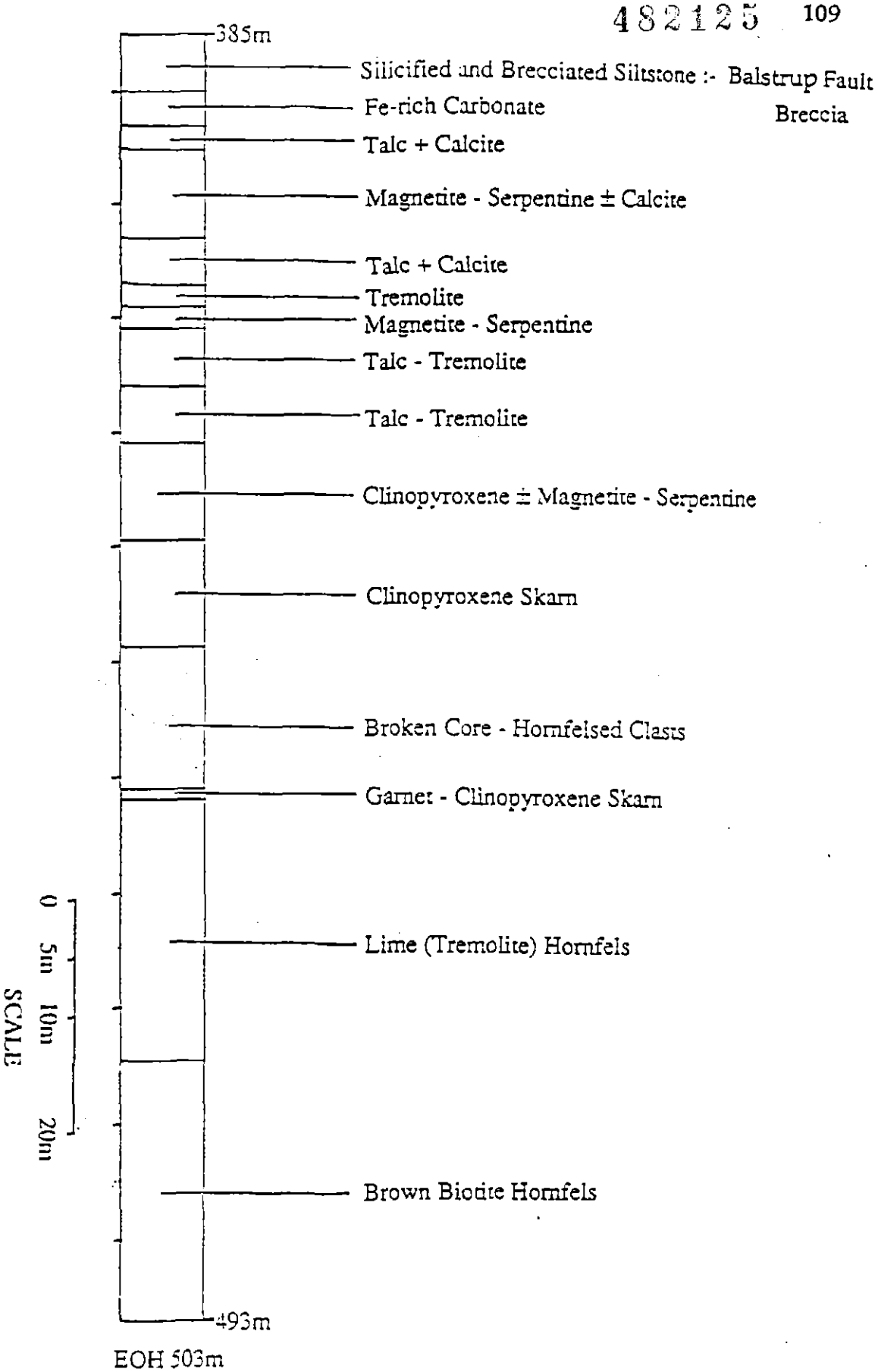

Figure 9.3 Schematic diagram showing the distribution of skarn in drill hole SY014.

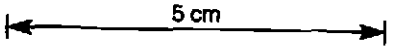

resulted in greater thicknesses of skarn and sulphide mineralisation in the crestal portions of the folded carbonate.

9.2.2 Faults and fractures

The occurrence of sulphide and skarn mineralisation being intimately associated with major faults and fractures is documented throughout the Sylvester prospect. The principal structural control in relation to the late stage serpentine-magnetite skarn and Comstock massive sulphide mineralisation is the Balstrup Fault, which has acted as the main conduit for mineralising fluids.

The importance of the Balstrup Fault is illustrated by the fact that the entire Comstock sulphide body is located within ~15 m of the footwall of the fault, abutting the structure in places, along a strike length of over 1 km. Over this distance the Balstrup Fault is a well defined structure (Crossing, 1989), however, the continuation of the fault past the areas of mineralisation (east of SY003; Fig. 4.9) is marked by the fault becoming a composite structure, consisting of multiple discrete fault zones. This strongly suggests that the well defined section of the Balstrup Fault acted as a focus for hydrothermal fluids, whereas the composite sections of the structure lacked the ability to focus fluids, most probably dispersing the hydrothermal fluids.

Fractures in the more competent non-carbonate units of the Oonah Formation are the dominant control on stockwork vein mineralisation. Metal distribution diagrams (Chapter 6; Figs. 6.1-6.4) illustrate this close spatial association between minor faults are fractures and the numerous occurrences of minor Pb, Zn and Cu grades which correspond to stockwork veins.

CHAPTER TEN

CONCLUSIONS

On the basis of stratigraphic, structural, mineralogical, morphological, and isotopic data, the skarn and sulphide mineralisation of the Sylvester prospect is interpreted as metasomatic replacements of carbonate horizons of the Late Precambrain Upper Oonah Formation by hydrothermal fluids, heated by and at least in part supplied by the emplacement of the Late Devonian Heemskirk Granite. The sequence of events is summarised as the follows:

1. A Late Precambrian succession of massive sandstones, interbedded siltstones-sandstones and shales (Lower Oonah Formation) grading into sandstones-siltstones, shales and dolomitic carbonates towards the top of the succession (Upper Oonah Formation) accumulated, and was uncomformably overlain by a sequence of Eo-Cambrian turbiditic mudstones, greywackes and volcaniclastics (Crimson Creek Formation) in a marine environment.

2. The tectonic (?) emplacement of a composite body of serpentinites, gabbros and mafic volcanics occurred in the Early Cambrian.

3. Folding and faulting of the host rocks occurred during a period of Early to late Middle Devonian deformation (Tabberraberan Orogeny) resulting in large scale (1 to 1.5 Km) NNW plunging open folding and the development of regional scale NNW trending faults (eg Balstrup Fault).

4. The Late Devonian Heemskirk Granite, an S-type granitic pluton was emplaced into the Precambrian rocks. The presence of the body beneath the Sylvester prospect is indicated by gravity modelling of the subsurface morphology of the granite.

5. The emplacement of the granite resulted in metamorphism of the country rocks. In the Sylvester prospect metamorphism was restricted to the development of biotite hornfels in the pelitic rocks of the Oonah Formation and extensive recrystallisation of the carbonate units of the Upper Oonah Formation to dolomitic marble.

6. During a late phase of intrusion of the Heemskirk Granite high temperature (400° - 500°C), relatively low XCO_2 metasomatic fluids (0.1 to 0.2 XCO_2) exsolved from the granite passed upward into the Oonah Formation along fracture and lithological boundaries resulting in the replacement of carbonate units by a calc-silicate assemblage of garnet, diopside, tremolite, talc and calcite± chlorite.

7. Concurrent with the crystallisation and cooling of the granite was the development of a hydrothermal cell within the Upper Oonah Formation which channelled hydrous low temperature (~200° - 500°C), low XCO_2 (<0.05) metasomatic fluids up the Balstrup Fault and produced extensive serpentine-magnetite ± brucite skarn in the carbonate units in the footwall of the Fault.

8. Closely associated with the late (hydrous) skarn phase is the formation of massive pyrrhotite + sphalerite + galena + chalcopyrite mineralisation replacing carbonates and late stage skarn in the immediate footwall of the Balstrup Fault. Pyrite + sphalerite + galena + boulangerite mineralisation occurs at the margins of the sulphide mineralisation, and

pyritic stockwork veins and fracture fillings were developed in the Oonah Formation and the Balstrup Fault. The late stage hydrous skarn and sulphide mineralisation is interpretated as derived from a hydrothermal system located in the country rock based on carbon and oxygen isotopes which show depletion in ^{18}O (~6‰) in calcite formed in the late stage skarn phase, and sulphur isotopes which have higher values (+6 - +7‰) than expected for purely magmatic fluids.

9. Minor phases of vug fillings and very late stage quartz and carbonate veins followed skarn development and sulphide mineralisation.

REFERENCES

Anderson, J A., 1986. The geology of the Zeehan cassiterite-sulphide deposits, Tasmania. *Genesis of Tin-Tungsten. Dep. and Assoc. Granitoids.*

Berry, R. F., and Crawford, A. J., 1988. The tectonic significance of the Cambrian allochthonous mafic-ultramafic complexes in Tasmania. *Aust. J. Earth Sci.* v.34(4) pp. 161-171.

Berry, R. F., Elliott, C. G., and Grey, D. R., 1990. Excursion Guide E3 - Structure and tectonics of western and northern Tasmania. 10th Australian Geological Convention.

Blissett, A. H., 1962a. Geology and structure of the Zeehan region, western Tasmania. Unpub. M.Sc. Thesis, University of Tasmania.

Blissett, A. H., 1962b. *Zeehan, Tasmania.* Tasm. Dep. Mines 1 Mile Geol. Atlas Series Expl. Rep., Sheet 50 (7914S).

Both, R. A., Rafter, T. A., Solomon, M. and Jensen, M. L., 1969. Sulfur isotopes and zoning of the Zeehan mineral field. *Econ. Geol.* v. 64, pp. 618-628.

Both, R. A., and William, K. L., 1968. Mineralogical zoning in the lead-zinc ores of the Zeehan Field, Tasmania; Part I and II. *J. Geol. Soc. Aust.* .v.15 (1) and (2) pp. 121-137, pp. 217-243.

Bowman, J.R., Covert, J. J., Clark, A. H., and Mathieson, G. A., 1985. The CanTung E zone scheelite skarn orebody, Tungsten, northwest Territories: Oxygen, hydrogen and carbon isotope studies. *Econ. Geol.* v.80, pp. 1872-1895.

Brooks, C., 1966. The rubidium-strontium ages of some Tasmanian igneous rocks. *J. Geol. Soc. Aust.* v.13, pp. 457-469.

Brown, A. V., 1986. The geology of the Dundas-Mt Lindsay-Mt Youngbuck area, Western Tasmania. Unpub. Ph.D Thesis, University of Tasmania

Brown, P. E., Bowman, J. R., and Kelly, W. C., 1985. Petrologic and stable constraints on the source and evolution of skarn-forming fluids at Pine Creek, California. *Econ. Geol.* v.80, pp. 72-95.

Buseck, P. R., 1967. Contact metamorphism and ore deposition. Tem Piute, Nevada. *Econ Geol.* v.62, pp. 331-353.

Carroll, G., 1990. MinTab v 1.1, Mineral recalculation and tabulation computer program. University of W.A.

Collins, P. L. F., and Williams, E., 1986. Metallogeny and tectonic development of the Tasman Fold Belt system in Tasmania. *Ore Geol. Rev.* v.1, pp. 153-201.

Crossing, D. J. F., 1989. E.L. 42/87, Zeehan area, Annual Report. 1988/89. Unpub. RGC Rpt T/89/3

Crossing, D. J. F., 1990. E.L.42/87, Zeehan area Annual Report. 1989/90. Unpub. RGC Rpt T/90/13.

Crossing, D. J. F., 1991. E.L. 42/87, Incorporating M.L.'s 43M/85 and 123M/47, Zeehan area, Annual Report for the period Oct. 1990 to Sept. 1991. Unpub. RGC Rpt T/91/23.

Crossing, D. J. F., 1992. E.L. 42/87, Incorporating M.L.'s 43M/85 and 123M/47, Zeehan area, Annual Report for the period Oct. 1991 to Sept. 1992. Unpub. RGC Rpt T/92/33.

Dick, L. A. and Hodgson C. J., 1982. The MacTung W-Cu (Zn) contact metasomatic and related deposits of the northeastern Canadian Cordilleria: *Eco Geol,* v. 77. pp. 845-867

Dickson, T. W., 1981. Tenth Legion Prospect (IMI joint venture). Interim Report Nov. 1980-Aug 1981. CRA Exp. Unpub.

Edwards, A. B., 1953. The Heemskirk-Zeehan mineral field. *5th Emp. Min. and Metal. Congr.*, v.1, pp. 1166-1778.

Einaudi, M. T., Meinert, L. D and Newberry, R. J., 1981. Skarn deposits: Eco Geol, 75th Anniversary Volume. pp. 317-391.

Everad, J. L., Findlay, R. H., McClenaghan, M. P., Seymour, D. B., and Brown, A. V., 1992. Current systematic regional mapping - new potentials for mineral discovery *Bull. Geol. Surv. Tasm.* v.70, pp. 70-82.

Findlay, R. H., and Brown, A. V., 1992. The Tenth Legion Thrust, Zeehan District: Distribution, interpretation and regional significance. *Rep Dep. Mines Tasm.* 1992/02.

Hajitaheri, J., 1985. The origin of mineralisation in south Heemskirk Granite, western Tasmania. Australia. Unpub. Ph.D. Thesis, University of Tasmania.

Johnson, B. D., 1967 . A regional gravity survey of westcoast of Tasmania. *The geology of western Tasmania.* A symposium [Unpub] Dept. of Geology, University of Tasmania.

Klominsky, J., 1972. The Heemskirk Granite massif, western Tasmania-a study of chemical variability in plutonic rocks. Unpub. Ph.D Thesis, University of Tasmania.

Kwak, T. A. P., and Askins, P. W., 1981. Geology and genesis of the F-Sn-W-(Be-Zn) skarn (wrigglite) at Moina, Tasmania. *Econ. Geol.* v.76, pp. 439-467.

Layne, G. D., Longstaff, F. J., and Spooner, E. T. C., 1991. The J.C. Tin skarn deposit, southern Yukon Territory: a carbon, oxygen, hydrogen and sulfur stable isotope study. *Econ. Geol.* v.86, pp. 48-65.

Leake, B. E., 1978. Nomenclature of amphiboles. *Can. Mineral.* v. 16, pp. 501-520.

Leaman, D. E., 1990. Gravity and magnetic evaluation of the Sylvester grid. *In* RGC Exploration Pty. Ltd. Annual Report Oct. 1990 to Sept. 1991. Unpub.

Leaman, D. E., and Richardson R. G., 1989. The granites of west and north-west Tasmania -a geophysical interpretation. *Geol. Surv. Bull.* No. 66.

McClenaghan, M. P., 1989. Mid-Palaeozoic Granitoids., *In* Burrett, C. F., and Martin, E.L. (ed). Geology and mineral resources of Tasmania. *Spec. Publ. geol. Soc. Aust.* v.15, pp. 250-269.

McCrea, J. M., 1950. On the isotopic chemistry of carbonates and a palaeotemperature Scale: *Journ. Chem. Physics,* v.18, pp. 849-857.

Ohmoto, H., 1986. Stable isotope geochemistry of ore deposits. *Rev . Mineral* v.16, pp. 491-556.

Olubus, P. E., 1988. The geology of the McIvor Hill Complex. Unpub. BSc. (Hons) Thesis, University of Tasmania.

Robinson, B. W., and Kusakabe, M., 1975. Quantitative preparation of SO_2, for $^{34}S/^{32}S$ analysis, from sulphides by combustion with cuprous oxide. *Analytical Chem* v.47, No. 7, pp. 1179-1181.

Shein, Y. H., and Taylor, H. P. Jr., 1969. Oxygen and carbon isotope studies of contact metamorphism of carbonate rocks: *Journ. Pet,* v.10, pp. 307-331.

Shimazaki, H., Shimizu, M., and Nakano, T., 1986. Carbon and oxygen isotopes of calcites from Japanese skarn deposits. *Geochem. Jour.* v.20, pp. 297-310.

So, C. S., Rye, D. M., and Shelton, K. L., 1983. Carbon, hydrogen, oxygen and sulphur isotope and fluid inclusion study of the Weolag Tungsten-Molybdenum deposit, Republic of Korea: Fluid histories of metamorphic and ore-forming events. *Econ,. Geol.* v.78, pp. 1551-1573.

Solomon, M., 1981. An introduction to the geology and metallic ore deposits of Tasmania. *Econ. Geol.*, v.76, pp. 194-208.

Taylor, B. E., and O'Neil, J. R., 1977. Stable isotope studies of metasomatic Ca-Fe-Al-Si skarns and associated metamorphic and igneous rocks, Osgood Mountains, Nevada: *Contr. Min. Pet.* v.62, pp. 1-50.

Titley, S. R., 1961. Genesis and control of the Linchburg orebody Socorro County, New Mexico. *Econ. Geol.* v.56 pp. 695-722.

Turner, F. J., 1981. Metamorphic petrology, Mineralogical and field aspects. McGraw Hill, N.Y.

Turner, N. J., 1989. Precambrian. *In* Burrett, C. F., and Martin, E.L. (ed). Geology and mineral resources of Tasmania. *Spec. Publ. geol. Soc. Aust.* v.15, pp. 84-153.

Twelvetrees, W. H., and Ward, L. K., 1910. The ore bodies of the Zeehan Field, *Bull. Geol. Surv. Tasm.* 8.

Walker, R. G., 1979b. Facies Models 8: Turbidites and associated course clastic deposit *In* Walker, R. G., (Ed)., Facies Models., Geoscience Canada, Reprint Series 1 pp. 91-103.

Will, T. M., and Powell, R. and Holland, T. J. B., 1990. A calculated petrogenetic grid for ultramafic rocks in the system CaO - FeO - MgO - Al_2O_3 - SiO_2 - CO_2 - H_2O at low pressures:. *Contr. Min. Pet.* v.105, pp. 347-358.

Williams, E., and Seymour, D. B., 1989. Mid-Palaeozoic Deformation. *In* Burrett, C. F., and Martin, E.L. (eds). Geology and mineral resources of Tasmania. *Spec. Publ. Geol. Soc. Aust.* v.15, pp. 239-250.

Williams, K. L., and Both, R. A., 1971. Mineralogy of the mines and prospects of the Zeehan field. *Rec. Tasm. Geol. Surv.* 11.

Waller, G. A., 1902. Report on the Western Silver mine, Zeehan. *Tasm. Dep. Mines.*

Waller, G. A., 1904. Report on the Zeehan silver-lead mining field. *Tasm. Dep. Mines.* Unpub. Rep.

Viezer, J., and Hoefs, J., 1976. The nature of $^{18}O/^{16}O$ and $^{13}C/^{12}C$ secular trends in sedimentary carbonate rocks: *Geochem. et Cosmochim. Acta.*, v.40, pp. 1387-1395.

Zharikov, V. A., 1970. Skarns: Internat. Geology Rev., v. 12 pp. 541-599, 619-647, 760-775.

APPENDIX A

ELECTRON MICROPROBE ANALYSES

(GARNETS)

Garnet

Sample No.	T35571	T35571	T35571	T35571	T35571	T35571	T35571	T35571	T35571	T35571	T35571	T35571
	Ring 1core	Ring 1 (2)	Ring 1 (3)	Ring 2 core	Ring 2 (2)	Ring 2 (3)	Ring 2 rim	Ring 2 (2)	Ring 2 (3)	Ring 2 (4)	Ring 2 (5)	Ring 2 (6)
SiO2	33.960	33.670	33.550	34.500	34.050	34.330	35.210	34.770	34.340	34.400	34.260	35.470
TiO2	0.000	0.000	0.000	0.000	0.000	0.000	0.000	0.000	0.000	0.000	0.000	0.000
AL2O3	0.200	0.240	0.110	1.210	0.350	0.090	4.860	1.860	0.420	0.500	0.890	1.000
Cr2O3	0.000	0.000	0.000	0.000	0.000	0.000	0.000	0.000	0.000	0.000	0.000	0.000
MgO	0.000	0.000	0.000	0.000	0.050	0.020	0.000	0.010	0.060	0.060	0.520	1.220
CaO	30.790	32.710	32.840	32.860	32.370	32.540	32.390	32.510	32.610	32.190	31.610	31.090
MnO	3.390	0.590	0.470	0.650	0.690	0.380	1.290	0.840	0.770	0.790	0.850	0.690
Fe2O3	30.641	31.084	31.278	29.450	30.658	31.291	24.556	28.120	30.413	29.830	29.936	27.894
Total	98.970	98.290	98.260	98.660	98.170	98.660	98.300	98.130	98.610	97.790	98.070	97.370
CATIONS												
Si	2.918	2.900	2.892	2.941	2.933	2.946	2.958	2.969	2.941	2.969	2.947	3.039
Ti	0.000	0.000	0.000	0.000	0.000	0.000	0.000	0.000	0.000	0.000	0.000	0.000
Al	0.021	0.024	0.012	0.121	0.036	0.009	0.481	0.187	0.043	0.051	0.090	0.101
Fe3+	1.981	2.015	2.029	1.889	1.987	2.021	1.553	1.807	1.960	1.937	1.938	1.799
Mg	0.000	0.000	0.000	0.000	0.006	0.003	0.000	0.001	0.008	0.007	0.062	0.156
Ca	2.834	3.018	3.033	3.001	2.987	2.992	2.916	2.974	2.992	2.977	2.876	2.854
Mn	0.247	0.043	0.034	0.047	0.051	0.027	0.092	0.061	0.056	0.058	0.062	0.050
Total Cation	8.000	8.000	8.000	8.000	8.000	8.000	8.000	8.000	8.000	8.000	8.000	8.000
Oxy Equiv	12.000	12.000	12.000	12.000	12.000	12.000	12.000	12.000	12.000	12.000	12.000	12.000
MOLE%												
Pyrope	0.000	0.000	0.000	0.000	0.190	0.110	0.000	0.000	0.200	0.200	2.174	5.100
Hydrogrossular	0.980	1.190	0.590	5.910	1.580	0.300	24.000	8.430	1.843	1.801	2.492	0.000
Calderite	7.970	1.400	1.090	1.480	1.670	0.890	3.000	1.780	1.804	1.846	1.994	1.570
Andradite	91.050	97.410	98.410	92.610	96.560	98.700	73.000	89.790	96.153	96.153	93.340	93.330

APPENDIX B

ELECTRON MICROPROBE ANALYSES

(CLINOPYROXENES)

clinopyroxenes data

Sample No	T41943 Ring 1 (1)	T41943 Ring 1 (2)	T41943 Ring 1 (3)	T41943 Ring 1 (4)	T41943 Ring 1 (5)	T41943 Ring 1 (6)	T41943 Ring 2 (1)	T41943 Ring 2 (2)	T41943 Ring 2 (3)	T41943 Ring 3 (1)	T41943 Ring 3 (2)
SiO2	54.710	53.562	53.299	53.124	52.955	53.919	53.521	53.141	53.627	54.240	54.378
TiO2	0.000	0.008	0.029	0.000	0.036	0.000	0.000	0.009	0.000	0.000	0.000
Al2O3	0.020	0.179	0.138	0.168	0.046	0.045	0.032	0.300	0.077	0.005	0.035
Cr2O3	0.010	0.000	0.024	0.011	0.000	0.006	0.000	0.000	0.013	0.000	0.000
MgO	17.237	15.715	16.481	15.953	14.793	16.188	16.779	16.554	17.037	17.917	17.911
CaO	26.331	26.030	26.438	25.816	25.497	25.722	26.184	26.069	26.386	26.244	26.028
MnO	0.094	0.347	0.156	0.259	0.718	0.280	0.241	0.331	0.513	0.215	0.033
FeO	1.489	3.852	2.434	3.231	4.995	2.984	1.622	1.980	1.761	0.930	0.392
Total	100.464	100.179	99.571	99.035	99.457	99.510	98.857	98.898	99.925	99.986	99.259
CATIONS											
Si	7.918	7.873	7.847	7.876	7.892	7.934	7.897	7.858	7.848	7.881	7.921
Ti	0.000	0.000	0.003	0.000	0.004	0.000	0.000	0.001	0.000	0.000	0.000
Al	0.000	0.031	0.024	0.030	0.008	0.008	0.006	0.052	0.010	0.001	0.006
Cr	0.000	0.000	0.003	0.001	0.000	0.000	0.000	0.000	0.001	0.000	0.000
Mg	3.718	3.443	3.617	3.525	3.286	3.550	3.690	3.649	3.716	3.880	3.889
Ca	4.083	4.100	4.171	4.101	4.071	4.055	4.139	4.130	4.137	4.086	4.062
Mn	0.012	0.043	0.019	0.033	0.091	0.035	0.030	0.041	0.064	0.026	0.005
Fe	0.180	0.473	0.300	0.401	0.623	0.367	0.200	0.245	0.216	0.113	0.047
MOLE%											
Diopside	95.100	86.960	91.910	89.080	82.190	89.850	94.130	92.750	93.040	96.540	98.700
Hedenbergite	4.610	11.940	7.600	10.100	15.560	9.290	5.100	6.200	5.380	2.810	1.200
Johannsenite	0.280	1.080	0.480	0.800	2.250	0.860	0.770	1.050	1.580	0.650	0.100

clinopyroxenes data

T41943	T41968	T41968	T41968	T41968	T35571	T35571	T35571
Ring 3 (3)	Ring 1 (1)	Ring 2 (1)	Ring 2 (2)	Ring 3 (2)	Ring 3 (1)	Ring 3 (2)	Ring 3 (3)
54.273	52.609	53.143	52.526	53.102	50.376	50.075	50.443
0.030	0.000	0.046	0.034	0.008	0.000	0.000	0.000
0.030	0.140	0.307	0.372	0.092	0.097	0.069	0.068
0.000	0.004	0.000	0.000	0.011	0.000	0.000	0.000
17.916	14.419	14.693	14.250	14.909	8.102	7.757	8.579
26.730	25.402	25.462	25.579	25.545	23.726	24.043	24.100
0.110	0.455	0.350	0.252	0.293	0.868	0.954	0.952
0.297	6.017	5.597	5.716	5.233	15.567	16.022	14.111
99.828	99.621	100.058	99.330	99.714	99.353	99.594	98.866
7.881	7.854	7.874	7.851	7.885	7.890	7.856	7.898
0.003	0.000	0.005	0.004	0.001	0.000	0.000	0.000
0.000	0.025	0.054	0.066	0.016	0.018	0.013	0.120
0.000	0.000	0.000	0.000	0.001	0.000	0.000	0.000
3.878	3.209	3.245	3.175	3.299	1.892	1.181	2.002
4.159	4.063	4.042	4.096	4.064	3.981	4.041	4.045
0.013	0.058	0.044	0.032	0.037	0.115	0.126	0.124
0.036	0.751	0.694	0.715	0.650	2.039	2.102	1.847
98.750	79.880	81.510	80.990	82.800	46.750	44.880	50.360
0.920	18.700	17.410	18.220	16.290	50.140	52.000	46.470
0.330	1.420	1.080	0.790	0.910	2.840	3.120	3.170

APPENDIX C

DRILLHOLE ASSAY DATA

SY003

Metres	Cu (ppm)	Pb (ppm)	Zn (ppm)	Sn (ppm)	Au (ppb)	Ag (ppm)	As (ppm)	Sb (ppm)
91.10	135.00	190.00	1000.00	4.00	0.00	0.00	28.00	4.60
93.00	125.00	75.00	610.00	9.00	0.00	0.00	20.00	3.40
95.00	105.00	100.00	870.00	3.00	0.00	0.00	30.00	6.60
97.00	120.00	135.00	656.00	6.00	0.00	0.00	25.00	4.90
99.00	45.00	50.00	640.00	10.00	0.00	0.00	18.00	3.50
101.00								
103.00	100.00	90.00	1350.00	12.00	0.00	0.00	21.00	4.50
105.00	120.00	5.00	305.00	5.00	0.00	0.00	5.00	2.00
108.00	90.00	60.00	265.00	4.00	0.00	0.00	16.00	4.20
120.00	55.00	20.00	225.00	9.00	0.00	0.00	8.90	4.20
134.00	30.00	50.00	235.00	4.00	0.00	0.00	64.00	18.00
136.00	40.00	35.00	105.00	6.00	0.00	0.00	13.00	4.00
138.00	25.00	60.00	105.00	7.00	0.00	0.00	21.00	7.00
140.00	35.00	105.00	115.00	11.00	0.00	0.00	21.00	7.00
142.00	55.00	100.00	95.00	6.00	0.00	0.00	37.00	12.00
144.00	70.00	360.00	160.00	9.00	0.00	0.00	14.00	8.00
146.00	40.00	200.00	100.00	17.00	0.00	0.00	75.00	10.00
147.00	40.00	1600.00	1700.00	42.00	0.00	0.00	89.00	17.00
148.00	55.00	5400.00	10500.00	59.00	0.00	0.00	26.00	26.00
148.70	105.00	29400.00	60300.00	28.00	0.00	57.00	399.00	355.00
150.00	50.00	24800.00	52700.00	43.00	0.00	67.00	351.00	109.00
151.00	750.00	52500.00	173000.00	34.00	0.00	50.00	52.00	116.00
152.00	350.00	46700.00	145000.00	15.00	0.00	55.00	20.00	151.00
153.00	400.00	60300.00	68600.00	3.00	0.00	32.00	8.00	90.00
154.00	260.00	71200.00	69300.00	6.00	0.00	46.00	5.00	64.00
155.00	255.00	24000.00	46800.00	19.00	0.00	43.00	9.00	35.00
156.00	230.00	5650.00	5200.00	4.00	0.00	20.00	21.00	23.23
157.00	885.00	4500.00	6350.00	13.00	0.00	21.00	22.00	44.90
158.20	10.00	290.00	1990.00	14.00	0.00	0.00	12.00	18.00
160.00	10.00	1200.00	920.00	16.00	0.00	0.00	21.00	19.00
162.00	5.00	756.00	4758.00	8.00	0.00	0.00	29.00	18.00
164.00	70.00	3000.00	2800.00	50.00	0.00	0.00	33.00	46.40
166.00	130.00	20400.00	4575.00	67.00	0.00	52.00	180.00	250.00
168.00	40.00	9800.00	175.00	10.00	0.00	22.00	33.00	47.10
170.00	15.00	117000.00	2450.00	8.00	0.00	16.00	180.00	43.40
172.00	15.00	4350.00	180.00	11.00	0.00	13.00	18.00	21.60
174.00	10.00	500.00	85.00	0.00	0.00	0.00	57.00	4.30
176.00	25.00	230.00	110.00	7.00	0.00	0.00	328.00	8.90
178.00	10.00	155.00	100.00	4.00	0.00	0.00	351.00	6.90
180.00	95.00	860.00	170.00	0.00	0.00	0.00	207.00	4.30
182.00	20.00	1250.00	80.00	8.00	0.00	0.00	278.00	7.00
184.00	15.00	280.00	145.00	7.00	0.00	0.00	130.00	5.00

SY003

Metres	Cu (ppm)	Pb (ppm)	Zn (ppm)	Sn (ppm)	Au (ppb)	Ag (ppm)	As (ppm)	Sb (ppm)
185.00	75.00	2000.00	345.00	0.00	17.00	0.00	100.00	22.70
190.00	10.00	40.00	65.00	3.00	8.00	0.00	974.00	3.30
194.00	10.00	20.00	50.00	13.00	0.00	0.00	35.00	0.50
200.00	445.00	5950.00	345.00	0.00	10.00	29.00	588.00	32.00
201.00	275.00	1030.00	286.00	3.00	0.00	6.00	215.00	13.00
202.00	55.00	60.00	60.00	6.00	0.00	0.00	90.00	6.30
214.00	210.00	535.00	2600.00	3.00	8.40	5.00	256.00	2.40
220.00	10.00	50.00	55.00	0.00	0.00	0.00	18.00	0.37
227.00	225.00	750.00	1000.00	17.00	9.50	0.00	901.00	6.30
232.00	320.00	260.00	375.00	6.00	110.00	0.00	56.00	29.80
237.00	10.00	10.00	65.00	4.00	0.00	0.00	110.00	0.62
239.00	15.00	15.00	50.00	0.00	0.00	0.00	120.00	0.62
244.00	25.00	2350.00	850.00	10.00	7.90	0.00	680.00	6.10
245.00	180.00	7000.00	12400.00	50.00	37.00	0.00	660.00	14.00
246.00	15.00	285.00	160.00	0.00	0.00	0.00	316.00	1.70
247.00	15.00	275.00	165.00	4.00	0.00	0.00	170.00	1.60
248.00	15.00	90.00	125.00	5.00	0.00	0.00	60.00	1.00
249.00	270.00	9200.00	45900.00	118.00	22.00	16.00	200.00	17.00
250.00	125.00	4100.00	16000.00	49.00	18.00	5.90	613.00	8.20
251.00	15.00	185.00	345.00	0.00	0.00	0.00	50.00	1.20
256.00	10.00	55.00	105.00	0.00	0.00	0.00	52.00	1.00
260.00	10.00	15.00	65.00	0.00	0.00	0.00	36.00	0.56
270.00	55.00	65.00	185.00	12.00	7.90	0.00	77.00	14.00
280.00	60.00	75.00	115.00	6.00	0.00	0.00	66.00	17.00
290.00	20.00	20.00	55.00	5.00	0.00	0.00	27.00	1.60
310.00	60.00	30.00	135.00	10.00	0.00		26.00	19.00
316.00	80.00	60.00	165.00	5.00	0.00	0.00	81.00	22.00
320.00	25.00	25.00	60.00	6.00	0.00	0.00	16.00	6.90
330.00	15.00	35.00	150.00	9.00	0.00	0.00	110.00	19.00
340.00	10.00	20.00	30.00	0.00	0.00	0.00	6.03	3.50
350.00	5.00	15.00	20.00	4.00	0.00	0.00	4.00	1.80
360.00	65.00	230.00	200.00	18.00	0.00	0.00	83.00	28.00
370.00	20.00	115.00	170.00	6.00	0.00	0.00	28.00	16.00
378.00	20.00	1100.00	80.00	8.00	0.00	0.00	57.00	436.00
380.00	80.00	2850.00	55.00	22.00	0.00	0.00	190.00	30.00
381.00	30.00	2650.00	50.00	15.00	0.00	0.00	150.00	110.00
382.00	245.00	5150.00	50.00	84.00	0.00	0.00	140.00	500.00
383.00	15.00	270.00	40.00	3.00	0.00	0.00	226.00	69.00
384.00	10.00	195.00	30.00	0.00	0.00	0.00	72.00	69.90
385.00	10.00	60.00	40.00	0.00	0.00	0.00	65.00	13.00
386.00	10.00	175.00	30.00	0.00	13.00	0.00	361.00	33.40
387.00	25.00	3350.00	120.00	23.00	18.00	0.00	502.00	60.00

482145

SY003

Metres	Cu (ppm)	Pb (ppm)	Zn (ppm)	Sn (ppm)	Au (ppb)	Ag (ppm)	As (ppm)	Sb (ppm)
388.00	610.00	42800.00	43400.00	129.00	31.00	93.00	805.00	281.00
389.00	1500.00	94800.00	100300.00	263.00	19.00	220.00	489.00	409.00
390.00	15.00	600.00	525.00	6.00	0.00	0.00	38.00	8.90
400.00	10.00	155.00	125.00	5.00	0.00	0.00	2.00	13.00
411.00	10.00	95.00	105.00	4.00	0.00	0.00	140.00	7.00
413.00	10.00	90.00	45.00	0.00	0.00	0.00	120.00	6.30
417.00	20.00	620.00	100.00	3.00	0.00	0.00	36.00	22.00
420.00	10.00	152.00	55.00	0.00	0.00	0.00	23.00	9.40
428.00	10.00	55.00	35.00	0.00	0.00	0.00	5.10	0.69
440.00	5.00	50.00	35.00	0.00	0.00	0.00	15.00	1.70
450.00	10.00	65.00	35.00	0.00	0.00	0.00	19.00	2.00
460.00	10.00	60.00	60.00	0.00	0.00	0.00	0.00	0.65
471.00	10.00	85.00	30.00	4.00	0.00	0.00	5.00	4.40
474.00	10.00	65.00	40.00	8.00	0.00	0.00	13.00	4.20
476.00	10.00	20.00	260.00	0.00	0.00	0.00	64.00	5.20
478.00	10.00	0.00	40.00	3.00	0.00	0.00	12.00	1.10
480.00								
482.00	5.00	0.00	30.00	9.00	0.00	0.00	18.00	2.20
484.00	10.00	10.00	50.00	0.00	0.00	0.00	15.00	2.80
486.00	25.00	150.00	175.00	3.00	0.00	0.00	28.00	8.20
489.00	25.00	415.00	425.00	0.00	0.00	0.00	59.00	20.00
490.00	25.00	80.00	75.00	7.00	0.00	0.00	13.00	8.90
494.00	25.00	5.00	60.00	0.00	0.00	0.00	3.00	3.00
495.00	25.00	0.00	75.00	0.00	0.00	0.00	8.00	2.20
502.00	150.00	65.00	90.00	0.00	0.00	0.00	24.00	15.00
509.00	905.00	27200.00	31800.00	33.00	0.00	27.00	42.00	17.00
514.00	75.00	50.00	130.00	6.00	0.00	0.00	24.00	5.30
521.00	100.00	1450.00	6200.00	8.00	0.00	0.00	8.00	4.60
523.00	35.00	1500.00	260.00	5.00	0.00	0.00	33.00	5.00
					0.00			

SY 005

Metres	Cu (ppm)	Pb (ppm)	Zn (ppm)	Sn (ppm)	Au (ppm)	Ag (ppm)	W (ppm)
110.00	10.00	10.00	30.00	0.00	0.00	0.00	0.00
111.00	10.00	10.00	25.00	0.00	0.00	0.00	0.00
111.80	10.00	70.00	70.00	0.00	0.00	0.00	0.00
112.00	8.00	40.00	25.00	0.00	0.00	0.00	0.00
236.00	115.00	65.00	110.00	5.00	0.00	0.00	0.00
237.00	65.00	60.00	70.00	20.00	0.00	0.00	0.00
237.80	60.00	6650.00	9250.00	12.00	0.00	8.00	159.00
238.00	20.00	60.00	95.00	0.00	0.00	1.00	0.00
239.00	10.00	0.00	35.00	0.00	0.00	0.00	0.00
240.00	20.00	0.00	35.00	0.00	0.00	0.00	0.00
241.00	10.00	0.00	30.00	0.00	0.00	0.00	0.00
242.00	10.00	0.00	45.00	0.00	0.00	0.00	0.00
243.00	35.00	80.00	1000.00	0.00	0.00	0.00	0.00
244.00	10.00	15.00	75.00	0.00	0.00	0.00	0.00
245.00	5.00	0.00	30.00	0.00	0.00	0.00	0.00
246.00	0.00	0.00	30.00	0.00	0.00	0.00	0.00
247.00	0.00	0.00	30.00	0.00	0.00	0.00	0.00
248.00	0.00	5.00	30.00	0.00	0.00	0.00	0.00
249.00	15.00	50.00	55.00	0.00	0.00	1.00	0.00
251.00	5.00	10.00	55.00	0.00	0.00	0.00	0.00
252.00	5.00	10.00	45.00	0.00	0.00	0.00	0.00
253.00	5.00	15.00	30.00	0.00	0.00	0.00	0.00
254.00	5.00	15.00	45.00	0.00	0.00	1.00	0.00
255.00	10.00	105.00	150.00	0.00	0.00	0.00	0.00
256.00	0.00	0.00	35.00	14.00	0.00	0.00	0.00
257.00	5.00	0.00	70.00	16.00	0.00	0.00	0.00
257.50	5.00	0.00	35.00	0.00	0.00	0.00	0.00
258.00	5.00	0.00	60.00	13.00	0.00	0.00	0.00
259.00	5.00	0.00	70.00	0.00	0.00	0.00	0.00
260.00	0.00	0.00	55.00	0.00	0.00	0.00	0.00
261.00	0.00	15.00	40.00	0.00	0.00	0.00	0.00
378.00	0.00	85.00	135.00	0.00	0.00	0.00	0.00
379.00	0.00	15.00	75.00	0.00	0.00	0.00	0.00
380.00	30.00	270.00	335.00	10.00	0.01	0.00	0.00
381.00	35.00	155.00	6600.00	0.00	0.01	0.00	110.00
382.00	40.00	195.00	16600.00	0.00	0.01	0.00	263.00
383.00	60.00	195.00	6750.00	0.00	0.00	1.00	118.00
384.00	50.00	105.00	2100.00	0.00	0.00	0.00	0.00
385.00	20.00	45.00	360.00	0.00	0.01	0.00	0.00
386.00	0.00	60.00	70.00	0.00	0.00	0.00	0.00
387.00	0.00	20.00	55.00	0.00	0.11	4.00	112.00
392.00	75.00	2000.00	5800.00	0.00	0.11	4.00	112.00

SY 005

Metres	Cu (ppm)	Pb (ppm)	Zn (ppm)	Sn (ppm)	Au (ppm)	Ag (ppm)	W (ppm)
396.00	0.00	35.00	355.00	0.00	0.00	0.00	0.00
398.00	15.00	10.00	185.00	0.00	0.00	0.00	0.00
400.00	55.00	10.00	1750.00	0.00	0.03	0.00	37.00
402.00	25.00	5.00	190.00	42.00	0.00	0.00	0.00
404.00	335.00	0.00	6400.00	26.00	0.11	0.00	141.00
406.00	50.00	0.00	295.00	6.00	0.02	2.00	28.00
410.00	20.00	130.00	1650.00	0.00	0.03	0.00	31.00
414.00	15.00	140.00	375.00	0.00	0.00	0.00	0.00
418.00	45.00	20.00	640.00	5.00	0.00	0.00	0.00
422.00	60.00	15.00	220.00	8.00	0.02	0.00	27.00
426.00	15.00	15.00	55.00	5.00	0.00	0.00	0.00
429.10	210.00	2450.00	3100.00	102.00	0.00	0.00	0.00
430.00	15.00	110.00	375.00	112.00	0.02	0.00	27.00
431.00	30.00	695.00	1800.00	58.00	0.00	4.00	0.00
432.00	10.00	280.00	310.00	69.00	0.00	0.00	0.00
433.00	35.00	560.00	1450.00	69.00	0.04	3.00	44.00
434.00	15.00	100.00	210.00	79.00	0.00	0.00	0.00
435.00	10.00	245.00	400.00	52.00	0.02	2.00	22.00
436.00	10.00	330.00	405.00	62.00	0.01	1.00	0.00
437.00	10.00	585.00	400.00	68.00	0.00	3.00	0.00
438.00	155.00	1550.00	3800.00	100.00	0.08	10.00	89.00
438.80	70.00	105.00	230.00	51.00	0.00	0.00	0.00
440.00	165.00	365.00	340.00	196.00	0.00	1.00	0.00
441.00	140.00	300.00	345.00	86.00	0.02	1.00	22.00
442.00	25.00	45.00	100.00	127.00	0.00	0.00	0.00
443.00	90.00	150.00	265.00	118.00	0.02	0.00	24.00
444.00	50.00	270.00	345.00	76.00	0.00	0.00	0.00
445.00	10.00	50.00	80.00	49.00	0.00	0.00	0.00
446.00	0.00	15.00	110.00	40.00	0.00	0.00	0.00
447.00	10.00	50.00	160.00	50.00	0.00	0.00	0.00
451.00	45.00	95.00	170.00	155.00	0.00	0.00	0.00
452.00	120.00	235.00	740.00	50.00	0.04	0.00	49.00
453.00	75.00	80.00	400.00	32.00	0.00	0.00	0.00
456.00	85.00	0.00	50.00	0.00	0.02	0.02	26.00
458.00	80.00	0.00	190.00	0.00	0.02	0.00	27.00
460.00	45.00	10.00	60.00	0.00	0.00	0.00	0.00
463.00	75.00	295.00	4200.00	0.00	0.08	0.00	83.00
464.00	70.00	420.00	4100.00	0.00	0.09	0.00	92.00
465.00	100.00	80.00	470.00	0.00	0.00	0.00	0.00
465.70	65.00	10.00	145.00	4.00	0.02	0.00	21.00
467.00	25.00	5.00	200.00	20.00	0.00	0.00	0.00
468.00	250.00	340.00	2450.00	5.00	0.02	1.00	24.00

SY 005

Metres	Cu (ppm)	Pb (ppm)	Zn (ppm)	Sn (ppm)	Au (ppm)	Ag (ppm)	W (ppm)
469.00	410.00	95.00	900.00	36.00	0.02	2.00	27.00
470.00	260.00	35.00	2200.00	42.00	0.07	1.00	76.00
471.00	915.00	140.00	10200.00	27.00	0.03	3.00	282.00
472.00	255.00	20.00	1976.00	43.00	0.05	5.00	50.00
473.00	260.00	10.00	900.00	49.00	0.00	1.00	0.00
474.00	420.00	15.00	2150.00	44.00	0.04	2.00	46.00
475.00	360.00	15.00	2600.00	41.00	0.04	2.00	42.00
476.00	360.00	35.00	2750.00	33.00	0.04	2.00	49.00
477.00	145.00	40.00	400.00	40.00	0.00	0.00	0.00
478.00	55.00	15.00	100.00	41.00	0.00	0.00	0.00
479.00	180.00	30.00	200.00	45.00	0.00	0.00	0.00
480.00	25.00	10.00	100.00	43.00	0.00	0.00	0.00
481.00	15.00	0.00	300.00	44.00	0.00	0.00	0.00
482.00	40.00	15.00	225.00	77.00	0.02	0.00	25.00
483.00	40.00	0.00	170.00	99.00	0.00	0.00	0.00
484.00	105.00	0.00	215.00	110.00	0.02	0.00	24.00
485.00	150.00	0.00	675.00	99.00	0.00	0.00	0.00
486.00	50.00	0.00	75.00	55.00	0.03	0.00	35.00
487.00	115.00	0.00	155.00	67.00	0.00	0.00	0.00
488.00	70.00	0.00	55.00	48.00	0.02	0.00	29.00
489.00	25.00	0.00	75.00	56.00	0.02	0.00	29.00
490.00	15.00	0.00	100.00	40.00	0.00	0.00	0.00
491.00	15.00	10.00	200.00	75.00	0.00	0.00	0.00
492.00	15.00	0.00	100.00	108.00	0.00	0.00	0.00
493.00	10.00	0.00	60.00	196.00	0.00	0.00	0.00
494.00	10.00	125.00	115.00	120.00	0.00	0.00	0.00
495.00	10.00	10.00	125.00	87.00	0.00	0.00	0.00
496.00	10.00	90.00	160.00	77.00	0.00	0.00	0.00
497.00	10.00	0.00	85.00	77.00	0.00	0.00	0.00
498.00	10.00	70.00	595.00	92.00	0.02	0.00	21.00
499.00	10.00	0.00	80.00	144.00	0.00	0.00	0.00
500.00	15.00	0.00	85.00	178.00	0.00	0.00	0.00
501.00	15.00	0.00	95.00	118.00	0.00	0.00	0.00
502.00	30.00	0.00	145.00	102.00	0.00	0.00	0.00
503.00	30.00	0.00	135.00	197.00	0.00	0.00	0.00
504.00	20.00	0.00	100.00	223.00	0.00	0.00	0.00
505.00	10.00	0.00	100.00	168.00	0.00	0.00	0.00
506.00	110.00	0.00	85.00	180.00	0.00	0.00	0.00
507.40	960.00	45.00	730.00	169.00	0.00	3.00	0.00
508.00	2350.00	31800.00	39800.00	240.00	0.00	36.00	909.00
509.00	2800.00	46800.00	47100.00	264.00	0.00	70.00	1210.00
510.00	3150.00	40700.00	41600.00	150.00	0.00	44.00	1090.00

SY 005

Metres	Cu (ppm)	Pb (ppm)	Zn (ppm)	Sn (ppm)	Au (ppm)	Ag (ppm)	W (ppm)
511.00	1800.00	37800.00	13100.00	134.00	0.02	35.00	314.00
512.00	3700.00	99400.00	29200.00	182.00	0.00	78.00	510.00
513.00	4050.00	18500.00	66600.00	80.00	0.00	35.00	1350.00
514.00	570.00	1250.00	7700.00	1150.00	0.00	8.00	116.00
515.00	110.00	180.00	1050.00	672.00	0.00	1.00	0.00
516.00	35.00	295.00	1700.00	747.00	0.00	2.00	0.00
517.00	65.00	55.00	275.00	530.00	0.00	0.00	0.00
518.00	2575.00	3350.00	80600.00	139.00	0.00	10.00	1640.00
519.00	2650.00	4500.00	39300.00	43.00	0.00	10.00	984.00
520.00	2250.00	10900.00	49600.00	206.00	0.00	12.00	1160.00
521.00	1750.00	11200.00	25200.00	67.00	0.02	12.00	632.00
522.00	795.00	840.00	10200.00	60.00	0.03	0.00	315.00
523.00	345.00	760.00	7300.00	86.00	0.05	0.00	396.00
524.00	575.00	1150.00	44500.00	98.00	0.02	1.00	1130.00
525.00	0.00	0.00	0.00	0.00	0.00	0.00	0.00
526.00	1900.00	59000.00	62900.00	471.00	0.01	36.00	1310.00
527.00	1750.00	105600.00	29000.00	616.00	0.01	50.00	524.00
528.00	1700.00	2100.00	10700.00	100.00	0.00	7.00	390.00
529.00	1500.00	17100.00	109300.00	282.00	0.00	12.00	2430.00
530.00	1500.00	1850.00	23500.00	427.00	0.01	7.00	609.00
530.90	795.00	4050.00	15800.00	208.00	0.00	3.00	312.00
532.00	1550.00	4000.00	11900.00	499.00	0.00	10.00	258.00
533.00	775.00	6850.00	23900.00	838.00	0.00	9.00	525.00
534.00	675.00	220.00	3300.00	118.00	0.00	4.00	81.00
535.00	930.00	15.00	120.00	60.00	0.00	1.00	80.00
535.80	350.00	15.00	80.00	7.00	0.00	1.00	0.00
537.00	290.00	10.00	120.00	32.00	0.00	2.00	0.00
538.00	225.00	0.00	100.00	35.00	0.00	0.00	0.00
539.00	450.00	0.00	85.00	13.00	0.00	0.00	0.00
540.00	340.00	10.00	45.00	7.00	0.00	0.00	0.00
541.00	400.00	0.00	45.00	11.00	0.00	0.00	0.00
542.00	370.00	0.00	60.00	210.00	0.00	0.00	0.00
543.00	515.00	20.00	150.00	345.00	0.00	0.00	0.00
544.00	195.00	0.00	55.00	22.00	0.00	0.00	0.00
545.00	130.00	0.00	40.00	73.00	0.00	0.00	0.00
546.00	290.00	15.00	40.00	164.00	0.00	0.00	0.00
547.00	210.00	15.00	40.00	48.00	0.00	0.00	0.00
548.00	135.00	0.00	40.00	228.00	0.00	0.00	0.00
549.00	180.00	20.00	35.00	38.00	0.00	0.00	0.00
550.00	200.00	0.00	85.00	621.00	0.00	0.00	0.00
551.00	400.00	15.00	90.00	36.00	0.03	0.00	0.00
	[illegible]	[illegible]	[illegible]	984.00	0.00	0.00	89.00

SY 005

Metres	Cu (ppm)	Pb (ppm)	Zn (ppm)	Sn (ppm)	Au (ppm)	Ag (ppm)	W (ppm)
553.00	275.00	0.00	90.00	488.00	0.00	0.00	0.00
554.00	845.00	50.00	60.00	0.00	0.00	0.00	84.00
555.00	1200.00	15.00	45.00	0.00	0.04	0.00	214.00
556.00	1300.00	75.00	50.00	0.00	0.20	1.00	0.00
557.00	1300.00	275.00	45.00	7.00	0.22	1.00	0.00
558.00	905.00	0.00	30.00	0.00	0.10	1.00	50.00
559.00	880.00	25.00	285.00	119.00	0.02	0.00	101.00
560.10	500.00	40.00	250.00	2392.00	0.02	0.00	73.00
561.20	35.00	995.00	6350.00	670.00	0.00	3.00	101.00
562.00	15.00	50.00	4950.00	237.00	0.00	3.00	67.00
563.00	15.00	130.00	3750.00	148.00	0.00	1.00	73.00
564.00	35.00	196.00	9450.00	192.00	0.00	1.00	142.00
565.00	945.00	50.00	3350.00	18.00	0.00	1.00	138.00
566.00	955.00	150.00	1700.00	24.00	0.00	3.00	0.00
567.00	435.00	510.00	2250.00	52.00	0.00	3.00	53.00
568.00	445.00	330.00	420.00	0.00	0.00	2.00	0.00
569.00	360.00	40.00	1600.00	19.00	0.00	2.00	0.00
570.00	125.00	70.00	2000.00	77.00	0.00	1.00	51.00
571.00	340.00	50.00	430.00	25.00	0.00	1.00	0.00
572.00	695.00	40.00	360.00	37.00	0.00	1.00	0.00
572.80	70.00	405.00	2950.00	110.00	0.00	3.00	30.00
574.00	235.00	65.00	80.00	67.00	0.00	1.00	0.00
575.00	106.00	60.00	85.00	55.00	0.00	2.00	0.00
576.10	250.00	40.00	55.00	9.00	0.00	2.00	0.00
577.10	255.00	90.00	90.00	0.00	0.00	2.00	0.00
578.00	190.00	90.00	75.00	0.00	0.03	0.00	39.00
579.00	205.00	105.00	160.00	14.00	0.00	1.00	0.00
579.90	50.00	330.00	360.00	174.00	0.00	0.00	0.00
581.00	55.00	670.00	1000.00	66.00	0.00	0.00	0.00
582.00	80.00	525.00	800.00	105.00	0.00	0.00	0.00
583.00	160.00	715.00	2600.00	53.00	0.00	0.00	25.00
584.00	70.00	110.00	75.00	23.00	0.00	3.00	0.00
585.00	285.00	295.00	1050.00	89.00	0.20	3.00	197.00
586.00	500.00	235.00	1000.00	162.00	0.03	0.00	33.00
610.00	30.00	25.00	75.00	4.00	0.00	0.00	0.00
619.00	35.00	20.00	50.00	6.00	0.00	0.00	0.00
635.00	30.00	0.00	75.00	4.00	0.00	0.00	0.00
639.00	25.00	0.00	25.00	23.00	0.00	0.00	0.00
[illegible]	[illegible]	[illegible]	[illegible]	37.00	0.00	0.00	29.00

SY 008

Metres	Cu (ppm)	Pb (ppm)	Zn (ppm)	Sn (ppm)	Ag (ppm)
26.000	39.000	381.000	1615.000	0.000	0.000
34.000	40.000	249.000	1824.000	0.000	0.000
42.000					
50.000	14.000	219.000	93.000	5.000	5.000
89.000	74.000	91.000	149.000	5.000	7.000
92.000	360.000	766.000	120.000	20.000	10.000
96.000	51.000	2327.000	14300.000	9.000	8.000
100.000					
102.000	131.000	131700.000	451400.000	74.000	334.000
105.000	25.000	1347.000	3659.000	6.000	2.000
110.000	36.000	831.000	1224.000	0.000	0.000
115.000	80.000	923.000	953.000	3.000	0.000
121.000	41.000	16200.000	10000.000	9.000	11.000
123.000	26.000	4965.000	7774.000	9.000	5.000
125.000	14.000	4698.000	12400.000	49.000	3.000
127.000					
129.000	135.000	79200.000	87400.000	127.000	42.000
130.000	335.000	93800.000	183400.000	245.000	61.000
132.000	32.000	2819.000	8007.000	25.000	5.000
134.000	97.000	10400.000	14200.000	55.000	
136.000	212.000	12000.000	11700.000	11.000	10.500
138.000	121.000	18600.000	48500.000	86.000	22.000
139.000	26.000	299.000	1031.000	3.000	0.000
142.000	21.000	244.000	1674.000	0.000	0.000
144.000	31.000	223.000	1343.000	4.000	0.000
145.000	16.000	2060.000	2205.000	0.000	0.000
148.000	38.000	222.000	2707.000	0.000	
150.000	34.000	206.000	399.000	6.000	
152.000	40.000	113.000	447.000	0.000	
154.000	26.000	141.000	170.000	4.000	
160.000	13.000	19.000	59.000	0.000	
165.000	15.000	145.000	153.000	4.000	
171.000	17.000	112.000	96.000	0.000	
178.000	30.000	10.000	50.000	5.000	
180.000	32.000	48.000	185.000	5.000	
182.000	25.000	331.000	164.000	15.000	
188.000	32.000	19.000	27.000	7.000	
190.000	49.000	110.000	186.000	15.000	
192.000	55.000	132.000	51.000	7.000	
200.000	28.000	78.000	63.000	4.000	
210.000	31.000	46.000	31.000	4.000	
220.000	47.000	67.000	56.000	0.000	

SY 008

Metres	Cu (ppm)	Pb (ppm)	Zn (ppm)	Sn (ppm)	Ag (ppm)
224.000	39.000	0.000	31.000	0.000	
228.000	57.000	71.000	37.000	0.000	
232.000	47.000	0.000	32.000	4.000	
236.000	53.000	126.000	35.000	6.000	
240.000	51.000	96.000	43.000	4.000	
250.000	61.000	17.000	32.000	4.000	
251.000	62.000	16.000	39.000	0.000	
252.000	72.000	25.000	528.000	8.000	
253.000	26.000	22.000	37.000	6.000	
260.000	48.000	39.000	26.000	0.000	
270.000	42.000	188.000	994.000	3.000	
280.000	37.000	42.000	159.000	0.000	
290.000	14.000	21.000	15.000	6.000	
300.000	0.000	15.000	109.000	4.000	
315.000	46.000	31.000	486.000	4.000	
322.000	32.000	1261.000	484.000	27.000	2.000
326.000	42.000	46.000	40.000	9.000	0.000
330.000	46.000	38.000	27.000	21.000	0.000
332.000	256.000	524.000	400.000	28.000	1.000
339.000	25.000	875.000	74.000	14.000	1.000
341.000	23.000	2917.000	4899.000	8.000	4.000
342.000	128.000	4600.000	11200.000	15.000	16.000
343.000	172.000	10300.000	11200.000	21.000	20.000
348.000	15.000	81.000	64.000	6.000	0.000
352.000	8.000	19.000	44.000	4.000	0.000
356.000	26.000	47.000	43.000	4.000	0.000
360.000	14.000	11.000	38.000	3.000	0.000
370.000	22.000	5.000	29.000	3.000	0.000
380.000	113.000	0.000	35.000	8.000	0.000
391.000	48.000	0.000	54.000	6.000	0.000
396.000	39.000	16.000	60.000	17.000	0.000
408.000	36.000	12.000	73.000	0.000	0.000
412.000	379.000	423.000	1046.000	22.000	4.000
416.000	15.000	5.000	26.000	7.000	0.000
420.000	41.000	26.000	44.000	13.000	0.000

SY 009

Metres	Cu (ppm)	Pb (ppm)	Zn (ppm)	Sn (ppm)	Ag (ppm)
502.00	0.00	11.00	89.00	113.00	0.00
506.00	21.00	7.00	116.00	658.00	0.00
510.00	0.00	43.00	115.00	42.00	0.00
514.00	0.00	9.00	91.00	11.00	0.00
517.00	187.00	55.00	803.00	37.00	1.00
519.00	196.00	239.00	6974.00	23.00	2.20
520.00	165.00	135.00	3218.00	8.00	1.20
524.00	14.00	0.00	115.00	10.00	0.00
528.00	67.00	19.00	132.00	17.00	0.50
530.00	59.00	17.00	54.00	20.00	0.00
532.00	79.00	100.00	195.00	15.00	0.00
534.00	187.00	171.00	313.00	11.00	0.80
536.00	101.00	7.00	144.00	22.00	0.00
538.00	107.00	322.00	1000.00	45.00	0.00
540.00	251.00	9.00	284.00	19.00	0.00
541.00	1275.00	8.00	122.00	30.00	0.00
542.00	200.00	9.00	33.00	20.00	0.00
543.00	22.00	41.00	117.00	17.00	0.00
546.00	94.00	11.00	36.00	18.00	0.00
547.00	220.00	26.00	47.00	9.00	0.00
548.00	191.00	649.00	2142.00	11.00	2.30
554.00	22.00	44.00	43.00	7.00	0.00
558.00	14.00	7.00	19.00	9.00	0.00
562.00	12.00	30.00	57.00	6.00	0.00
566.00	134.00	7.00	62.00	42.00	0.00
570.00	55.00	5.00	41.00	24.00	0.00
574.00	0.00	6.00	29.00	13.00	0.00
578.00	23.00	32.00	61.00	20.00	0.00
581.00	0.00	11.00	17.00	14.00	0.00
582.00	0.00	15.00	23.00	20.00	0.00
585.00	27.00	12.00	9.00	6.00	0.00
587.00	36.00	10.00	14.00	3.00	0.00
590.00	21.00	0.00	21.00	6.00	0.00

SY 009

Metres	Cu (ppm)	Pb (ppm)	Zn (ppm)	Sn (ppm)	Ag (ppm)
20.00	124.00	0.00	130.00	0.00	0.00
40.00	122.00	6.00	133.00	0.00	0.00
60.00	224.00	0.00	126.00	6.00	0.00
80.00	145.00	9.00	220.00	6.00	0.00
100.00	89.00	0.00	178.00	6.00	0.00
120.00	108.00	33.00	127.00	5.00	0.70
140.00	111.00	0.00	148.00	5.00	0.00
159.00	137.00	0.00	154.00	10.00	0.00
162.00	57.00	129.00	280.00	0.00	0.00
164.00	59.00	88.00	113.00	7.00	0.50
168.00	71.00	13.00	192.00	9.00	0.00
172.00	25.00	44.00	130.00	3.00	0.00
176.00	72.00	456.00	332.00	5.00	0.50
182.70	44.00	952.00	715.00	37.00	2.50
184.00	155.00	5200.00	10700.00	93.00	13.00
185.00	261.00	33500.00	13200.00	71.00	40.00
204.00	30.00	580.00	212.00	6.00	0.00
207.00	63.00	182.00	68.00	9.00	0.90
220.00	47.00	124.00	53.00	6.00	0.70
230.00	36.00	85.00	33.00	10.00	0.50
240.00	30.00	164.00	106.00	5.00	0.80
250.00	17.00	12.00	38.00	5.00	0.00
260.00	17.00	6.00	48.00	10.00	0.00
270.00	45.00	343.00	324.00	10.00	1.20
274.00	34.00	5941.00	5247.00	8.00	10.40
275.00	87.00	9100.00	11100.00	13.00	30.00
290.00	24.00	241.00	121.00	12.00	0.50
300.00	29.00	175.00	198.00	23.00	0.50
310.00	52.00	2754.00	810.00	22.00	7.60
320.00	190.00	8878.00	4400.00	25.00	22.00
330.00	12.00	34.00	48.00	7.00	0.50
340.00	5.00	9.00	85.00	18.00	0.00
347.00	12.00	44.00	2951.00	93.00	0.70
348.00	33.00	78.00	123.00	64.00	0.00
356.00	165.00	41.00	359.00	13.00	0.60
358.00	38.00	28.00	55.00	19.00	0.00
376.00	54.00	310.00	335.00	89.00	0.80
378.00	48.00	45.00	176.00	134.00	0.00
379.00	1028.00	12.00	33.00	11.00	1.10
380.00	1334.00	116.00	688.00	0.00	2.00
381.00	1339.00	1669.00	1037.00	30.00	4.40
382.00	1376.00	1248.00	3468.00	17.00	3.20

SY 009

Metres	Cu (ppm)	Pb (ppm)	Zn (ppm)	Sn (ppm)	Ag (ppm)
383.00	1362.00	7750.00	9185.00	107.00	10.20
384.00	1000.00	206.00	744.00	15.00	1.70
385.00	412.00	493.00	1003.00	74.00	1.00
386.00	112.00	63.00	237.00	118.00	0.00
387.00	1180.00	20.00	126.00	26.00	0.90
388.00	995.00	27.00	84.00	39.00	0.50
389.00	732.00	37.00	116.00	59.00	0.00
390.00	173.00	36.00	102.00	91.00	0.50
391.00	47.00	0.00	61.00	39.00	0.00
392.00	18.00	0.00	51.00	32.00	0.00
393.00	1000.00	27900.00	66000.00	83.00	38.00
394.00	934.00	53000.00	89000.00	46.00	64.00
395.00	117.00	126.00	214.00	73.00	0.80
397.00	9.00	0.00	92.00	125.00	0.00
402.00	10.00	41.00	143.00	117.00	0.00
406.00	9.00	22.00	98.00	612.00	0.00
410.00	13.00	25.00	72.00	37.00	0.00
414.00	53.00	9.00	46.00	20.00	0.00
418.00	7.00	114.00	109.00	16.00	0.00
419.00	439.00	35.00	129.00	40.00	0.90
420.00	174.00	33.00	101.00	35.00	0.00
421.00	186.00	8.00	62.00	45.00	0.00
422.00	396.00	0.00	359.00	24.00	0.00
428.00	10.00	6.00	44.00	325.00	0.00
430.00	0.00	8.00	82.00	439.00	0.00
434.00	12.00	17.00	104.00	39.00	0.00
438.00	13.00	6.00	63.00	276.00	0.00
442.00	8.00	12.00	83.00	22.00	0.00
446.00	43.00	19.00	197.00	17.00	0.00
450.00	8.00	27.00	102.00	155.00	0.00
454.00	23.00	55.00	250.00	23.00	0.00
458.00	6.00	63.00	673.00	63.00	0.00
462.00	38.00	268.00	3259.00	89.00	0.80
466.00	12.00	46.00	340.00	69.00	0.00
470.00	54.00	80.00	1455.00	212.00	0.60
474.00	0.00	58.00	186.00	74.00	0.00
478.00	49.00	38.00	1021.00	188.00	0.00
482.00	6.00	34.00	450.00	109.00	0.00
486.00	37.00	89.00	1454.00	22.00	0.50
490.00	32.00	6.00	50.00	7.00	0.00
494.00	7.00	16.00	333.00	65.00	0.00
498.00	0.00	22.00	94.00	17.00	0.00

SY 010

Metres	Cu (ppm)	Pb (ppm)	Zn (ppm)	Sn (ppm)	Ag (ppm)
30.000	28.000	12.000	165.000	3.000	0.000
40.000	29.000	30.000	100.000	0.000	0.000
50.000	29.000	16.000	147.000	0.000	0.000
60.000	27.000	15.000	75.000	0.000	0.000
70.000	28.000	14.000	92.000	5.000	0.000
80.000	26.000	82.000	336.000	6.000	0.000
90.000	32.000	19.000	112.000	4.000	0.000
100.000	78.000	159.000	145.000	0.000	0.000
102.000	52.000	184.000	112.000	0.000	0.000
104.000	65.000	470.000	125.000	0.000	0.800
107.000	135.000	308.000	19942.000	0.000	1.200
109.000	145.000	84.000	60.000	0.000	1.100
112.000	98.000	37.000	65.000	0.000	0.900
118.000	52.000	188.000	106.000	0.000	1.000
122.000	29.000	5.000	86.000	0.000	0.000
126.000	22.000	31.000	71.000	0.000	0.000
130.000	20.000	104.000	279.000	0.000	0.000
134.000	26.000	5.000	57.000	0.000	0.000
138.000	25.000	6.000	89.000	0.000	0.000
142.000	50.000	67.000	73.000	0.000	0.900
146.000	36.000	56.000	483.000	0.000	0.600
150.000	40.000	30.000	123.000	0.000	0.000
154.000	20.000	25.000	182.000	0.000	0.600
158.000	27.000	10.000	118.000	0.000	0.000
162.000	28.000	28.000	85.000	0.000	0.500
166.000	75.000	88.000	152.000	0.000	0.800
168.000	55.000	115.000	108.000	0.000	1.100
172.000	37.000	5.000	99.000	0.000	0.000
176.000	54.000	20.000	64.000	0.000	0.600
180.000	37.000	20.000	53.000	0.000	0.000
190.000	29.000	14.000	37.000	0.000	0.000
200.000	25.000	32.000	34.000	0.000	0.000
210.000	27.000	5.000	24.000	0.000	0.000
220.000	24.000	12.000	47.000	0.000	0.000
230.000	21.000	9.000	26.000	0.000	0.000
238.000	306.000	56.000	77.000	30.000	0.900
242.000	59.000	5.000	70.000	0.000	0.000
245.000	33.000	13.000	178.000	0.000	0.000
250.000	29.000	103.000	141.000	0.000	0.700
260.000	22.000	17.000	28.000	0.000	0.000
270.000	34.000	9.000	37.000	6.000	0.000
279.000	35.000	23.000	34.000	0.000	0.000
[illegible]	[illegible]	21.000	43.000	18.000	0.600

SY 010

Metres	Cu (ppm)	Pb (ppm)	Zn (ppm)	Sn (ppm)	Ag (ppm)
300.000	25.000	37.000	26.000	0.000	0.500
310.000	23.000	10.000	30.000	0.000	0.500
320.000	25.000	0.000	29.000	0.000	0.000
330.000	62.000	9.000	40.000	6.000	0.600
336.000	74.000	6500.000	4320.000	20.000	13.500
340.000	47.000	34.000	46.000	8.000	0.000
360.000	35.000	46.000	126.000	4.000	0.000
380.000	22.000	50.000	38.000	5.000	0.600
400.000	33.000	891.000	1720.000	0.000	5.700
410.000	65.000	14.000	36.000	0.000	0.500
415.000	72.000	39.000	62.000	6.000	0.000
417.000	50.000	48.000	82.000	4.000	0.000
418.000	56.000	84.000	702.000	7.000	1.300
419.000	17.000	432.000	209.000	0.000	1.900
420.000	17.000	203.000	84.000	0.000	1.000
421.000	19.000	65.000	75.000	0.000	0.700
422.000	8.000	21.000	37.000	0.000	0.000
423.000	9.000	15.000	37.000	0.000	0.000
424.000	9.000	25.000	73.000	0.000	0.000
425.000	21.000	3320.000	5390.000	4.000	12.100
426.000	10.000	763.000	1260.000	4.000	4.400
427.000	9.000	12600.000	3020.000	5.000	29.000
430.000	20.000	685.000	1060.000	6.000	4.700
434.000	10.000	169.000	343.000	6.000	1.100
438.000	28.000	6200.000	31.000	5.000	10.100
450.000	16.000	53.000	64.000	5.000	0.600
467.000	51.000	100.000	86.000	5.000	1.400
480.000	23.000	34.000	52.000	5.000	0.000
490.000	15.000	17.000	42.000	5.000	0.000
500.000	30.000	12.000	28.000	0.000	1.100
510.000	42.000	87.000	43000.000	50.000	1.400
511.000	32.000	72.000	1850.000	35.000	0.700
512.000	79.000	54.000	863.000	45.000	0.600
513.000	226.000	20.000	111.000	40.000	0.500
514.000	306.000	23.000	218.000	25.000	0.000
515.000	110.000	0.000	47.000	8.000	0.000
516.000	1100.000	98.000	135.000	0.000	1.300
517.000	346.000	0.000	80.000	35.000	0.000
518.000	192.000	28.000	238.000	40.000	0.000
520.000	66.000	6.000	40.000	16.000	0.000
522.000	53.000	28.000	60.000	30.000	0.000
526.000	64.000	24.000	69.000	18.000	0.000
530.000	89.000	5.000	32.000	11.000	0.000

SY 010

Metres	Cu (ppm)	Pb (ppm)	Zn (ppm)	Sn (ppm)	Ag (ppm)
534.000	56.000	0.000	38.000	21.000	0.000
538.000	69.000	5.000	35.000	13.000	0.000
542.000	70.000	44.000	98.000	12.000	0.000
546.000	173.000	15.000	64.000	24.000	0.000
547.000	22.000	0.000	103.000	130.000	0.000
551.000	10.000	0.000	70.000	1050.000	0.000
552.000	9.000	0.000	86.000	1250.000	0.000
556.000	0.000	27.000	390.000	350.000	0.000
560.000	6.000	0.000	50.000	520.000	0.000
564.000	5.000	32.000	203.000	100.000	0.000
570.000	8.000	240.000	806.000	40.000	0.800
582.000	173.000	5.000	114.000	30.000	0.000
600.000	6.000	21.000	41.000	55.000	0.500
620.000	13.000	0.000	51.000	20.000	0.000
640.000	6.000	0.000	85.000	30.000	0.500
651.000	23.000	0.000	47.000	18.000	0.000
652.000	45.000	0.000	61.000	20.000	0.000
655.000	75.000	0.000	46.000	15.000	0.000

SY012

letres	Cu (ppm)	Pb (ppm)	Zn (ppm)	Sn (ppm)	Au (ppm)	Ag (ppm)
2.200	105.000	0.000	138.000	0.000	0.000	0.000
2.100	80.000	11.000	332.000	0.000	0.000	0.000
10.000	110.000	243.000	1720.000	0.000	0.000	0.000
15.000	23.000	1080.000	1480.000	0.000	0.000	0.900
16.000	56.000	4090.000	4360.000	4.000	0.000	2.300
17.000	108.000	4680.000	5720.000	4.000	0.000	2.500
18.000	41.000	32.000	377.000	0.000	0.000	0.000
19.000	41.000	2890.000	4320.000	0.000	0.000	2.300
20.000	152.000	189.000	838.000	5.000	0.000	1.100
24.000	27.000	903.000	1240.000	0.000	0.000	1.000
25.000	17.000	9.000	135.000	0.000	0.000	0.000
51.800	127.000	0.000	211.000	0.000	0.000	0.700
00.000	87.000	13.000	159.000	0.000	0.000	0.500
40.000	77.000	0.000	100.000	0.000	0.000	0.000
80.000	92.000	0.000	154.000	0.000	0.000	0.000
91.000	113.000	430.000	1370.000	0.000	0.000	0.700
20.000	126.000	10.000	141.000	0.000	0.000	0.000
60.000	41.000	0.000	153.000	0.000	0.000	0.000
00.000	92.000	0.000	92.000	0.000	0.000	0.000
29.000	59.000	11.000	60.000	3.000	0.000	0.000
31.000	153.000	0.000	84.000	7.000	0.000	0.000
34.000	59.000	174.000	356.000	50.000	0.000	0.000
38.000	54.000	28.000	52.000	0.000	0.000	0.000
43.000	102.000	507.000	1026.000	55.000	0.000	4.000
43.800	170.000	1470.000	2110.000	40.000	0.011	12.000
45.000	70.000	250.000	85.000	5.000	0.030	0.000
46.000	160.000	100.000	60.000	5.000	0.066	0.000
47.000	910.000	0.000	55.000	0.000	0.039	0.000
48.000	1080.000	80.000	65.000	0.000	0.031	0.000
49.000	1150.000	180.000	630.000	19.000	0.024	0.000
50.000	950.000	5900.000	4900.000	8.000	0.067	15.000
51.000	280.000	5200.000	6000.000	55.000	0.033	14.000
52.000	610.000	10800.000	30800.000	6.000	0.045	20.000
53.000	240.000	26600.000	24800.000	19.000	0.077	50.000
54.000	440.000	19000.000	83000.000	100.000	0.054	37.000
55.000	740.000	3300.000	1800.000	7.000	0.026	12.000
56.000	350.000	8800.000	128000.000	0.000	0.055	15.000
57.000	76.000	1510.000	165.000	0.000	0.000	3.400
58.000	78.000	2080.000	101.000	0.000	0.000	4.300
59.000	28.000	3310.000	363.000	0.000	0.000	10.200
60.000	24.000	554.000	99.000	0.000	0.000	1.700
61.000	124.000	720.000	1230.000	0.000	0.000	1.800
				0.000	0.000	2.600

SY012

Metres	Cu (ppm)	Pb (ppm)	Zn (ppm)	Sn (ppm)	Au (ppm)	Ag (ppm)
463.000	18.000	912.000	452.000	0.000	0.000	2.700
464.000	16.000	95.000	124.000	0.000	0.000	0.800
465.000	11.000	131.000	176.000	0.000	0.000	0.600
466.000	22.000	1660.000	805.000	4.000	0.020	7.000
467.000	43.000	770.000	1140.000	0.000	0.000	0.700
468.000	17.000	155.000	264.000	0.000	0.000	0.000
469.000	62.000	4800.000	1310.000	45.000	0.019	23.000
474.000	6.000	254.000	245.000	0.000	0.000	1.000
477.000	31.000	876.000	540.000	0.000	0.000	0.900
478.000	22.000	51.000	4072.000	0.000	0.000	0.500
479.000	43.000	211.000	293.000	0.000	0.000	1.500
480.000	26.000	231.000	282.000	0.000	0.000	0.800
484.000	10.000	264.000	282.000	0.000	0.000	0.700
488.000	17.000	774.000	570.000	0.000	0.000	1.000
492.000	33.000	7.000	105.000	0.000	0.000	0.000
				0.000		

Sy 014

Metres	Cu (ppm)	Pb (ppm)	Zn (ppm)	Sn (ppm)	Au (ppm)	Ag (ppm)	W (ppm)
40.000	5.000	5.000	63.000	6.000	0.000	0.000	0.000
78.000	8.000	12.000	47.000	30.000	0.000	0.000	0.000
80.000	23.000	0.000	24.000	11.000	0.000	0.000	0.000
82.000	25.000	0.000	16.000	17.000	0.000	0.000	12.000
86.000	11.000	25.000	78.000	13.000	0.000	0.000	0.000
90.000	60.000	44.000	133.000	16.000	0.000	0.000	0.000
94.000	11.000	20.000	26.000	7.000	0.000	0.000	0.000
110.000	15.000	91.000	106.000	12.000	0.000	0.000	0.000
111.000	24.000	742.000	992.000	13.000	0.000	1.000	0.000
112.000	24.000	529.000	975.000	17.000	0.000	0.700	0.000
113.000	572.000	26300.000	136000.000	50.000	0.027	39.000	0.000
114.000	1131.000	106000.000	73000.000	60.000	0.021	169.000	0.000
115.000	170.000	1557.000	1090.000	35.000	0.000	4.000	0.000
116.000	184.000	1500.000	64000.000	60.000	0.026	11.000	0.000
117.000	29.000	490.000	4852.000	50.000	0.010	1.100	0.000
118.000	10.000	877.000	2103.000	45.000	0.080	1.000	0.000
119.000	23.000	3400.000	8600.000	70.000	0.000	5.000	0.000
120.000	0.000	335.000	890.000	65.000	0.000	0.000	0.000
121.000	23.000	28.000	88.000	13.000	0.000	0.000	0.000
130.000	52.000	323.000	365.000	55.000	0.000	1.000	0.000
132.000	467.000	21000.000	5600.000	75.000	0.225	35.000	0.000
180.000	25.000	54.000	68.000	9.000	0.000	0.000	0.000
221.000	12.000	9.000	39.000	19.000	0.000	0.000	0.000
222.000	344.000	171.000	1100.000	35.000	0.000	2.100	0.000
223.000	126.000	1586.000	4382.000	65.000	0.000	9.300	0.000
224.000	467.000	266.000	1951.000	75.000	0.000	1.000	0.000
225.000	677.000	576.000	1566.000	700.000	0.000	3.000	0.000
226.000	2004.000	368.000	351.000	400.000	0.000	2.200	3000.000
227.000	63.000	34.000	160.000	710.000	0.000	0.000	950.000
228.000	42.000	38.000	108.000	220.000	0.000	0.000	0.000
229.000	100.000	56.000	141.000	70.000	0.000	0.000	0.000
233.000	4532.000	188.000	326.000	330.000	0.000	4.000	0.000
234.000	639.000	87.000	2546.000	100.000	0.000	0.000	0.000
235.000	152.000	16.000	2013.000	30.000	0.000	0.000	0.000
236.000	38.000	12.000	157.000	14.000	0.000	0.000	0.000
237.000	57.000	83.000	1309.000	25.000	0.000	0.000	0.000
238.000	125.000	173.000	1473.000	30.000	0.000	0.000	0.000
239.000	89.000	218.000	441.000	20.000	0.000	0.000	0.000
240.000	45.000	339.000	1893.000	15.000	0.000	0.000	0.000
241.000	118.000	586.000	1355.000	20.000	0.000	2.000	0.000
242.000	155.000	733.000	2750.000	16.000	0.000	2.000	0.000
243.000	20800.000	10100.000	42200.000	160.000	0.134	95.000	0.000
[illegible]	[illegible]	700.000	1625.000	40.000	0.012	8.000	0.000

Sy 014

Metres	Cu (ppm)	Pb (ppm)	Zn (ppm)	Sn (ppm)	Au (ppm)	Ag (ppm)	W (ppm)
245.000	1906.000	432.000	1150.000	45.000	0.010	8.000	0.000
247.000	423.000	100.000	674.000	45.000	0.000	2.000	0.000
249.000	114.000	47.000	257.000	110.000	0.000	0.000	0.000
251.000	141.000	83.000	808.000	25.000	0.000	0.000	0.000
264.000	55.000	43.000	83.000	12.000	0.000	0.000	0.000
265.000	55.000	650.000	2004.000	20.000	0.000	2.000	0.000
267.000	58.000	24.000	75.000	20.000	0.000	0.000	0.000
269.000	30.000	53.000	134.000	30.000	0.000	0.000	0.000
306.000	33.000	139.000	844.000	12.000	0.000	0.600	0.000
347.000	309.000	51.000	3684.000	18.000	0.000	0.000	0.000
380.000	46.000	125.000	317.000	15.000	0.000	0.000	0.000
390.000	9.000	87.000	209.000	25.000	0.010	0.700	0.000
391.000	7.000	109.000	1190.000	80.000	0.021	0.600	45.000
393.000	0.000	12.000	666.000	40.000	0.314	0.000	0.000
395.000	0.000	0.000	147.000	45.000	0.000	0.000	55.000
397.000	0.000	175.000	197.000	40.000	0.000	0.000	0.000
399.000	0.000	30.000	324.000	40.000	0.000	0.000	30.000
401.000	0.000	58.000	311.000	40.000	0.000	0.000	0.000
404.000	0.000	41.000	1237.000	35.000	0.011	0.000	0.000
406.000	0.000	0.000	110.000	30.000	0.000	0.000	0.000
408.000	18.000	200.000	3574.000	35.000	0.000	0.011	0.000
410.000	0.000	12.000	86.000	70.000	0.000	0.000	45.000
412.000	5.000	56.000	655.000	25.000	0.000	0.000	0.000
416.000	0.000	110.000	173.000	80.000	0.000	0.000	0.000
420.000	16.000	35.000	191.000	55.000	0.000	0.000	0.000
424.000	0.000	15.000	87.000	55.000	0.000	0.000	16.000
428.000	0.000	15.000	90.000	45.000	0.000	0.000	10.000
432.000	0.000	5.000	0.000	20.000	0.000	0.000	0.000
436.000	0.000	6.000	0.000	70.000	0.000	0.000	20.000
440.000	25.000	10.000	249.000	14.000	0.000	0.000	0.000
450.000	35.000	44.000	385.000	1350.000	0.028	0.028	1690.000
460.000	16.000	33.000	69.000	55.000	0.000	0.000	0.000
480.000	0.000	0.000	210.000	11.000	0.000	0.000	0.000
500.000	88.000	5.000	128.000	15.000	0.000	0.000	0.000

482164

ALLEGIANCE MINING N.L.

PUBLIC ANNOUNCEMENT

10th March 1999

NICKEL SULFIDE DISCOVERY – ZEEHAN TASMANIA

We are pleased to report that further drill testing of the Avebury nickel sulfide deposit on Tasmania's West Coast has resulted in the discovery of a second zone of mineralisation.

Cored drill hole A003 was recently completed at 339m and intersected a 50m wide zone of significant nickel sulfide mineralisation, including two high-grade intervals. Details of the intersection are as follows:

Hole No.	Collar Dip	Bearing	Intersection(m) From	To	Drill Hole Width (m)	%Ni
A003	-50	004 AMG	223.7	274.1	50.4	0.83
Including at 0.5% Ni cut-off			223.7	246.9	23.2	1.02
			262.0	274.1	12.1	1.14
Including at 1.0% Ni cut-off			237.2	246.9	9.7	1.39
			271.1	274.1	3.0	2.29

This new zone of mineralisation lies on the northern margin of an ultramafic body, approximately 150m north of the previously announced discovery (A001: 10.7m of 1.15% Ni) which lies on the southern margin of the same ultramafic body.

Substantial magnetite generally in the range of 30-50% accompanies the nickel mineralisation. This may present an opportunity for process preconcentration and upgrading of nickel sulfide by the early stage low cost removal of magnetite.

Magnetite so produced is viewed as a potentially saleable by-product to nickel sulfide recovery, and is of definite commercial significance.

Preliminary petrological studies of A003 mineralisation indicates all of the nickel is present as relatively coarse pentlandite, which is the only sulfide present. This suggests that treatment of this mineralisation may result in the low cost recoveries of nickel sulfide into high-grade concentrates, along with a clean magnetite concentrate.

(/doc/announce/nickel-zeehan)

482165

Avebury represents the discovery of a new style of a potentially commercial nickel sulfide mineralisation within the already renowned western Tasmanian mineral province. The geological setting and the factors thought to control the formation of these new discoveries are extensive within the Allegiance tenements west of Zeehan.

To date, drilling has focused on a relatively small section of one ultramafic body. Seven (7) drill holes have now been completed. Significant nickel sulfide mineralisation was intersected in six (6) of these drill holes over a strike length of 1,500m. Geological environments similar to Avebury are currently thought to exist over at least a further 20 kilometres of cumulative strike length, and remain untested by drilling.

Allegiance is currently undertaking a range of geophysical and geochemical test surveys over the Avebury deposits. Results from these surveys will determine the most efficient exploration techniques to be applied to the substantial additional areas of prospective geology.

These latest drilling results are exciting for several reasons.

- **potential exists to discover a very large deposit. The encouraging results to date have been obtained from focused drilling of a relatively small section of a geological environment which is extensive within the Allegiance controlled tenements.**
- **deposit characteristics suggest they may be amenable to low cost underground mining methods**
- **petrological studies indicate the mineralisation may be amenable to simple, low cost treatment to produce both a high quality nickel sulfide concentrate and a magnetite by-product concentrate.**
- **the deposits are located close to the mining town of Zeehan with consequent infrastructure cost savings.**

Core drilling at Avebury is continuing to further test both the northern and southern deposits.

Allegiance Mining N.L. are operators of the Trial Harbour joint venture and are currently earning a 90% interest from Rio Tinto Exploration Pty Limited.

A.W. Howland-Rose
MSc, DIC, FGS, FIMM, FAusIMM, FAIG, CEng
Chairman

(/doc/announce/nickel-zeehan)

LEGEND

PERMIAN
- Pt — ZEEHAN GLACIAL FM.

CAMBRIAN
- €d — DUNDAS GP. GRITS AND CONGLOMERATE
- €c — CRIMSON CK. FM. TURBIDITES

PROTEROZOIC
- Pou — UPPER OONAH FM., UNDIFFERENTIATED
- Pocs — CARBONATES AND CARBONACEOUS SHALE
- Post — SANDSTONE AND SILTSTONE
- Pom — MONTANA MELAPHYRE VOLCANICS
- Po — LOWER OONAH FM. PSAMMO–PELITES

INTRUSIVE
- Dp — DEVONIAN PORPHYRY
- €g — CAMBRIAN GABBRO
- €us — CAMBRIAN SERPENTINITE

MINERALISATION
- Fe — IRONSTONE
- Mg — MAGNETITE
- Py — PYRITE

BASE METAL VEINS
DYKE
FAULT
MINERALISED FAULT
LITHOLOGICAL CONTACT
BEDDING TREND
UNCONFORMITY
SHEAR FABRIC
VERTICAL BEDDING
BEDDING ATTITUDE 0–29°
" " 29–59°
" " 60–90°
ANTCLINE
SYNCLINE

GRID CONVERGENCE 1.2?
GN TN MN
GRID/MAGNETIC 11.6?

482166

TCR 99-4380

RGC EXPLORATION PTY. LTD.

COMPILED	J.CROSSING
DRAWN	M.WALTER
DATE	7/92
CHECKED	
1:25,000 REFERENCE	

Fig. 1-4.

GEOLOGICAL INTERPRETATION

5 cm

100 0 100 200 500

SCALE: 1 : 5,000

356 000mE
357 000mE
358 000mE
359 000mE
363 000mN
362 000mN
361 000mN
360 000mN
359 000mE
358 000mE

1000m
2000m
3000m
4000m

Eo
Eou
Ec

PbZn
PbZn(Cu)
FePy
Fe
FeMn

SY001 193.00
SY002 534.50
SY003 536.50
SY004 343.50
SY005 666.50
SY008 421.00
SY009 687.90
SY010 670.80
SY011 218.00
SY012 554.40
SY013 154.50
SY014 503.30
SY015 412.50
SY016 413.00

SYLVESTER FT.
TENTH LEGION FT.
BALSTRUP FT. (AT M.S.L.)
BALSTRUP FT. (AT SURFACE)
08
70
45

GABBRO

LEGEND

- MASSIVE SULPHIDES/GOSSAN (SURFACE)
- MASSIVE SULPHIDES AT M.S.L.
- MAGNETITE–SERPENTINITE SKARN (SURFACE)
- MAGNETITE SERPENTINITE SKARN AT M.S.L.
- RECRYSTALLISED CARBONATE (SURFACE)
- RECRYSTALLISED CARBONATE AT M.S.L.
- OUTER LIMIT OF CALC–SILICATE METASOMATISM
- OUTER LIMIT OF INTENSE HORNFELS/SILICIFICATION
- DEPTH TO GRANITE (GRAVITY INTERP)
- PYRITIC VEINS + Pb Zn Ag
- QUARTZ TOURMALINE VEINS
- MINES
- FAULT, SURFACE
- FAULT, AT M.S.L.
- REPLACEMENT MASSIVE SULPHIDE
- MAGNETITE–SERPENTINITE SKARN
- RECRYSTALLISED CARBONATE
- OTHER MINERALISATION (VEIN, STOCKWORK)
- CALC. SILICATES

482167

TCR 99-4320

FIGURE 4.1

SKARN AND SULPHIDE MINERALISATION SYLVESTER PROSPECT

Modified after Crossing, 1992--RGC Exploration

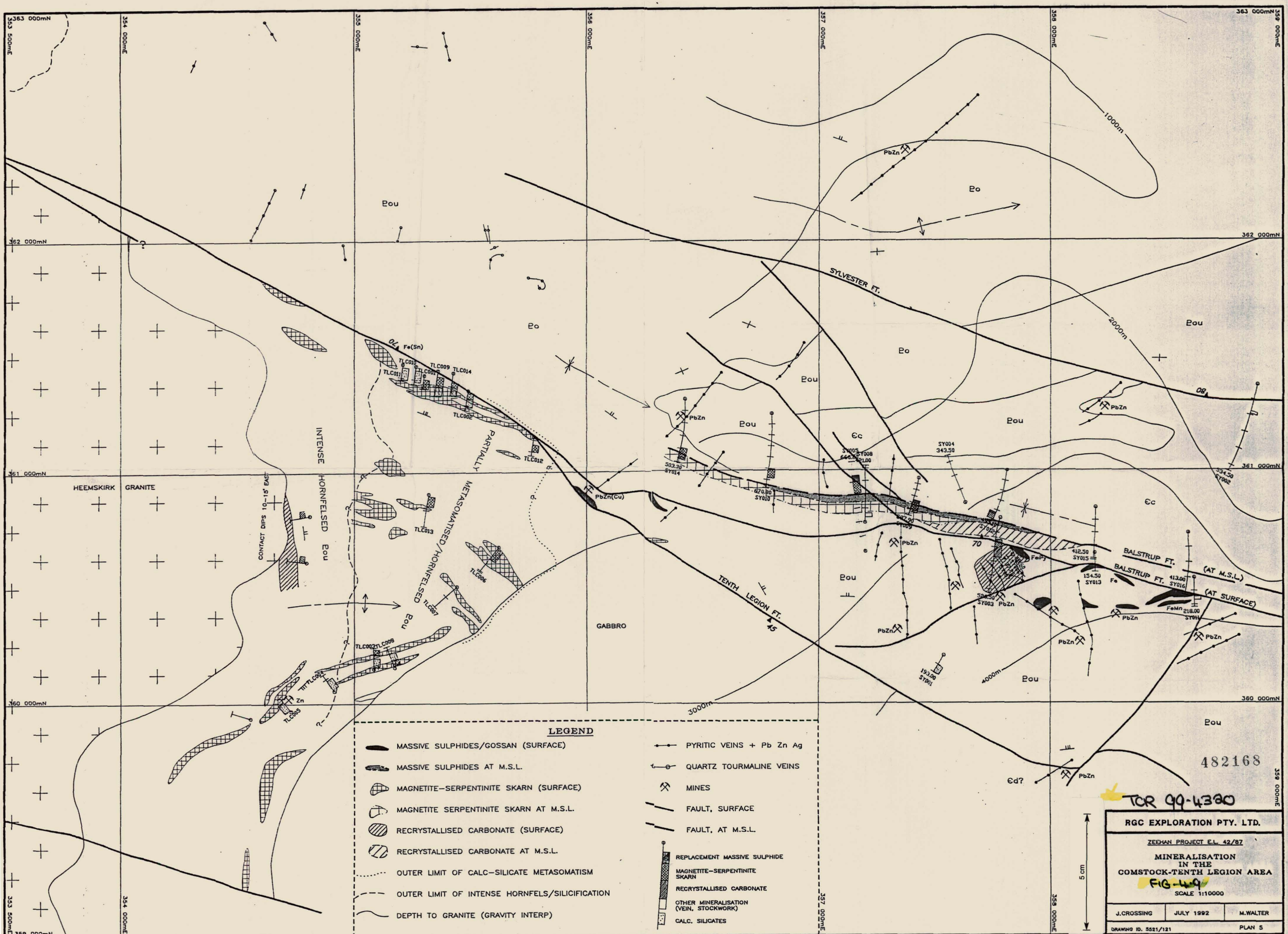
363 000mN
353 500mE
354 000mE
355 000mE
356 000mE
357 000mE
358 000mE
359 000mE
362 000mN
361 000mN
360 000mN
359 000mN
Ɛou
Ɛo
Ɛc
Ɛd?
1000m
2000m
3000m
4000m
SYLVESTER FT.
TENTH LEGION FT.
BALSTRUP FT. (AT M.S.L.)
BALSTRUP FT. (AT SURFACE)
HEEMSKIRK GRANITE
GABBRO
INTENSE HORNFELSED Ɛou
PARTIALLY METASOMATISED/HORNFELSED Ɛou
CONTACT DIPS 10-15° EAST
PbZn
PbZn(Cu)
Fe(Sn)
FePy
FeMn
Fe
Zn
TLC001
TLC002
TLC003
TLC005
TLC006
TLC007
TLC008
TLC009
TLC010
TLC011
TLC012
TLC013
TLC014
SY002
SY003
SY004
SY005
SY008
SY009
SY010
SY011
SY013
SY014
SY015
SY016
LEGEND
MASSIVE SULPHIDES/GOSSAN (SURFACE)
MASSIVE SULPHIDES AT M.S.L.
MAGNETITE-SERPENTINITE SKARN (SURFACE)
MAGNETITE SERPENTINITE SKARN AT M.S.L.
RECRYSTALLISED CARBONATE (SURFACE)
RECRYSTALLISED CARBONATE AT M.S.L.
OUTER LIMIT OF CALC-SILICATE METASOMATISM
OUTER LIMIT OF INTENSE HORNFELS/SILICIFICATION
DEPTH TO GRANITE (GRAVITY INTERP)
PYRITIC VEINS + Pb Zn Ag
QUARTZ TOURMALINE VEINS
MINES
FAULT, SURFACE
FAULT, AT M.S.L.
REPLACEMENT MASSIVE SULPHIDE
MAGNETITE-SERPENTINITE SKARN
RECRYSTALLISED CARBONATE
OTHER MINERALISATION (VEIN, STOCKWORK)
CALC. SILICATES
482168
TCR 99-4320
5 cm
RGC EXPLORATION PTY. LTD.
ZEEHAN PROJECT E.L. 42/87
MINERALISATION IN THE COMSTOCK-TENTH LEGION AREA
FIG-4.9
SCALE 1:10000
J.CROSSING
JULY 1992
M.WALTER
DRAWING ID. 5521/121
PLAN 5